

Optimising Qubit Designs for Topological Quantum Computation

Robert Ainsworth

B.Sc.



**Maynooth
University**
National University
of Ireland Maynooth

Thesis presented for the degree of

Doctor of Philosophy

to the

National University of Ireland Maynooth

Department of Mathematical Physics

October 2014

Department Head

Professor Daniel M. Heffernan

Research advisor

J. K. Slingerland

To my parents.

Declaration

This thesis has not been submitted in whole, or in part, to this or any other university for any other degree and is, except where otherwise stated, the original work of the author.

Robert Ainsworth, November 4, 2014

Abstract

The goal of this thesis is to examine some of the ways in which we might optimise the design of topological qubits. The topological operations which are imposed on qubits, in order to perform logic gates for topological quantum computations, are governed by the exchange group of the constituent particles. We examine representations of these exchange groups and investigate what restrictions their structure places on the efficiency, reliability and universality of qubits (and multi-qubit systems) as a function of the number of particles composing them. Specific results are given for the limits placed on d -dimensional qudits where logic gates are imposed by braiding anyons in 2+1 dimensions.

We also study qudits designed from ring-shaped, anyon-like excitations in 3+1 dimensions, where logic gates are implemented by elements of the loop braid group. We introduce the concept of local representations, where the generators of the loop braid group are defined to act non-trivially only on the local vector spaces associated with the rings which undergo the motion. We present a method for obtaining local representations of qudits and show how any such representation can be decomposed into representations which come from the quantum doubles of groups. Due to the dimension of the local representation being related to the number of generators, any non-Abelian properties of the representation are not compromised with an addition of extra operations, we conclude that universal representations may be easier to find than in previously discussed cases (though not for topological operations alone).

We model a ring of Ising anyons in a fractional quantum Hall fluid to study how interactions in a real environment may impact any qubits we have created. Fractional quantum Hall liquids are currently one of the most promising possibilities for the physical realisation of TQC and so present a natural choice of system in which to study these effects. We show how interactions between the anyons compromise the practicality of qubits defined by the fusion channels of anyon pairs and explore the use of the fermion number parity sectors as qubit states. Interactions between the anyon ring and the edge of the liquid are modelled to study the effect they will have on the state of the qubit. We perform numerical simulations, for a small system, to give some indication of how the edge interaction will influence the reliability of the qubit.

Acknowledgements

Firstly, I need to thank my incredible supervisor, Dr. Joost Slingerland. I could not have reached this point without his advice, guidance and (most importantly) patience over the last five years. I will always be grateful for how accommodating and approachable he was over the years as well as his unwavering enthusiasm and support.

To the other members of the group; Olaf, Jorgen, Ivan and Niall, thanks for helping me over all those mental blocks and also for the many post-conference beers around Europe.

For being delightful distractions and protectors of my sanity, I'll be forever indebted to my office/lunch mates; Aoife, Úna, Glen, Graham, Sepanda and John. And thanks also to all the other members of the Maths Physics department, especially Prof. Daniel Heffernan and Monica Harte for keeping the department running so smoothly.

A big thank you to all my friends from Dunboyne and Maynooth for being so supportive and understanding. A special thanks, in particular, to my housemates over the last few years; Niall, Rob, Darragh and Sandra, for always being there to come home to and for always managing to make my day a little bit better, no matter how impossible it seemed.

Lastly I must thank my family, my parents; Joe and Mary, my sister, Niamh, and brother, Niall. I will never be able to express the extent of my gratitude for their endless support, encouragement and reassurance, for always staying positive, especially when I couldn't, and for always guaranteeing that I ate at least one decent meal every week.

I also acknowledge financial support from the Science Foundation Ireland through the Ireland Principal Investigator award 08/IN.1/I1961

Thank you all.

Contents

1	Introduction	1
1.1	Topological Quantum Computation	2
1.2	Anyons	4
1.3	The Braid Group	5
1.4	Fusion Trees	8
1.5	Conformal Field Theory	11
1.6	Thesis Outline	15
2	Topological Qubit Design	17
2.1	Standard TQC Scheme	17
2.2	The Optimal Qubit	19
2.2.1	Maximum Number of Anyons	21
2.2.2	Universality	23
2.3	Qudits	25
2.3.1	Optimal Qutrit	26
2.3.2	General Anyon Number Limits	29
2.3.3	Upper Limit for the Braid Group	36
2.4	Multi-Qudit Gates	38
2.4.1	Two-Qubit Gates	39
2.4.2	Two-Qutrit and Qubit-Qutrit Gates	42
2.5	Conclusion	43
3	TQC with Anyonic Rings	45
3.1	The Motion Group	46
3.2	Qubits Using Slides	50
3.3	Induced Representations of \mathfrak{Mot}_n	52
3.4	Local Representations	55

3.4.1	2 Dimensional Local Vector Spaces	58
3.4.2	Representations of Slide and Flip Groups	64
3.4.3	Canonical Flip Basis	66
3.5	Local Representations for $d > 2$	69
3.5.1	6 Dimensional Example	80
3.6	Conclusion	82
4	Interacting Ising Anyons	84
4.1	The Fractional Quantum Hall Effect	84
4.2	The Ring Model	88
4.3	Anyon Ring Hamiltonian	92
4.3.1	The Transverse Field Ising Model	96
4.3.2	TFIM - Ising CFT Correspondence	103
4.3.3	Qubit Definition	110
4.4	Edge Interaction	113
4.4.1	Double Chain System	115
4.4.2	Computing Elements of H_I	119
4.4.3	Reintroducing Chirality	125
4.4.4	Scaling Interaction Energies	127
4.5	Perturbation Theory	128
4.5.1	Interacting System Eigenstates	134
4.5.2	Time Evolution	135
4.6	Numerical Simulations	138
4.6.1	Non-Chiral System	142
4.6.2	Chiral Edge System	149
4.7	Optimal Design	156
4.8	Conclusion	160
	Conclusions	162
	Bibliography	167

Introduction

Topological quantum computation (TQC) is a field which is still very much in its infancy. A number of models of how a topological quantum computer may be implemented have been devised (see refs. [1, 2, 3] for examples) but there has not yet been any definitive experimental proof of the existence of the necessary non-Abelian, anyonic excitations on which these designs are based, though simpler types of topological excitations and some intriguing experimental results which point to non-Abelian anyons have been observed [4, 5, 6]. Even at this early stage of development, it is useful to consider how the device may be optimally designed. The work in this thesis was then motivated by an interest in answering this question for the basic components of a topological quantum computer, i.e. the qubits. We wanted to understand the theoretical conditions under which a qubit might possess the most useful properties which would inform us of certain limits that could feasibly be reached by the computer.

To this end, chapters 2 and 3 of the thesis will be primarily focused on the study of the representations of various exchange groups associated with the movements of anyonic excitations within a topological quantum system. We will be concerned with finding the most general properties of representations of these exchange groups as the physics of any excitations which are subject to the exchange group are of more interest than the properties of particular anyon models given by specific representations.

These representations are useful as they allow us to study topological excitations outside of the constraints imposed by the physical materials which harbour them. The results found then apply to any realisation of these excita-

tions and we can specialise to specific systems by adding in any extra physical restrictions imposed.

Representations of exchange groups are also of interest in TQC where the representation of the generators of the exchange group gives the possible logic gates which can be implemented on a topological qubit by allowing the constituent anyons to undergo this exchange. Study of this general representation, for anyonic excitations defined by a particular exchange group, then enables us to determine what design optimisations are possible within the limits allowed by the presentation of their exchange group. This highlights the essential properties which are necessary for an “ideal” topological quantum computer and allows us to identify systems which could potentially approach such ideal limits.

By inserting the constraints of particular anyon models into this general framework we can see the extent to which these ideal conditions must be compromised and assess the practicality of the system to see whether it can meet the requirements of TQC.

The work presented in this thesis is separated into three distinct, but closely related, projects; two of which, examined in chapters 2 and 3, study the optimal design of topological qubits discussed above and the other, discussed in chapter 4, examines the effects of introducing some physical restrictions into the design. Each these projects have been given a dedicated chapter in this thesis but there are some deep connections and common ideas which arise in all three chapters which I will introduce first. How each of the concepts relates specifically to the work will be explained in detail in the body of the thesis, I will just provide a quick overview of some of the important terminology and concepts here.

1.1 Topological Quantum Computation

Topological quantum computing is a method of implementing quantum computations by storing information in certain quantum states which can only be altered by manipulating the topology of the system, see ref. [1, 7, 8, 9, 10] for a comprehensive introduction to TQC theory.

Other designs for quantum computers encode information in local quan-

tum states of a system. Such states are extremely unstable and will decohere through interaction with the environment, this places a high demand on the isolation of the system and speed of the computation, making the system difficult to scale. Storing information in non-local, topological degrees of freedom of a system means there is a much lower probability of loss or corruption of the information due to local perturbations. Operations can then be performed with less worry about disturbing the sensitive local quantum states. Topological quantum computers aim to utilise these more robust, non-local quantum states in order to produce a quantum computer which scales with greater ease.

However, in order to obtain the topological particles that will be used in the computation, such machines must be built from complex topological systems which, so far, have not been found in nature and are difficult to achieve in the lab. Many of the challenges with topological quantum computation then are not in the implementation of the actual computations but in discovering and producing the complex and delicate topological phases of matter which display the necessary properties, as discussed in ref. [9].

The basic units of information in quantum computation are two-level, quantum systems called qubits, see e.g. ref. [11, 8]. Topological qubits are then two-level, quantum systems whose state can be altered through a topologically nontrivial operation. In general a topological qubit will consist of a collection of topological (quasi-)particles whose configuration dictates the state of the qubit. Moving these (quasi-)particles around in a certain manner then amounts to imposing quantum gates on the qubit.

While two-level systems (bits) are sufficient for classical computing, the case is slightly more complex for quantum computation. Quantum mechanical systems with more than two states exist and we may be forced, or choose, to use such systems as our basic unit of information. The analogy to a classical bit is then somewhat lost and so we alter the name to make this change obvious, a three state system is then referred to as a *qutrit*, a four state system as a *quqart*, and so on. In general, we call a d -state system a *qudit*.

A topological system will have many states, to create a qudit from this system we must choose d states to encode the information we wish to store. Ideally we should ensure the chosen states are topologically degenerate, i.e. states at the same energy level but which require some topological operation in the de-

generate subspace in order to move between them. There should also be an energy gap to the other states of the system to protect the qubit from slipping out of the computational space [1, 12].

1.2 Anyons

Quantum statistics is a property by which we can distinguish between different types of particles, usually bosons and fermions. If we have a wavefunction, ψ , which describes a system of two particles, then the quantum statistics of these particles determines what effect exchanging their position will have on ψ . If ψ remains unchanged by such an operation then the wavefunction is symmetric under exchange and we call the particles bosons, alternatively if ψ becomes $-\psi$ then the wavefunction is antisymmetric under exchange and the particles are referred to as fermions. In our everyday, (3+1)-dimensional world these are the only two possibilities, however, more exotic results are found when we move to 2+1 dimensions [13].

To understand what happens in moving to a (2+1)-dimensional system we should first look at the mathematical explanation of these exchange statistics. Instead of just performing one exchange we consider the case where we exchange two particles twice, so that they return to their original positions. It is not difficult to see that this operation is equivalent to leaving one particle, which we will call p_2 , in place and moving the other particle, p_1 , completely around it and back to its starting position.

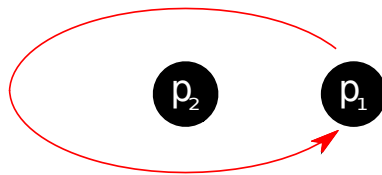


Figure 1.1: Moving one particle around another, equivalent to two exchanges.

If we track the path, or worldline, of p_1 (shown in red above) we see that it traces out a loop around p_2 with a base point on p_1 . In (3+1)-dimensional space we can picture taking this loop and, using the dimension perpendicular to the plane it lies in, pull it around p_2 , we can then shrink it down in size until it becomes a single point located at p_1 .

This operation is done without breaking or cutting the loop in any way. In topological terms we call this form of operation a continuous deformation, i.e. a deformation of one object into another which does not involve cutting or gluing the original object. If one object can be transformed into another by a continuous deformation we say that they are homeomorphic and from a topological perspective they are equivalent, see for example ref. [14].

We see, therefore, that a loop encircling a point in 3+1 dimensions is homeomorphic to a point at the loop's base. A point is a topologically trivial object so we have in fact shown that the path which p_1 takes around p_2 is equivalent to a trivial path. Thus the operation of double exchange of particles in 3+1 dimensions is completely trivial, in other words, if τ exchanges two such particles, then $\tau^2 = 1$. A single exchange then must be a root of the identity so we get; $\tau = \pm 1$, and so we have produced the exchange statistics for bosons and fermions.

Moving to 2+1 dimensions makes things more complicated. The loop can no longer be contracted to a point, this is because the dimension which we used to pull the loop around p_2 is not present in this system. So we would have to either pull the loop through p_2 or cut it, both of which would mean the result is not homeomorphic to the loop we started with. Therefore the path of p_1 is not equivalent to the trivial path and so $\tau^2 = 1$ is not a requirement for this system. There is then more freedom in the values τ can take.

In fact, if ψ is a wavefunction describing two particles in 2+1 dimensions then it picks up a phase factor, $e^{i\vartheta}$, under exchange; $\tau\psi \mapsto e^{i\vartheta}\psi$ [15, 16]. The exact value of ϑ is determined by the species of particles we are dealing with. For $\vartheta = 0$ we get $e^0 = 1$ so we have bosons and for $\vartheta = \pi$ we have $e^{i\pi} = -1$ and so we get fermions. However, ϑ is not constrained to these two values and can actually take any value between 0 and 2π . Thus the particles are dubbed *anyons*, and they can be considered a generalisation of bosons and fermions.

1.3 The Braid Group

The exact nature of the exchange operators, τ , mentioned in section 1.2, and hence also the nature of the anyonic phase factors, ϑ , are determined by the braid group, B_n , on n 'strands' [17]. The braid group has generators, τ_i , which

exchange strands i and $i + 1$ in the manner depicted in figure (1.2).

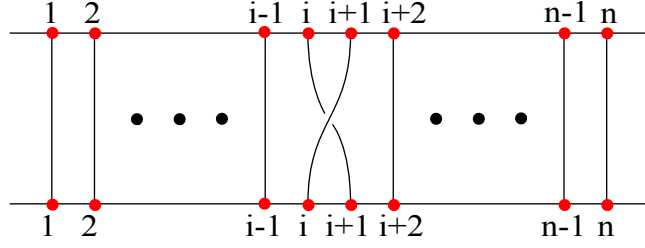


Figure 1.2: τ_i braids the i^{th} and $(i + 1)^{th}$ strands.

The worldlines of particles in 2+1 dimensions act in an equivalent way to the strands and so exchanging these particles can be viewed as the braiding of their worldlines. Braids can be multiplied together by simply stacking them on top of each other and the inverse of a braid is found by inverting the crossing of the two strands.

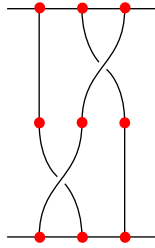


Figure 1.3: The braid $\tau_1\tau_2$

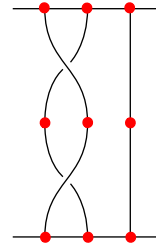


Figure 1.4: The braid $\tau_1\tau_1^{-1}$

The presentation of the braid group, as described by Artin [18], is given by generators τ_i , for $i = 1, 2, \dots, n - 1$, which obey the following group relations:

$$\tau_i\tau_j = \tau_j\tau_i \quad \{\text{for } |i - j| \geq 2\} \quad (1.1)$$

$$\tau_i\tau_{i+1}\tau_i = \tau_{i+1}\tau_i\tau_{i+1} \quad (1.2)$$

Relation (1.1) here is simply a statement of how spatially separated braids have no influence on each other so it does not matter which order we do them in. Relation (1.2) is a form of the well-known Yang-Baxter relation which will be discussed in much greater detail several times later in this thesis.

An important property of the braid generators is that they are conjugate to each other. We can take any generator, τ_j and produce any other generator in the group, say τ_k , by conjugating τ_j by the appropriate braid, X , which is some combination of the generators of B_n ; $\tau_k = X\tau_jX^{-1}$, figure 1.5 shows this diagrammatically.

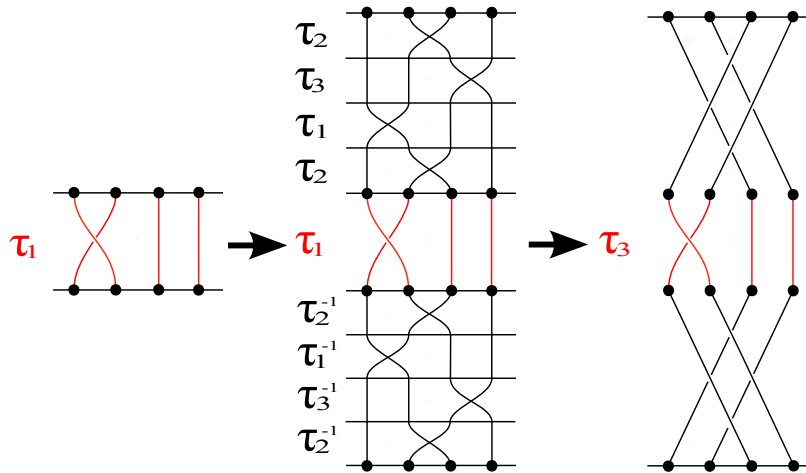


Figure 1.5: This shows if we conjugate τ_1 by another braid, $\tau_2\tau_3\tau_1\tau_2$, we get the same effect as if we just performed τ_3 .

This property is useful as it means all braid group generators are equivalent, they only differ by our labelling convention. The generators then share the same properties, specifically they all have the same eigenvalues and so their trace and determinants are all equal.

Finally if the system is described by a wavefunction, ψ , then representations of the braid group can be obtained by examining the effect of the generators ψ on configurations of the system. One dimensional representations of the braid group will always exist, where the wavefunction picks up a phase factor, $\tau\psi \mapsto e^{i\theta}\psi$, when particles are braided. Here then we see the anyonic nature of the two-dimensional particles emerging directly from representations of their exchanges.

The order in which we apply the braid generators will clearly not affect the outcome, as the phase factors commute with each other. Particles whose exchanges can be described by one-dimensional representations of the braid group are then termed Abelian anyons. However, the presentation of B_n permits higher dimensional, irreducible representations. The matrix representations of the braids in these cases will, in general, not all commute and so the order in which we apply them does affect the outcome. Particles whose exchanges are described by higher dimensional, irreducible representations of B_n are then called non-Abelian anyons [19].

For TQC purposes, information can be stored in the configuration of the anyons, to create qudits. Logic gates can then be implemented on these qudits by manipulating this configuration through braiding of the anyons. Qudits

built from Abelian anyons then will only be able to undergo operations which change their state by some trivial phase factor. To enable us to perform a larger set of logic operations (potentially any desired logic operation) we then require non-Abelian anyons. For our purposes then we will primarily be concerned with non-Abelian representations of the braid group and Abelian representations will be regarded as significantly less useful.

It is interesting to note here, that if we were to move back to a (3+1)-dimensional system then any braid which brings all particles back to their starting position can be untangled, such braids are called *pure* or *coloured* braids. This is not obvious from figures 1.2 - 1.5 above as it is difficult to imagine another dimension in these diagrams, but we will always be able to continuously deform the strands until any pure braid is completely untangled.

Every pure braid is then equivalent to the trivial braid in 3+1 dimensions. The square of any braid is clearly a pure braid so we get an extra group relation of the form:

$$\tau_i^2 = 1 \tag{1.3}$$

But the braid group along with relation (1.3) is actually the presentation the symmetric group, S_n . The symmetric group has also been well studied and most importantly is known to have only representations which correspond to those of bosons and fermions, specifically it has two one-dimensional representations, $\tau_i = \pm 1$, corresponding to bosons and fermions and higher dimensional representations which can all be decomposed into one of the one-dimensional representations by assigning an extra quantum number to each particle [20, 9].

1.4 Fusion Trees

The topological charge of an anyon is specified by the phase factor its wavefunction picks up when braided. In a system with multiple anyons present, multiple species of anyons inevitably emerge. Groups of anyons can move close together and act effectively as a single anyon with a different topological charge, see for example [9, 21]. For any two non-Abelian anyons this new topological charge may take on a range of values, called fusion channels. The fusion channels are

determined by the fusion rules of the particular anyon model, which can be given as a fusion algebra of the form [8, 22]:

$$a \times b = \sum_{c \in T} N_{a,b}^c c \quad (1.4)$$

where: a, b and c are topological charges, $N_{a,b}^c$ is an integer referred to as a fusion coefficient which determines the probability of that fusion outcome and T is the set of allowed topological charges in the anyon model. Notice that the fusion can possibly have multiple outcomes (provided $|T| > 1$), such “multi-channel” fusions will then present a multi-level system which can be utilised as a qudit.

There are many example of such models (see for example ref. [22]), the most well known being the Fibonacci model [23, 24] which we will use as an illustrative example. The Fibonacci model contains two particles species; one of topological charge 1, called the vacuum, and another of charge τ , called the Fibonacci anyon. The fusion rules for the system are then given as:

$$\begin{aligned} 1 \times 1 &= 1 & 1 \times \tau &= \tau \\ \tau \times \tau &= 1 + \tau \end{aligned}$$

These can be interpreted as: combining any anyon with a topologically trivial particle leaves it unaltered, while combining two Fibonacci anyons produces either a single Fibonacci anyon or a vacuum anyon with equal probability.

We can design systems of anyons using these models and examine how the different species of anyons interact with each other in an attempt to describe what is happening in real topological systems. Fusion trees give a useful diagrammatic display of how the anyons in a system are behaving [25].

A fusion tree contains edges, which represent the anyons in the system, and vertices where two edges meet, which represents the fusion of two anyons or the splitting of an anyon into two separate anyons. To draw a fusion tree we start with an edge for each anyon in the system, the edges depict the worldlines of the anyons so we can have braiding or joining of edges at different points in the diagram depending on how the anyons behave at those times. It should be noted that an edge can have multiple labels, if two edges meet at a vertex and

the fusion outcome of the anyons they represent have more than one possibility, then the edge which exists this vertex must bear both possible labels.

The “tree” title stems from a common method of obtaining the overall topological charge of a system whereby we pick one anyon in the system and let it fuse with each of the other anyons one at a time, as if we are zooming out in discrete steps, until we are left with the overall topological charge of the whole system. The resultant structure resemble a trees as seen figure 1.6.

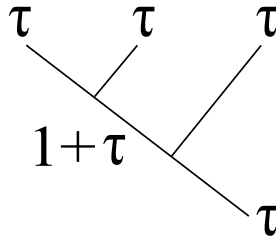


Figure 1.6: Fusion tree for three Fibonacci anyons with a total charge of τ .

Given that certain fusions can have more than one outcome, a given fusion tree can have multiple different possible labellings. The labellings then represent different states the system of anyons can be in. Therefore, we obtain a basis for the system by writing down all possible fusion tree labellings for the collection of anyons.

Notice above we just picked a charge at random to start with, this choice will affect the shape of the resulting fusion tree but the overall topological charge of the anyons shouldn't change. The multiple different fusion trees which can be drawn for any group of anyons will correspond to different basis choices. It can often be useful to change between different bases, if the fusion of a certain two anyons is desired we can move to a basis where these fuse together first before their fusion product fuses with the rest of the anyons in the collection. Such a basis change is achieved using a so-called *F-move* [24], which changes the order in which three particles are fused together by acting with an appropriate transformation, called an *F-matrix*, on the original basis.

In figure 1.7, F is the transformation matrix linking the two bases, it is a function of the charges of the three anyons, a , b and c , the two possible initial fusion channels, x and \tilde{x} , and the total outcome of the fusion, d .

Exchange of the anyons may alter the fusion outcome as it affects the state of the system non-trivially, we then need to account for braiding in the fusion

$$\begin{array}{c} a \\ \diagdown \\ \text{x} \\ \diagup \\ b \end{array} \begin{array}{c} c \\ \diagdown \\ \text{x} \\ \diagup \\ d \end{array} = \left[\mathbf{F}_d^{a,b,c} \right]_{x, \tilde{x}} \begin{array}{c} a \\ \diagdown \\ \text{x} \\ \diagup \\ b \end{array} \begin{array}{c} c \\ \diagdown \\ \text{x} \\ \diagup \\ d \end{array}$$

Figure 1.7: The order the anyons a , b and c are fused in is changed by moving to a basis where b and c fuse before combining with a . Note the resultant charge d remains unchanged by this operation.

tree method. This is done by altering the basis to one in which two anyons are exchanged via application of the R -matrix.

$$\mathbf{R}_{a,b} \begin{array}{c} a \\ \diagdown \\ \text{c} \\ \diagup \\ b \end{array} = \begin{array}{c} b \\ \diagdown \\ \text{c} \\ \diagup \\ a \end{array} = \mathbf{R}_c^{b,a} \begin{array}{c} b \\ \diagdown \\ \text{c} \\ \diagup \\ a \end{array}$$

Figure 1.8: The braiding of anyons a and b is accounted for by moving to a new basis using an R -move.

In figure 1.8, R is the transformation matrix moves to a basis where anyons a and b are in the opposite order, it depends on the two braided anyons, a and b , and their fusion outcome, c .

The form of the F and R -matrices is determined by consistency equations, known as the pentagon and hexagon equations [26, 2], which ensure that certain combinations of F and R -moves will return the system to its original state.

1.5 Conformal Field Theory

As mentioned in section 1.2, systems which contain the anyonic excitations necessary for topological quantum computation are (2+1)-dimensional in nature. However many important elements of these systems, such as the edge (see e.g. ref. [27]), are in fact (1+1)-dimensional.

These (1+1)-dimensional quantum systems can often be described by a two-dimensional, conformally-invariant quantum field theory. Such theories will then be useful in modelling anyon systems and so we will give a brief introduction. The overview here follows the treatment in many conformal

field theory books and reviews such as ref. [28, 29, 30, 31].

For any statistical model we can define a pair correlation function, $\Gamma(i-j)$, which gives a measure of the statistical dependence of an interaction between two sites. This function will naturally depend on the nature of the interaction, but more importantly for us it will also be a function of the distance between the two sites. In general, this pair correlation function will decay exponentially with the distance over which the interaction takes place;

$$\Gamma(i-j) \sim \exp\left(-\frac{|i-j|}{\xi}\right) \quad (1.5)$$

where ξ is a characteristic length and is termed the ‘correlation length’ of the interaction. However, at a quantum critical point the correlation length will diverge, it exceeds the system size and the pair correlation is instead limited by the linear size of the system. The exponential decay in equation (1.5) is replaced by an inverse power decay:

$$\Gamma(i-j) \sim \frac{1}{|i-j|^{d-2+\eta}} \quad (1.6)$$

where d is the dimension of space and η is some exponent characterising interaction taking place. For correlations over distances which are large compared to the lattice spacing, i.e. in the continuum limit, the absence of the correlation length, ξ , indicates that $\Gamma(i-j)$ will be independent of the scale of the system. A (quantum) field theory description of this model would then be invariant under conformal transformations, i.e. angle preserving transformations, as this is known to be true of all such scale-invariant, (1+1)-dimensional quantum field theories [32].

Conformally-invariant quantum field theories, more commonly referred to as *conformal field theories*, are very useful in (1+1)-dimensional systems as they are often completely solvable using only symmetry arguments due to the infinite dimensionality of the conformal symmetry algebra (or Virasoro algebra).

We start with a particular two-dimensional quantum field, $\phi(z, \bar{z})$, written in terms of holomorphic (and antiholomorphic) coordinates, $z = x + iy$. Its behaviour under a conformal transformation is governed by the field’s scaling

dimension, Δ , and its spin, S , which are combined into quantities known as the holomorphic conformal dimension, $h = \frac{1}{2}(\Delta + S)$, and its antiholomorphic counterpart, $\bar{h} = \frac{1}{2}(\Delta - S)$. If such a field also obeys the following conformal transformation of its holomorphic coordinates, as $z \mapsto f(z)$:

$$\phi(z, \bar{z}) \mapsto \left(\frac{\partial f}{\partial z}\right)^{-h} \left(\frac{\partial \bar{f}}{\partial \bar{z}}\right)^{-\bar{h}} \phi(f(z), \bar{f}(\bar{z})) \quad (1.7)$$

then it is called a primary field and its action on the absolute vacuum at $z = 0$ produces an eigenstate, $|h, \bar{h}\rangle$, of the Hamiltonian, with an energy $h + \bar{h}$. The holomorphic and antiholomorphic parts of a conformal field are mostly decoupled from each other, enough that they can be considered in isolation. From here on we will consider only holomorphic operators which act on the holomorphic part of $\phi(z, \bar{z})$ but it should be noted that each of these operators will have an antiholomorphic counterpart which acts on the antiholomorphic part.

The holomorphic energy-momentum tensor of the theory can be expanded in terms of mode operators L_n ; $T(z) = \sum_{n \in \mathbb{Z}} z^{-n-2} L_n$. These modes satisfy a commutator algebra known as the Virasoro algebra, defined by the commutation relations:

$$\begin{aligned} [L_n, L_m] &= (n - m)L_{n+m} + \frac{c}{12}n(n^2 - 1)\delta_{n+m,0} \\ [L_n, \bar{L}_m] &= 0 \end{aligned} \quad (1.8)$$

The operator c is known as the central charge of the conformal field theory. As c commutes with the Virasoro operators, L_n and \bar{L}_n , we can choose a representation of the Virasoro algebra such the c is diagonal. The value of c obtained by acting on the states of some CFT then defines the commutation relations of the Virasoro algebra. We can then obtain a representation of the CFT described by this c value by acting with the Virasoro generators on some initial lowest weight state.

The variation of a state under a conformal transformation is then given by acting on the state with the appropriate generator, L_n . The subspace of the Hilbert space generated by the action of the L_n on the state $|h, \bar{h}\rangle$ is closed under the action of the conformal generators and so forms a representation of

the Virasoro algebra called a Verma module, $V(c, h)$.

The constraint of regularity of $T(z)|0\rangle$ at $z = 0$ indicates that $L_n|0\rangle = 0$ for all $n \geq -1$, and the hermiticity of $T(z)$ results in the relation $L_{-n} = L_n^\dagger$. Together these properties, with relations (1.5), imply that the L_n and \bar{L}_n act as raising ($n \leq -1$) and lowering ($n \geq 1$) operators of the eigenvalues of L_0 and \bar{L}_0 and thus will produce the states of the Verma module by acting in various combinations on the lowest weight state.

The commutation relations between the energy-momentum tensor and the field operator show that $|h, \bar{h}\rangle = \phi(0, 0)|0\rangle$ is this lowest weight state, and so it is often called a primary state. Such a primary state is annihilated by all L_n, \bar{L}_n with $n > 0$, and it produces other states within the same conformal family, called descendant states, $\phi^{(-n)}|0\rangle$, under action of L_{-n}, \bar{L}_{-n} .

The operator $(L_0 + \bar{L}_0)$ is proportional to the Hamiltonian. It has the eigenvalues which are the conformal dimensions of the states in the module, e.g. $(L_0 + \bar{L}_0)|h, \bar{h}\rangle = (h + \bar{h})|h, \bar{h}\rangle$, which can then be interpreted as the energy of the state. Similarly the operator $(L_0 - \bar{L}_0)$ is proportional to the momentum operator.

We can then produce the spectrum of a conformal field theory. For the value of c associated with the particular theory, we obtain a Verma module for each primary field, $\phi_i(z, \bar{z})$, by building a tower of descendant states. This is done through the action of the generators of the Virasoro algebra which behave as ladder operators on the lowest weight states, created by applying the primary fields to the vacuum state.

A Verma module will give an irreducible representation of the Virasoro algebra unless there exists a state, $|\chi\rangle$ (which is not the lowest weight state $|h, \bar{h}\rangle$), for which $L_n|\chi\rangle = 0$ {for $n > 0$ }. Such states are called null states and can be considered to be the primary states of their own Verma (sub)module. A Verma module can then be reduced into irreducible representations of each of its null states.

The Kac determinant [33] can be used to obtain the conformal dimensions, $h_{p,q}$, of any null states within a Verma module, $V(c, h)$. From the Kac determinant we find that all theories with $c < 1$ have positive, real conformal dimensions. It also shows that the central charge, c , and the conformal dimensions of any null states, $h_{p,q}$, can be expressed in terms of a new parameter

$m = \frac{1}{2} \pm \frac{1}{2} \sqrt{\frac{25-c}{1-c}}$ as:

$$c = 1 - \frac{6}{m(m+1)} \quad (1.9)$$

$$h_{p,q} = \frac{[(m+1)p - mq]^2 - 1}{4m(m+1)} \quad (1.10)$$

For $m \geq 2$, $1 \leq p \leq m-1$, $1 \leq q \leq m$, this defines the conformal dimensions for all constituent primary fields of a conformal field theory with a particular central charge, provided $c < 1$. Note this actually gives twice the number of fields for each theory but we find that $h_{p,q} = h_{m-p,m+1-q}$ and the corresponding fields can be identified with each other, i.e. the representations of these fields are isomorphic. Models defined by relations (1.9) and (1.10) are referred to as minimal models and in principle “everything” about these conformal field theories can be fully determined.

Conformal field theory also furnishes us with rules for fusing fields together, which are derived from the operator product expansion (OPE) of the correlators the conformal fields. Taking $\phi_{i,j}$ to be a primary field with conformal dimension $h_{i,j}$, the constraints placed on the operator algebra due to existence of null states in the theory allows us to derive the following fusion rules for primary fields from their OPE:

$$\phi_{a_1,z_1} \times \phi_{a_2,z_2} = \sum_{a_3=A_{int}, A_+=1}^{2m-1-a_1-a_2} \sum_{z_3=Z_{int}, Z_+=1}^{2m+1-z_1-z_2} \phi_{a_3,z_3} \quad (1.11)$$

where $Z_{int} = |z_1 + z_2| + 1$, $A_{int} = |a_1 + a_2| + 1$, $A_+ = (a_1 + a_2 + a_3) \bmod 2$, $z_+ = (z_1 + z_2 + z_3) \bmod 2$ and m is the parameter of the CFT defined by the conformal charge, see equation (1.9).

1.6 Thesis Outline

As stated at the beginning of the introduction, this thesis covers work on three separate projects and a chapter has been dedicated to each of them.

In chapter 2 we give the most general description of a qudit. We then examine what properties a qudit must display to be defined as optimally designed. We force our general qudit to display these properties and then discuss

what restrictions this places on it. Finally we compare current qudit models to this optimally designed, general qudit to see how well they match. We use a similar method to examine multi-qudit gates and look into the issue of information leakage from such systems, using our general qudit approach to search for leakage-free, universal systems.

In chapter 3 we consider a system of anyonic ring-shaped excitations in 3+1 dimensions which can utilize several types of motion in three spatial dimensions to produce quantum computations. We study the possible implementations of qudits in this system and compare the results to those found for general exchange groups in chapter 2. We also study systems in which each ring has an internal vector space associated with it and introduce local representations to define a certain type of action of the exchange group generators on such a system. We discuss the advantages and difficulties of using this ring system for TQC over the current more conventional (2+1)-dimensional implementations.

In chapter 4 we move away from the more abstract tone of the previous two chapters in order to examine the reality of implementing these designs in a physical system. We model Ising type anyons in a fractional quantum Hall fluid and discuss how the anyons composing the qubits in the bulk can interact with the current on the edge of the sample. Using numerical simulations we predict how the interactions will affect the state of the qubits over time and discuss what demands this places on how the qubits should be designed.

Chapter 2

Topological Qubit Design

A natural question to ask when considering the design of a quantum computer is; “What is the optimal way in which to design a qudit?”. As the computer will be built from these qudits, an efficient design would be essential to the overall efficiency of the quantum computer.

There has been many schemes suggested for the implementation of a topological quantum computer, however, they all stem from the same basic premise. We have a collection of qubits which are composed of (quasi-)particles that are topological in nature. Information is encoded in the topology of the qubit and logic gates are implemented on the qubit by altering this topology in some way.

The topological particles we are referring to are 2+1 dimensional anyonic particles, which we discussed in section 1.2, and the information is stored in the arrangement of the anyons within the qubit. We can alter this topological feature by exchanging the anyons and so logic gates are implemented by braiding the anyons around each other. Thus every operation that can be performed on these qubits is an element of the braid group, which was described in section 1.3.

Representations of the braid group then yield the possible operations we can perform with a specific qubit. The goal of this chapter will be to look at various different topological qubit designs and attempt to find representations of the braid group for said qubits which have certain desirable properties.

2.1 Standard TQC Scheme

We start with a collection of anyons, we have some two-dimensional system wherein excitations display anyonic statistics. We will not consider the exact

properties of the anyons, i.e. their topological charge and fusion rules, or the specific nature of the system containing them. This allows us to keep our results as general as possible and we can restrict to specific anyon models later on.

The Hilbert space of the system is just the fusion space of the anyons, states in this space are then labelled by the possible ways in which the anyons in the system can fuse together. This Hilbert space does not have a natural tensor product structure which makes it difficult to fit these states to the standard computation models, based on collections of two-level systems. To solve this, we group anyons together into smaller collections (of usually 3 or 4) which we call qubits. The qubit is defined by restricting the overall fusion charge of the group of anyons to a set value (often the vacuum, 1, which is convenient as the qubit then has trivial topological charge and can be exchanged without effecting the system), this value is conserved under any operations which take place inside the qubit.

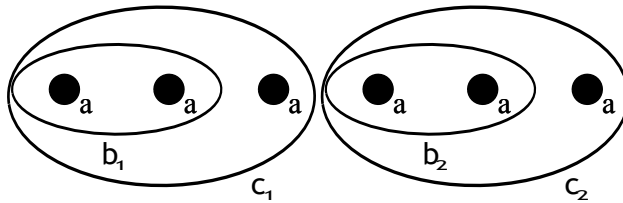


Figure 2.1: A possible qubit space for a system of six anyons. Here a is the anyon charge and the circles, b_i and c_i , represent anyon fusion with their labels denoting the fusion outcomes. c_1 and c_2 are the charges of the qubits, they are fixed, b_1 and b_2 can have multiple values which can be altered by braiding the other anyon around one of the anyons inside the b circle. To define the full qubit space we must also fix the overall charge of all 6 anyons.

The qubit space (or computational space) is composed of the possible ways in which the anyons can be fused together under the consideration that certain groups of anyons are required to fuse to specific values, i.e. the anyons within a qubit must fuse to the topological charge of the qubit.

This computational space does have a natural tensor product structure [1] making it much easier to work with than the full Hilbert space. However, there is a price to pay for using this ‘simpler’ space; the computational space is, in general, smaller than the full Hilbert space of the system. While operations performed within a qubit do not alter its charge, multi-qubit operations, i.e. braiding anyons from different qubits around each other, may change

the topological charge of one or all of the qubits involved. This will result in some of the information, “leaking” out of the computational space into so-called “non-computational” states.

Information which is in a non-computational space cannot be accessed by single qubit operations but multi-qubit operations may exist which can access the information and couple it back into the computational space. This is known as leakage error but it is not an error in a conventional sense as the information is not lost but has been moved to the states in the Hilbert space which are not accessible with our chosen qubit implementation.

If we perform calculations using only braiding operations contained within a single qubit, then there will be no leakage errors as these operations do not alter the overall topological charge of the qubit. However, if we braid anyons from two different qubits around each other, it is possible to alter the topological charge of the qubits and risk losing information to states where the qubits have a different charge to the one used to define the qubit space. These are obviously non-computational states and so we can get leakage errors.

There exists TQC models for which leakage errors appear to be avoidable, see e.g. ref. [34], however these necessarily have trivial one qubit operations and are not universal. In more standard anyon models, leakage errors are unavoidable [7, 17, 23] and we can only work to reduce the amount of information that is lost.

2.2 The Optimal Qubit

We now need to ask ourselves what properties we desire an “optimal” qubit to have. There are three criteria which an optimal qubit should fulfil, (see e.g. ref. [8, 7, 23, 35]):

1. *Universality*: It should be possible to apply any logic operation we wish to the qubit.
2. *Robust against errors*: Logic operations should be implemented on the qubit with few or no errors.
3. *Efficiency*: Logic gates should be implemented quicker than is possible for other qubit designs.

From section 1.3 we know that any operation that can be performed on a qubit must be matrix representing an element of the braid group. As logic gates are unitary operations, a unitary representation of the braid group will then contain all logic operations which can possibly be applied to the qubit. If the representation of the braid group of the anyons within a qubit is non-Abelian, the qubit can possibly be universal (though this is not sufficient to guarantee universality). This is not true for an Abelian representation of the anyons, which has generators which all commute and so can be simultaneously diagonalised. The representation can then be reduced to 1-dimensional representations which are non-universal.

To maintain robustness we must ensure that information is not able to *leak* from the system. The fundamental principles of TQC ensure that it is robust against decoherence errors but it is still possible to lose information when we perform operations which move this information from the computational space to non-computational states.

Lastly if we assume that it is experimentally easy to manoeuvre anyons, then we would expect qubits containing greater numbers of anyons to be more efficient (this is not true of current experiments but we are anticipating future advancements of the field). The number of generators in the braid group is directly related to the number of anyons in the qubit (as there is a generator for every neighbouring pair of anyons) thus with more anyons, we have a greater number of generating matrices in the representation of the group. This gives us more distinct options to choose from when performing a braid and so we may be able to reach a desired gate in fewer operations than if we had fewer anyons, in other words we may be able to produce our desired logic gate quicker.

To summarise then, an optimal qubit should be composed of as many anyons as possible, with a non-Abelian representation of their braid group, where none of the operations leak information to non-computational states.

As we will see in the next section, the group relations, equations (1.1) and (1.2), put an upper limit on the number of generators the braid group can contain before all 2-dimensional representations must be Abelian. The question we want to answer is then; *What is the maximum number of anyons a qubit can contain while the braid group representation remains non-Abelian?*

2.2.1 Maximum Number of Anyons

We now want to find this maximal anyon number for qubits. Note that we are exclusively dealing with qubits here, i.e. 2-dimensional representations of the braid group, higher dimensional representations will be considered in a later section. First we note that all logic operations are unitary and a qubit is by definition a 2-dimensional system, therefore we can accurately represent all possible logic operations on the qubit through a 2-dimensional, unitary representation of the braid group.

Due to the conjugacy of the braid generators, they must all have the same eigenvalues. We choose a basis for our representation such that the first generator, τ_1 , is a diagonal matrix. If the two eigenvalues of the generators are equal, τ_1 will be some multiple of the identity, $\tau_1 = \lambda^{(1)}\mathbb{1}_2$ and is unaffected by any basis transformation. We can then change to a basis where some other generator, say τ_2 , is diagonal. But again τ_2 has 2 equal eigenvalues so it too is some multiple of the identity, $\tau_2 = \lambda^{(2)}\mathbb{1}_2$. This process can obviously be repeated to show that, if the eigenvalues of the generators are equivalent then all generators in the group have a trivial representation.

We look then, only at the case where the eigenvalues are distinct. It is important to point out here, that if a diagonal matrix has all distinct eigenvalues then any other matrix which commutes with it must itself be diagonal. This fact will come into use extensively throughout this chapter.

Again we choose a basis where τ_1 is diagonal but with distinct eigenvalues. We must now use the braid group relations to find the form of the other generators in this representation, we repeat these relations here for convenience:

$$\begin{aligned}\tau_i\tau_j &= \tau_j\tau_i \quad \{\text{for } |i-j| \geq 2\} \\ \tau_i\tau_{i+1}\tau_i &= \tau_{i+1}\tau_i\tau_{i+1}\end{aligned}$$

If all of the other generators must also be represented by diagonal matrices, we know the braid group representation is Abelian.

A 2-anyon qubit has only one possible exchange, τ_1 , and so all generators have a diagonal representation. For the braid group of a 3-anyon qubit there are two generators, τ_1 and τ_2 , and the group relations place only one restriction

on them, namely that they must obey equation (1.2), the Yang-Baxter relation. This allows for the representation of the braid group to be non-Abelian. For 4-anyon qubits we have one extra generator, τ_3 . Equation (1.1) requires this to commute with τ_1 so it can be simultaneously diagonalised. So τ_1 and τ_3 are diagonal matrices but τ_2 can still be non-diagonal and so the representation of B_4 can be non-Abelian.

However, it turns out that four is the maximum number of anyons for which this can occur. If we consider a 5-anyon qubit then we have one more generator, τ_4 . Again we can simultaneously diagonalise τ_1 and τ_3 . The extra generator, τ_4 , is physically separated from, and so must commute with, τ_1 , however, it is not physically separated from τ_3 . The basis transformation used to simultaneously diagonalise τ_1 and τ_3 should then not also diagonalise τ_4 . But τ_1 has all distinct eigenvalues therefore, in order for τ_4 to commute with it, it too must be diagonal. Now τ_2 must commute with τ_4 , which is a diagonal matrix with all distinct eigenvalues, and so τ_2 must also be diagonal. Therefore for $N = 5$, all four generators must have a diagonal representation, thus the representation of B_5 is Abelian.

It is relatively easy to see that this will be the case for any number of anyons higher than 4. All odd numbered generators form a commuting set and so they can all be diagonalised simultaneously. Any even numbered generator which is physically separated from τ_1 , must also be diagonal in order for the two to commute (as τ_1 has distinct eigenvalues). The only remaining generator is τ_2 , if a generator exists which is physically separated from both τ_2 and τ_1 , then τ_2 must also be diagonal. This will be true for $N > 4$ and we are left with an Abelian representation for these cases.

The only cases in which this does not occur is when there is three or four anyons in the braid group, these are then the only cases for which there can potentially be non-Abelian representations. And so we have our final result; three or four anyons represent the optimal number from which to compose a qubit. We still do not know if the braid groups for these qubits are universal, or even non-Abelian, but we can say that all other options are definitely not universal.

It is important to highlight that this argument is only true for two-dimensional representations of the braid group. The result relies heavily on the fact that

the eigenvalues of two dimensional matrices can only be either all similar or all distinct. A matrix which commutes with a diagonal matrix with all distinct eigenvalues must itself be diagonal, whereas if the eigenvalues are similar the diagonal matrix is a multiple of the identity and any matrix will commute with it.

In higher dimensions, our above results will be repeated, i.e. if all eigenvalues are similar, any representations are trivial and if all eigenvalues are distinct, only representations of B_3 and B_4 can be non-Abelian. However in higher than 2 dimensions there is more available options, we can choose different groupings of the eigenvalues to be similar and distinct, this relaxes some of the restrictions on commuting matrices. We will examine this in greater detail in section 2.3.

2.2.2 Universality

We now need to examine whether the optimal anyon numbers found in the previous section can have a universal representation of their braid groups. In this section it will be necessary to explicitly refer to which representation we are using, therefore we will first describe our representation, η , of the braid group.

As stated in the previous section we start with a 2-dimensional, unitary representation of the braid group: $\eta' : B_n \rightarrow U(2)$, however we can simplify this a bit further by demanding that the representation is also special, i.e. $\eta : B_n \rightarrow SU(2)$.

This is easy to justify as the determinant of a representation is itself a representation and a valid representation is given by dividing a representation by some one-dimensional representation. All generators in the braid group are conjugate to each other. This means they all have the same eigenvalues and thus determinant, so we can divide our representation by the square root of this determinant so that all generators now have a determinant of 1 and the representation is special: $\eta = \frac{\eta'}{\sqrt{\det(\eta')}}$. We can recover all $U(d)$ representations by simply multiplying these $SU(d)$ representations by one-dimensional unitary representations.

As before we can choose the basis of the representation so that $\eta(\tau_1)$ is

diagonal. $\eta(\tau_2)$ is not, in principal, diagonal but we have some freedom left in our basis choice which we can use to ensure the off-diagonal elements of $\eta(\tau_2)$ are real. Using the standard general form of $SU(2)$ matrices and the Yang-Baxter relation (equation (1.2)) gives the following matrix representations:

$$\eta(\tau_1) = \begin{pmatrix} a & \\ & \bar{a} \end{pmatrix} \quad \eta(\tau_2) = \begin{pmatrix} \frac{1}{a-a^3} & b \\ -b & \frac{1}{\bar{a}-\bar{a}^3} \end{pmatrix} \quad (2.1)$$

Where $a = e^{i\phi}$, for some phase ϕ and $|a|^2 + |b|^2 = 1$. We will assume that the eigenvalues of the generators, a and \bar{a} , are distinct, as allowing them to be equal immediately renders the representation Abelian, as stated in the previous section. The choice of b to be real gives a restriction on the values of a . From the determinant of τ_2 , we have $b^2 = 1 - \frac{1}{2-\bar{a}^2-a^2} \geq 0$, this gives: $\frac{1}{2-\bar{a}^2-a^2} \leq 1$ which in turns gives: $-\pi/6 \geq \phi \geq \pi/6$. This fully defines all possible representations of B_3 which are non-Abelian.

In B_4 we have an extra generator, τ_3 , and we will assume τ_1 and τ_2 have the same form as above. τ_3 must commute with τ_1 and so it is also diagonal. Therefore, as the eigenvalues of all generators must be the same, there are only two possibilities: $\tau_3 = \tau_1$ or $\tau_3 = \bar{\tau}_1$. In the first case we get no new restrictions on ϕ and so $-\pi/6 \geq \phi \geq \pi/6$ as in the B_3 case. In the second case the Yang-Baxter relation between τ_2 and τ_3 does impose some extra restrictions on ϕ and we find that a must be a primitive 8^{th} root of unity, i.e. $a = \pm e^{\pm i\pi/4}$. Anyons with such exchange statistics are known as Ising anyons and will be discussed in much greater detail in chapter 4, for now we will just mention that these anyons are known to be non-universal [36].

Vafa's theorem [37] states that any representation of the braid group arising from an anyon model (or CFT) with a finite number of topological charges must have eigenvalues of its exchanges which are roots of unity at some finite order. Therefore, not all values of ϕ are permitted, instead only those for which a is a root of unity are allowed.

It will prove useful to identify the well-studied, Jones representation, ρ_r , for B_3 within the full set of representations we have given here. Ref. [38] gives

the following explicit form for the braid generators:

$$\rho_r(\tau_1) = \begin{pmatrix} q & \\ & -1 \end{pmatrix} \quad \rho_r(\tau_2) = \begin{pmatrix} -\frac{1}{q+1} & \sqrt{[3]_q} \\ -\sqrt{[3]_q} & \frac{q^2}{q+1} \end{pmatrix} \quad (2.2)$$

where: $[x]_q = \frac{q^{\frac{x}{2}} - q^{-\frac{x}{2}}}{q^{\frac{1}{2}} - q^{-\frac{1}{2}}}$ and $q = e^{i\frac{2\pi}{r}}$, with $r \in \mathbb{N}, r > 3$.

We can see that our representation, η , will exactly match the Jones representation if we multiply η by a factor of $-a$, then perform a coordinate transformation such that the off-diagonal terms pick up a factor of i . Then the two representations will be exactly equal with $q = -a^2$. We then have; $q = -a^2 = -e^{2i\phi} = e^{i(2\phi-\pi)}$, but $-\pi/6 \geq \phi \geq \pi/6$ so, allowing q to take the values $q = e^{i\psi}$, for $-2\pi/3 \geq \psi \geq 2\pi/3$, the Jones representation describes all possible representations of B_3 .

Freedman *et. al* [38] provided universality results for the Jones representation. They found that the images of the representations ρ_r are dense in an $SU(2)$ subgroup of $U(2)$ when $r \geq 5$ and $r \neq 6, 10$. More recent universality results by Kuperberg [39] cover the other roots of unity and even arbitrary eigenvalues of Jones representations. He states that the images of the representations of B_3 and B_4 are all dense in $SU(2)$ unless $q = e^{i\theta}$ with $|\theta| = \pi - 2\pi/t$, where θ is some angle and $t \in \mathbb{Z}, t \geq 3$ or q is a root of unity of order 10. Note that $t = 3, 4, 6$ are the only cases where $\pi - 2\pi/t$ is of the $2\pi/r$ form examined in ref. [38] (with $r = 6, 4, 3$ respectively). Thus the cases for which the universality results do not hold, where ϕ is a primitive root of unity, are exactly those exceptions which were found by Freedman *et al*.

We can conclude then that η will give a representation which is dense in $SU(2)$ for all possible values of a , except $a = e^{i\psi}$ where $\psi = \pm(\pi - \pi/2t)$ for $t \in \mathbb{Z}, t \geq 3$ or a is a root of unity of order 10. Therefore, our general representation, η , contains possible anyon models from which we can design qubits which are universal.

2.3 Qudits

In section 2.2 we analysed under what conditions qubits composed of three or four anyons are universal. If we stick to one qubit operations, we know that

there will be no leakage errors in the system. The only optimal property which has not been addressed then is efficiency.

The qubits discussed in the previous section are only able to produce two or three generating operations so, while the group is dense in $SU(2)$, it may take a lengthy and complicated braid in order to achieve a desired logic operation. This is an issue in terms of computing time and also in terms of the demand it puts on our ability to control anyons for extended periods of time. We would like to find a way to increase the number of anyons that we can braid without their braid group becoming Abelian

One idea to increase the maximal number of anyons is to move from a 2-dimensional *qubit* to a d -dimensional *qudit*. As mentioned in section 2.2, the advantage here is that in a dimension greater than 2 we can have a multiplicity of the eigenvalues of the generators which is not 1 or d . So it should be possible to fit more anyons into a qudit, without the representation becoming Abelian, if we choose the eigenvalues carefully enough to ensure that a generator commuting with a diagonal matrix does not necessarily have to be diagonal itself.

Given a qudit of dimension, d , it would then be useful to be able to say what is the maximum number of anyons such a qudit can contain while retaining its potential for universality. If we can relate the maximum number, N , of anyons the representation can take before becoming Abelian to its dimension, d , we will be able to easily identify how to optimally design a general qudit so that it could potentially be universal.

2.3.1 Optimal Qutrit

It is useful to first examine a specific example to introduce some of the concepts we will need later on, we will look at the case of $d = 3$ or a *qutrit*.

As was found in the qubit case, if the representation has 3 different eigenvalues then we will only have non-Abelian representations for 3 and 4-anyon qutrits and if the representation has only one eigenvalue then it will be Abelian for any number of anyons. We should then look at the new case which can't exist in two dimensions, i.e. where one of the eigenvalues has a multiplicity of 2. We construct a three-dimensional representation, ρ , of the exchange group

on n generators, each of which have two eigenvalues λ and μ , where λ occurs twice in the matrix representation of each generator.

We can choose the basis of the representation such that all odd numbered generators are simultaneously diagonalised, this satisfies equation (1.1). If two odd numbered generators have the exact same matrix representation, then any generator which commutes with one must also commute with the other. If $N \geq 5$ there will always be at least one even numbered generator which is spatially separated from one of these odd generators but not the other, but if both odd generators are equal this even generator must commute with its neighbouring odd generator.

As the braid generators are all conjugate to each other, the product of two neighbouring generators can be transformed into the product of any other neighbouring pair through conjugation by an appropriate braid. Thus if a neighbouring pair of generators commutes, all such pairs will commute and the representation is Abelian. If two odd numbered generators are equal then this forces the representation to become Abelian (in fact this is true for any two spatially separated generators).

As the odd generators are all diagonal matrices, they can only differ by the arrangement of the eigenvalues along their diagonal. There are only three distinct arrangements of the eigenvalues, λ and μ , within a diagonal matrix, namely $\{\lambda, \lambda, \mu\}$, $\{\mu, \lambda, \lambda\}$ or $\{\lambda, \mu, \lambda\}$, thus there can be at most three odd numbered generators and so six generators in total; $\tau_1 \rightarrow \tau_6$

A given arrangement of the eigenvalues along the diagonal of a τ_{odd} will partition the basis vectors on which the representation acts. Specifically it groups vectors together into eigenspaces which are acted on by similar eigenvalues of τ_{odd} . Any matrix which commutes with this τ_{odd} must preserve this partitioning.

The form of the even numbered generators, τ_2 , τ_4 and τ_6 , is then restricted as they must commute with all spatially separated odd numbered generators and hence must preserve the eigenspaces created by each partitioning of the basis vectors by these τ_{odd} . τ_2 and τ_4 will preserve the same eigenspaces as τ_5 and τ_1 respectively, but τ_6 will have the most restricted form as it commutes with both τ_1 and τ_3 and so must preserve the eigenspaces of both of these odd numbered generators (τ_1 and τ_3 must have a different ordering of the

eigenvalues so we know they will group the basis vectors differently).

We denote our basis vectors β_1 , β_2 and β_3 and we can choose an ordering such that $\{\beta_1, \beta_2\}$ is the 2-dimensional eigenspace preserved by τ_1 , $\{\beta_2, \beta_3\}$ is the eigenspace preserved by τ_3 and $\{\beta_1, \beta_3\}$ is the eigenspace preserved by τ_5 .

If we look at τ_6 , we see that it must preserve the 2-dimensional eigenspace formed by β_1 and β_2 and also that formed by β_2 and β_3 , it can only preserve both spaces simultaneously if it does not map any of the basis vectors into any of the other basis vectors, i.e. it must be diagonal. As a result τ_6 will commute with τ_5 and the representation of B_7 becomes Abelian.

We should then eliminate τ_6 from our system by reducing the number of particles to 6. Now there is no even generator which commutes with two odd generators and so no generator is required to preserve two 2-dimensional eigenspaces simultaneously. τ_2 and τ_4 need only preserve one 2-dimensional eigenspace each, this is still possible if they are both non-diagonal provided they have the following form:

$$\rho(\tau_2) = \begin{pmatrix} M_{11}^{(1)} & M_{12}^{(1)} & 0 \\ M_{21}^{(1)} & M_{22}^{(1)} & 0 \\ 0 & 0 & \mu \end{pmatrix} \quad \rho(\tau_4) = \begin{pmatrix} \mu & 0 & 0 \\ 0 & M_{11}^{(2)} & M_{12}^{(2)} \\ 0 & M_{21}^{(2)} & M_{22}^{(2)} \end{pmatrix}$$

where M^1 and M^2 are unitary, 2×2 matrices and μ is the eigenvalue of multiplicity 1. However, we must take into account that these two generators must also commute with each other. But the two matrices, $\rho(\tau_2)$ and $\rho(\tau_4)$, will only preserve the same eigenspaces if they are both diagonal. Commutation of the even numbered generators then causes B_6 to have an Abelian representation.

Moving to $N = 5$ finally solves the problem, τ_5 is eliminated and so τ_2 must only commute with τ_4 . Choosing τ_4 to have the form of $\rho(\tau_4)$ listed above, we are free to choose the same form for τ_2 , thereby allowing the two even numbered generators to preserve the same eigenspaces while remaining non-diagonal. Note while τ_2 and τ_4 have the same form, the matrices should not be equal, for the same reason we require this of the odd numbered generators.

Thus we get a 3-dimensional, non-Abelian representation for B_5 . For the group of possible logical operations on a qutrit to have a non-Abelian representation (and so present a possibility for universality), the qutrit should be

composed of a maximum of 5 anyons, thus we can have one more anyon in qutrits over qubits.

Performing this same argument for even higher dimensional cases is more difficult, as we can choose the multiplicities of the eigenvalues such that the eigenspaces which must be conserved split the basis vectors into multiple groups which contain more than one vector. This makes it very difficult to determine the nature of the restrictions that come from the commutation of even numbered generators.

2.3.2 General Anyon Number Limits

We want to generalise this results of qubits and qutrits to arbitrary dimensional qudits. It will also be useful to further generalise by not restricting ourselves to the specific structure of the braid group. Instead we consider only properties common to all exchange groups, our result will then hold for qudits composed from anyonic excitations other than the point-like two dimensional particles which we have considered so far. For example, the motion group for ring-shaped excitations in 3 dimensions, defined by Dahm [40, 41], which we will look at in detail in chapter 3. Specifically, we will require only the following properties of exchange group representations:

1. Generators that do not involve the same object (i.e. particles and strands) commute.
2. The group is represented unitarily.
3. The generators in our favoured set are conjugate to each other and any adjacent pair of generators is conjugate to any other adjacent pair.

The first property here, like the first braid group relation, is connected with the basic physical principle that spatially separated operations commute. The second property comes from the unitarity of time evolution. Both of these properties are therefore natural assumptions to make when dealing with any exchange group.

The third property, the availability of a set of conjugate generators, is more special. However, whenever all generators of a group perform the same action, just on different objects, then the only difference between two distinct

operations is the ordering of the objects they are acting on. One would expect in this case that the generators would all be conjugate to each other. If, on the other hand, there were different types of generators (such as exchanges of distinguishable types of particles) then this property will no longer hold (we will consider an example of this in chapter 3). The inclusion of property 3 allows us to use the argument introduced in the previous section that, through conjugation, if any neighbouring generators commute the representation must be Abelian.

We now define various versions of the 'maximal number of anyons':

- $N(d)$ is the largest n for which B_n has a non-Abelian representation of dimension d .
- $N(d, p)$ is the largest n for which B_n has a non-Abelian representation of dimension d , such that the elementary exchanges have p distinct eigenvalues.
- $N(d, \bar{m})$ is the largest n for which B_n has a non-Abelian, d -dimensional representation such that the exchanges have p distinct eigenvalues with multiplicities m_1, \dots, m_p given by the partition \bar{m} of d . For example if $\bar{m} = (2, 2, 1)$, then $d = 5$ and the representation is required to have three distinct eigenvalues, two of them with multiplicity 2 and one with multiplicity 1.
- $N(d, \bar{m}, \bar{q})$ is the largest n for which there is a non-Abelian, d -dimensional representation of B_n such that the exchanges have p eigenvalues, $\bar{\lambda} = (\lambda_1, \dots, \lambda_p)$, with multiplicities $\bar{m} = (m_1, \dots, m_p)$. q_i is the number of distinct eigenvalues with a multiplicity i and so $\bar{q} = (q_1, \dots, q_d)$ is a list of the number of λ with each eigenvalue multiplicity between 1 and d . For example if $\bar{q} = (2, 1, 0, 0)$ then $d = 4$ and there are 3 eigenvalues, 2 of which have multiplicity 1, 1 with multiplicity 2 and none with any higher multiplicities (\bar{q} will often be truncated to the highest non-zero multiplicity, for instance, $\bar{q} = (2, 1)$ in the previous example).

Our results so far for qubits and qutrits can be summarised using the above definitions as:

$$\begin{aligned}
N(2) &= N(2, 2) = 4 \\
N(3) &= N(3, 2) = N(3, (2, 1)) = 5 \\
N(3, 3) &= 4 \\
N(d, d) &= 4
\end{aligned}$$

We would like to obtain some relations which will allow us to calculate these maximal number of anyon figure for a general system. We will see that, while exact relations are difficult to produce without knowing certain specific details about the system, we will be able to provide some useful general limits.

Let us consider a d dimensional representation, η , of B_N . The representation matrices of all generators in B_N have the same eigenvalues, $(\lambda_1, \dots, \lambda_d)$, as they are all conjugate to each other.

As usual we choose a basis in which the representation matrices of all odd numbered generators are simultaneously diagonal. We have already shown, with arguments that relied only on properties (1) - (3), that representations of B_3 , B_4 and B_5 can be non-Abelian, thus these arguments will apply to the general exchange groups we are now considering. We will then concentrate on groups with $N \geq 5$.

Odd Numbered Generators

Property (3) guarantees that if any neighbouring pair of generators commute the representation will be Abelian, therefore no two of the diagonal matrices, $\eta(\tau_{odd})$, can be equal. Hence we get our first limit on how large N can be; a d -dimensional representation of B_N must yield a different arrangement of the eigenvalues in every one of the representation matrices of the odd generators. Therefore the maximum number of odd generators we can have is the number of possible ways in which we can arrange the eigenvalues of group.

The more distinct eigenvalues we have the larger this number will be thus if all eigenvalues have a multiplicity of 1 we get that the number of arrangements is $d!$ and $N(d) \leq 2d!$. However, if there is multiple occurrences of an eigenvalue,

then we must take into account that simply permuting these occurrences will not produce a distinct arrangement. Therefore if an eigenvalue, λ_i , has a multiplicity m_i then:

$$N(d, \bar{m}) \leq 2d! \prod_i \frac{1}{m_i!} \quad (2.3)$$

Finally we also need to consider that a τ_{even} does not see the value of the eigenvalues in a τ_{odd} when it commutes, it is simply the pattern of like and unlike eigenvalues in the τ_{odd} which allow it to commute with the τ_{even} . This means that if we have two eigenvalues, λ_k and λ_l , which have the same multiplicity, $m_k = m_l$, then we can swap the two eigenvalues, $\lambda_k \leftrightarrow \lambda_l$, to produce a new arrangement. However any τ_{even} which commutes with a τ_{odd} with the first arrangement of eigenvalues will also commute with the second. So when calculating the number of distinct arrangements which the odd generators can take we must exclude any which can be obtained by swapping eigenvalues with equal multiplicities in another arrangement, we then need to introduce \bar{q} as defined above:

$$N(d, \bar{m}, \bar{q}) \leq 2d! \prod_{i,k} \frac{1}{m_i! q_k!} \quad (2.4)$$

Note to obtain this result we have assumed that there is more than one distinct eigenvalue, i.e. $m_i < d$, otherwise the representation will be trivial and also that there is at least one eigenvalues with $m_i > 1$ otherwise $N \leq 5$ as argued in section 2.2.

We saw in the qutrit example that the actual upper limit on N was smaller than the one given by equation (2.4) and this will clearly be the case for any dimension larger than 2. The reason for this is that equation (2.4) only takes into account the restriction imposed by odd numbered generators being required to commute while remaining distinct from each other. But, as we have just seen with qutrits, there is a host of other factors which also contribute restrictions to the representation of the generators.

Even Numbered Generators

Next we need to examine the fact that each even numbered generator, τ_{even} , must commute with all odd numbered generators to which it is not adjacent, by property (1).

Firstly we should note that if a matrix must commute with two $\eta(\tau_{odd})$'s which group a certain subset of basis vectors into different eigenspaces, then this matrix preserves both groupings by only mapping the subset into basis vectors which both $\eta(\tau_{odd})$'s group with the subset. That is, if x , α , β and γ are all mutually exclusive subsets of the basis vectors, and τ_i and τ_j are odd numbered generators where $\eta(\tau_i)$ groups x with α and γ and $\eta(\tau_j)$ groups x with β and γ , then an even numbered matrix, $\eta(\tau_k)$, which commutes with both $\eta(\tau_i)$ and $\eta(\tau_j)$, must not map elements of x into any elements of α or β , but can map elements of x into elements of γ .

We know from the previous section that each $\eta(\tau_{odd})$ is a diagonal matrix with a different arrangement of the eigenvalues, $\{\lambda_i\}$. A given $\eta(\tau_{even})$ will then have its form restricted by the $\eta(\tau_{odd})$ it must commute with. We will assume there is an odd number of generators in total so that $N_{odd} = \frac{N+1}{2}$ and each $\eta(\tau_{even})$ must preserve the eigenspaces of all $\eta(\tau_{odd})$ except the two it is adjacent to. This is the most restrictive case, if there is an even number of generators there will be one $\eta(\tau_{even})$ which has only a single neighbouring $\eta(\tau_{odd})$ and so there is more freedom in its form.

Take some even numbered generator, τ_z , which is physically separated from, and so commutes with, one odd numbered generator, τ_a . Our representation, η , acts on a vector space, V , with elements, v_i . $\eta(\tau_a)$ will group these vectors into eigenspaces which $\eta(\tau_z)$ must preserve. The (i, j) element of $\eta(\tau_a)$ maps v_i into v_j , if these are in different eigenspaces (i.e. if the (i, i) and (j, j) elements of $\eta(\tau_a)$ are dissimilar) then this element of $\eta(\tau_z)$ must be zero. Thus $\eta(\tau_z)$ takes a form where entries which correspond to dissimilar eigenvalues in τ_a are zero.

For two dissimilar eigenvalues, λ_i and λ_j , which act on eigenspaces, e_i and e_j respectively, through $\eta(\tau_a)$, each vector in e_i cannot be mapped into the m_j vectors in e_j by $\eta(\tau_z)$. Thus the number of zero entries in $\eta(\tau_z)$ will then be

given by:

$$\sum_{i,j \neq i} m_i m_j = \sum_i m_i (d - m_i) = d^2 - \sum_i m_i^2 \quad (2.5)$$

Now assume that τ_z is physically separated from another odd numbered generator, τ_b . As each $\eta(\tau_{odd})$ must have a different arrangement of the eigenvalues we know that $\eta(\tau_b)$ will treat at least one basis vector as part of a different eigenspace to how $\eta(\tau_a)$ treats it. This means that more entries in $\eta(\tau_z)$ must be zero, the exact number of new zeroes corresponds to the multiplicity of the eigenvalues that have different positions between $\eta(\tau_a)$ and $\eta(\tau_b)$ but it must be at least 2 (this case arising from the exchange of an eigenvalue with $m = 1$ and another with $m = 2$).

Continuing this procedure we see that $\eta(\tau_a)$ will contain at least 2 extra zero entries for each other τ_{odd} it is spatially separated from. Thus $\eta(\tau_a)$ contains Q zero entries, where we define:

$$Q \geq d^2 - \sum_i m_i^2 + 2[N_{odd} - 3] \quad (2.6)$$

This accounts for $\sum_{i \neq j} m_i m_j$ zeros from commutation with the ‘‘initial’’ τ_{odd} and 2 extra zero from every other τ_{odd} except the two that neighbour τ_a . If Q is equal to the total number of off diagonal entries in a d -dimensional matrix then $\eta(\tau_z)$ must be diagonal, so for a non-Abelian exchange group we must have:

$$\begin{aligned} d^2 - \sum_i m_i^2 + 2[N_{odd} - 3] &\leq d^2 - d - 2 \\ \Rightarrow N(d, \bar{m}, \bar{q}) &\leq \sum_i m_i^2 - d + 4 \end{aligned} \quad (2.7)$$

In order to obtain the largest N we need to maximize the $\sum_{i \neq j} m_i m_j$ term. This will be largest when we have fewer distinct eigenvalues, with one eigenvalue having a much larger multiplicity than the others. Specifically this occurs if we reduce the number of eigenvalues to 2 with: $m_1 = d - 1$, $m_2 = 1$ (as we must always have more than one eigenvalue). For these values we get $N(d, (d - 1, 1), 0) = d^2 - 3d + 6$.

However our relation for Q only shows its minimum value, its derivation

relies on the assumption that each τ_{odd} (except the “initial” τ_{odd}) which τ_z commutes with forces only 2 extra entries in $\eta(\tau_z)$ to be zero. In general the number of extra zeros will depend on the extent of the changes in the arrangements of the eigenvalues of the τ_{odd} and the multiplicity of those eigenvalues that are exchanged. For the case with $m_1 = d - 1$, $m_2 = 1$, each of the $\eta(\tau_{odd})$'s differ by the location of λ_2 . For $\eta(\tau_z)$ to commute with a $\eta(\tau_{odd})$, where λ_2 is entry (j, j) , then all off diagonal elements of row j and column j in $\eta(\tau_z)$ must be zero. Therefore, each τ_{odd} forces $(2d - 2)$ elements in $\eta(\tau_z)$ to be zero, this gives a corrected result of; $N(d, (d - 1, 1), (1, 0, 0, \dots, 1, 0)) = d + 4$, which is lower than our previous result, assuming $d \geq 3$.

It is difficult therefore, to say exactly what partitioning of the eigenvalues will maximize N . Eigenvalues with large multiplicities allow for many distinct arrangements of the eigenvalues which still preserve a large eigenspace, thus an $\eta(\tau_{even})$ can commute with many $\eta(\tau_{odd})$ while maintaining a non-diagonal form in this eigenspace. However, eigenvalues with smaller multiplicities produce a greater number of smaller eigenspaces, thus each $\eta(\tau_{odd})$ a given $\eta(\tau_{even})$ commutes with requires less of its elements to be zero.

The two formulae we have found so far, equations (2.4) and (2.7), give two separate bounds for the number of odd generators. However neither limit can be exceeded and so the true limit will be given by the minimum of the two results. We must ensure that the number of odd generators does not exceed the number of eigenvalue arrangements but also that any $N_{odd} - 2$ of these arrangements preserve at least one eigenspace which is 2-dimensional or higher.

$$N(d, \bar{m}, q) \leq \min \left(\left[2d! \prod_i \frac{1}{m_i! q!} \right], \left[\sum_i m_i^2 - d + 4 \right] \right) \quad (2.8)$$

The number and multiplicities of the eigenvalues will determine which of the two is in fact the minimum.

The limit on N given by equation (2.8) will allow for all $\eta(\tau_{even})$ to have a non-diagonal form. However we must also consider that the τ_{even} are themselves physically separated, thus they must commute with each other. But, similar to the $\eta(\tau_{odd})$, no two of the $\eta(\tau_{even})$ can be equal, nor can they preserve all the same eigenspaces. The restrictions this places on the number of possible

non-diagonal $\eta(\tau_{even})$ will again depend on the number and multiplicity of the eigenvalues but it is difficult to obtain an explicit relation.

Clearly for two non-diagonal, even-numbered generators, $\eta(\tau_z)$ and $\eta(\tau_y)$, if a non-diagonal submatrix of $\eta(\tau_z)$ corresponds to a similar or trivial submatrix in $\eta(\tau_y)$ there is no effect on either submatrix. But these submatrices then preserve the same grouping of the basis vectors on which they act. $\eta(\tau_z)$ and $\eta(\tau_y)$ then must differ in their action on some other eigenspace.

If the non-diagonal submatrix of $\eta(\tau_z)$ corresponds to a diagonal submatrix of distinct eigenvalues in $\eta(\tau_y)$ then this forces the submatrix of $\eta(\tau_z)$ to also be diagonal, restricting its form quite severely. However, $\eta(\tau_y)$ and $\eta(\tau_z)$ can treat the same eigenspace differently without one of them necessarily acting on it with a diagonal submatrix, in this case the restrictions enforced by commutation are not so obvious.

As $\eta(\tau_z)$ and $\eta(\tau_y)$ must also commute with all other even generators in the system. Each $\eta(\tau_{even})$ must preserve at least one eigenspace differently and so impose new restrictions on $\eta(\tau_z)$ and $\eta(\tau_y)$. Clearly there will be some limit on N_{even} above which the $\eta(\tau_{even})$ will only all commute if at least one of them is diagonal and the representation becomes Abelian. This limit will depend heavily on the partitioning of the eigenvalues and so without knowing more about these eigenvalues and their multiplicities we cannot produce a precise relation for N .

We must stress then that the limit in equation (2.8) is an overestimation of the maximum number of objects an exchange group can contain before it must have an Abelian representation. However, a more specific bound on N for a general exchange group is beyond the scope of this thesis.

2.3.3 Upper Limit for the Braid Group

As discussed at length in previous sections, the braid group is the most relevant exchange group for us. This group has just one extra relation to the general case, the Yang-Baxter relation, which we would expect to lower the limit given in equation (2.8) (the conjugation criteria actually follows from this relation so we would expect most of the general exchange groups we defined in the previous section to feature it in their presentation). For B_n , an important

general result for $N(d)$ has been proved by Formanek in ref. [42]. There he shows that for the braid group specifically:

$$N(d) = d + 2 \tag{2.9}$$

This is the same result which we found in sections 2.2 and 2.3.1 for the cases $d = 2, 3$. Our results in those sections, however, were obtained from the physical properties of the exchange groups mentioned in section 2.3.2.

In ref. [43] all irreducible representations of B_n that are of dimension $d \leq n$ are classified. There are 11 cases, (A) through (K), listed in the paper. Cases (A) and (B), shown below, apply to any number of particles while the remaining cases are special cases, we will only mention the ones that are necessary for our calculations:

(A) A representation of Burau type, either:

- $\chi(y) \otimes \beta_n(z) : B_n \rightarrow GL_{n-1}(\mathbb{C})$, where $1 + z + \dots + z^{n-1} \neq 0$, or
- $\chi(y) \otimes \beta_n(z) : \hat{B}_n \rightarrow GL_{n-1}(\mathbb{C})$, where $1 + z + \dots + z^{n-1} = 0$

(B) A representation of standard type: $\chi(y) \otimes \gamma_n(z) : B_n \rightarrow GL_n(\mathbb{C})$ where $z \neq 1$.

In both cases, χ is a character of B_n (i.e. a 1D representation). Also $\beta_n(z)$ denotes the reduced Burau representation of B_n with parameter z , while $\hat{\beta}_n$ is the non-trivial composition factor of $\beta_n(z)$ which exists when z is an n th root of unity. Explicit formulae for β_n and $\hat{\beta}_n$ and also for the standard representation, γ_n , can be found in ref. [43].

The special cases all occur for $3 < n < 9$. We will mention the cases that are relevant for qutrits as an example of how they apply to our results which show that qutrits must have $2 \leq n \leq 5$.

The case $n = 2$ is uninteresting as it must be Abelian. For $n = 3$, we have case (B) above. For $n = 4$, we have β_4 from case (A) as well as the special case (D), which is given in ref. [43] as $\epsilon_4 : B_4 \rightarrow GL_3(\mathbb{C})$. Finally, for $n = 5$ we use the non-trivial composition factor, $\hat{\beta}_5(z)$ from case (A).

Ref. [43] deals with representations into $GL_d(\mathbb{C})$ so one might be concerned about unitarity. However, we find that, in each of the above cases, taking $\chi(y)$

to be unitary and restricting the values of the parameter, z , to roots of unity yields a unitary (or at least unitarisable) representation.

2.4 Multi-Qudit Gates

To fully realise a universal quantum computer we will need to consider multi-qudit gates, i.e. braiding of particles from different qudits around each other. All multi-qudit gates can be simplified to a succession of two-qudit and single qudit gates, therefore if we are able to construct a universal set of leakage-free, two-qudit gates, then we can perform universal quantum computation without leakage. However, even if we assume that no leakage occurs in single qudit gates it is still likely to plague multi-qudit gates, as we discussed in section 2.1.

A first simple question to ask is whether systems of two qudits exist in which all exchange processes are both leakage-free and universal. The computational Hilbert space of the system is then closed under the action of the braid group for the anyons in the two qudits, i.e. the computational Hilbert space carries a representation of the full two-qudit braid group.

We assume the qudits we are considering contain n_1 and n_2 anyons (where $n_1 + n_2 = n$ is the total number of anyons comprising the two qubits) and the dimensions of the qubit spaces are d_1 and d_2 .

We are then looking for a non-Abelian representation ρ , of B_n . In order for ρ to be leakage free we require that it decomposes as a tensor product of a d_1 and a d_2 -dimensional representation, that is, the two-qudit Hilbert space should be a tensor product of the two individual qudit spaces, so it has a dimension $d = d_1 d_2$. If no representations of this dimension exists then we must move to a higher dimensional representation, this means that in moving from two single qudits to a two-qudit gate we were forced to introduce states which were not accessible to the single qubits, these are non-computational states and we then have leakage of information from the qudits into these states which can not be accessed by the qubit operations. Of course we will easily be able to construct diagonal representations which satisfy these conditions but these will be Abelian so cannot meet the universality requirement, we therefore look only for non-Abelian representations.

Exchanges which only involve anyons from a single qudit will have a representation which is simply the single qudit representation of the exchange applied to the vector space of the qudit in which it takes place, with the identity matrix applied to the vector space of the other qudit. In other words, exchanges which feature only anyons from the first qudit will have a representation given by:

$$\rho(\tau_i) = \rho_1(\tau_i) \otimes \mathbb{1}_{d_2} \quad (1 \leq i \leq n_1 - 1) \quad (2.10)$$

where ρ_1 is the d_1 -dimensional representation of B_{n_1} on the Hilbert space of the first qudit. Similarly the exchanges which only feature anyons from the second qudit have a representation given by:

$$\rho(\tau_j) = \mathbb{1}_{d_1} \otimes \rho_2(\tau_j) \quad (1 \leq j \leq n_2 - 1) \quad (2.11)$$

where ρ_2 is the d_2 -dimensional representation of B_{n_2} on the Hilbert space of the second qudit. The representations ρ_1 and ρ_2 are obtained via the methods described in previous sections. Once these representations are fixed there is then only one generator for which we have to find a representation, τ_{n_1} . This is the only generator which exchanges anyons between the two qudits. We can find a representation for this generator by subjecting it to the constraint that it must satisfy the braid relations (equations (1.1) and (1.2)) with all other generators in the system.

If we can find a representation for τ_{n_1} then we have shown that the two-qudit Hilbert space can be decomposed into the tensor product of two single qudit spaces and thus we have a non-leaking two-qudit system. However, we will see that, for qudits of low dimension, such as qubits and qutrits, the constraints can usually not be satisfied, so that for almost all types of qubits and qutrits, it is unavoidable that leakage will appear for at least some of the possible exchange processes.

2.4.1 Two-Qubit Gates

We start with an analysis of two-qubit gates, i.e. $d_1 = d_2 = 2$. The individual qubits in our system must be non-Abelian so that we can achieve interesting

operations. From our results in section 2.2, this means there are three types of two-qubit gates which are of interest to us: firstly a gate between two qubits composed of three anyons ((3 + 3)-anyon gate), a gate between two qubits composed of four anyons ((4 + 4)-anyon gate) and a gate between a qubit composed of three anyons and a qubit composed of four anyons ((3 + 4)-anyon gate).

We are then looking for a non-diagonal, four-dimensional representation, ζ , of B_6 ((3+3)-anyon gate), B_8 ((4+4)-anyon gate) and B_7 ((3+4)-anyon gate). However, the result from ref. [42], mentioned in section 2.3.3, shows that no non-Abelian, d -dimensional representations of B_n exists when $d < n - 2$. Thus the only case which could potentially be useful is the (3 + 3)-anyon gate.

In B_6 we have five generators, where τ_1 and τ_2 exchange the anyons only within qubit 1 and τ_4 and τ_5 exchange the anyons only within qubit 2. As the two-qubit space is a tensor product of the single qubit spaces these four generators will simply be given by equations (2.10) and (2.11):

$$\begin{aligned}\zeta(\tau_{1/2}) &= \eta_1(\tau_{1/2}) \otimes \mathbb{1}_2 \\ \zeta(\tau_{4/5}) &= \mathbb{1}_2 \otimes \eta_2(\tau_{1/2})\end{aligned}\tag{2.12}$$

Where $\eta_{1/2}$ is the representation η from equation (2.1) but on the appropriate qubit space. By choosing a convenient basis, this gives us the following forms:

$$\begin{aligned}\zeta(\tau_1) &= \begin{pmatrix} a & & & 0 \\ & a & & \\ & & \bar{a} & \\ 0 & & & \bar{a} \end{pmatrix} & \zeta(\tau_2) &= \begin{pmatrix} \frac{1}{a-a^3} & 0 & c & 0 \\ 0 & \frac{1}{a-a^3} & 0 & c \\ -c & 0 & \frac{1}{a-a^3} & 0 \\ 0 & -c & 0 & \frac{1}{a-a^3} \end{pmatrix} \\ \zeta(\tau_4) &= \begin{pmatrix} \frac{1}{f-f^3} & g & & 0 \\ -g & \frac{1}{f-f^3} & & \\ & & \frac{1}{f-f^3} & g \\ 0 & & -g & \frac{1}{f-f^3} \end{pmatrix} & \zeta(\tau_5) &= \begin{pmatrix} f & & & 0 \\ & \bar{f} & & \\ & & f & \\ 0 & & & \bar{f} \end{pmatrix}\end{aligned}\tag{2.13}$$

where $f = a$ or $f = \bar{a}$ and hence $g = c = \sqrt{1 - \frac{1}{2-a^2-\bar{a}^2}}$. All that is left is to find a representation for τ_3 , which is the one braid that exchanges anyons between the two qubits. We use the group relations to find what $\zeta(\tau_3)$ should

2.4.2 Two-Qutrit and Qubit-Qutrit Gates

We can use a similar approach to examine if leakage-free braiding is possible for a two-qutrit gate. As detailed in section 2.3.1, all 3-dimensional representations of B_n are known and can be found in ref. [43]. We showed in the same section that it is possible to have non-Abelian qutrits composed of 3, 4 or 5 anyons. Thus we have 6 possibilities for a two-qutrit gate, i.e. using $(3 + 3)$, $(3 + 4)$, $(3 + 5)$, $(4 + 4)$, $(4 + 5)$ or $(5 + 5)$ anyons.

We are then looking for a non-diagonal, 9-dimensional representation of B_6 , B_7 , B_8 , B_8 , B_9 and B_{10} respectively. All of these cases satisfy Formanek's $N \leq d + 2$ result so we get no immediate restrictions.

We then proceed in the same way as in the previous section, first by fixing a representation of the exchanges which involve anyons from exclusively one qutrit, using equations (2.10) and (2.11), then examining whether a representation of τ_{n_1} exists. Doing this, however, we found that none of the cases give a result which is both non-Abelian and leakage-free. Therefore in two-qutrit systems having at least some braids with leakage is unavoidable.

There is another system which we can consider and where we have a gate between a qubit and a qutrit. This means we would have a 6-dimensional representation of B_n where the possibilities are a $(3 + 3)$, $(3 + 4)$, $(3 + 5)$ or $(4 + 4)$ -anyon gate, as a non-Abelian qubit has $n_1 = 3, 4$ and a non-Abelian qutrit has $n_2 = 3, 4, 5$. Again we directly calculate each of these possibilities and we find no leakage-free, non-Abelian representations.

In principle one may go on and, using the same method, test the possibilities for $d > 3$ two-qudit gates and it is indeed very straightforward for $d = 4, 5$ as all irreducible representations of B_3 for these dimensions are given in [44].

In fact it is known that if each anyon carries a representation of a quantum group (i.e. a quasitriangular Hopf algebra), the tensor product of these representations carries a braid group representation defined by exchanging tensor factors and applying the R-matrix of the quantum group. Since in such situations, each anyon must have a vector space of dimension at least 2 attached to it, we get a minimum of $d = 8$ dimensions for a qudit made up of three such anyons (or $d = 16$ for four anyons). This yields leakage-free, multi-qudit braiding, since there are no states outside the tensor product to leak into.

However, it is conjectured (see e.g. [45], conjecture 6.6) that the braid group representations that occur in this way always have a finite braid group image and therefore are never universal for quantum computation (although they can be non-Abelian). We will consider such representations in more detail when analysing the motion group in chapter 3.

So far we have shown that for systems consisting of qubits and qutrits, it is not possible to have a situation where all braidings are leakage free, except in an exceptional case with non-universal qubits of Ising type. However, it is actually only necessary for there to exist a single leakage-free, entangling exchange operation for a multi-qudit system to be universal. Therefore, if any of the systems above contain such an entangling operation, they will, in fact, be capable of leakage-free, universal quantum computation.

It would be of great interest to find the leakage-free subgroup of the braid group for representations that occur in simple anyon models, and of even greater interest to find the closure of the images of these representations in the corresponding unitary groups. Again, if braiding within qubits is universal and a single leakage-free entangling two-qubit gate exists, then the projective image of the leakage-free subgroup should be dense. Unfortunately, a leakage-free, entangling two-qudit braiding gate has yet to be found for any anyon model which has universal single-qudit braiding and finding such an operation is beyond the scope of this thesis.

2.5 Conclusion

In this chapter we have considered many questions concerning the optimal design of qudits composed of anyons in $2+1$ dimensions. The main result from the chapter was in section 2.2 where we showed that the optimal design for a qubit was using 3 or 4 anyons because this can potentially provide universal, leakage-free single qubit operations using only exchanges within the qubit.

More generally we showed using results of Formanek that a d -dimensional qudit should be composed of less than $d+2$ anyons, otherwise the representation of the braid group of those anyons must be Abelian and universal quantum computation cannot be achieved, within the single qubit system.

Generalising even further from braiding to an arbitrary exchange operation

as a means of implementing logic gates, we were able to indicate that an upper bound on the maximum number of anyons a qudit should contain such that universality is possible is:

$$N(d, \bar{m}, q) \leq \min \left(\left[2d! \prod_i \frac{1}{m_i! q!} \right], \left[\sum_i m_i^2 - d + 4 \right] \right)$$

as given in equation (2.8). However, we highlighted that this is an overestimation and in reality N will be much lower for a given d . Obtaining a more accurate limit on N should be a goal in any future work. A clear relation between the dimension of the representation of a qudit and the maximal number of anyonic components, for an arbitrary exchange group, will be a useful tool in the design considerations of a topological quantum computer.

In terms of two-qudit gates, we found that there are no universal multi-qudit systems, with dimensions 2 and 3, in which all operations are leakage-free. Note that it is conjectured [45], and known for the cases treated in ref. [46], that braid group representations coming from anyons with quantum dimensions that square to an integer are non-universal for TQC. However, whether any systems can exist with a single leakage-free, entangling operation remains an open question.

Chapter 3

TQC with Anyonic Rings

In chapter 2 we stressed how the fundamental ingredient in topological quantum computation is a system which picks up a non-trivial, anyonic phase under some exchange of its constituent particles. In section 1.2 we saw that, in order for particles to have such anyonic exchange statistics, we are forced to confine them to two spatial dimensions which ensures braiding of their worldlines is topologically non-trivial. However, this is only true of traditional, “point-like” particles. If the anyonic excitations are not restricted to be point-like, we can imagine a variety of differently shaped objects which could undergo exchanges that remain topologically non-trivial in 3+1 dimensions.

The case we will focus on is that of anyonic excitations which are ring-shaped. The number of possible topological operations ring-shaped excitations can undergo is much larger than just the simple braid exchanges the point-like particles are subject to. Ring-shaped excitations are governed by the motion group which contains within it three separate types of topologically non-trivial motions. A larger class of logic operations can then be performed on the qudits so, one would hope, this would make universality more feasible as well as making the system more efficient.

The goal of this chapter will be to examine various methods of implementing qubits in a system of anyonic rings and to assess the viability of such a system for topological quantum computation by using representation theory to obtain the properties of the qubits we have constructed.

3.1 The Motion Group

It has been shown, by Dahm [40], that the motion of such rings is governed by the motion group, \mathfrak{Mot}_n , on n rings.

A rigorous definition of \mathfrak{Mot}_n is provided in Dahm's paper. In general we can consider a manifold, M , along with a submanifold, S , which is the disjoint sum of n submanifolds, S_1, \dots, S_n .

If we take $\mathfrak{hom}_c(M)$ as the group of homomorphisms from M to itself with compact support, that is elements of $\mathfrak{hom}_c(M)$ send points on M to other points on M where the non-trivial homomorphisms of M are a compact subset of $\mathfrak{hom}(M)$. Now take $\mathfrak{hom}_c(M; S)$ as the subgroup of $\mathfrak{hom}_c(M)$ containing homomorphisms on M which act trivially on the submanifold S . Dahm then defines $\mathfrak{Mot}(M; S)$ as the relative homotopy group $\pi_1(\mathfrak{hom}_c(M), \mathfrak{hom}_c(M; S))$.

This can be understood as the group of homotopy distinct paths in the space of homomorphisms of M which leave the submanifold S unchanged. In other words the elements of $\mathfrak{Mot}(M; S)$ are motions of M which leave S alone but alter the loops of the fundamental group of M .

In this chapter we will only deal with the case where $M = \mathbb{R}^3$ and S is a disjoint union of n unlinked, unknotted circles. Therefore, \mathfrak{Mot}_n is the group of topologically distinct motions of distinct, unlinked circles in 3-dimensional space.

There is a more convenient way to look at the motion group. There exists a natural homomorphism, discovered by Dahm [41] and thus referred to as the Dahm homomorphism, from the motion group, \mathfrak{Mot}_n , into the automorphism group of the fundamental group of $M \setminus S$, i.e. $\mathfrak{Mot}_n \sim \mathfrak{Aut}(\pi_1(M \setminus S))$.

$M \setminus S$ is obtained when we take the manifold M and remove the submanifold S . The fundamental group on this space will contain homotopy distinct loops. These loops tell us about the holes in the manifold which occur due to the removal of S , along with any homotopy of M itself. The automorphism group on this fundamental group then contains the ways in which these loops can be mapped into other loops in the fundamental group while preserving products.

This formulation of the motion group is much easier to understand pictorially. When we remove S from M we are left with a 3-dimensional space with n annular holes. We choose a base point, b , through which each loop in

the fundamental group must pass. As the annular holes are 2-dimensional, we are able to pull loops over the annuli and contract them to the base point in our 3-dimensional space, thus the generating set of loops will be those which pass through the centres of the circles. We then draw all homotopy distinct loops which link with a single circle and contain the point b , these loops are the generators of the fundamental group $\pi_1(M \setminus S)$.

We can introduce the free group, F_n , which is isomorphic to $\pi_1(M \setminus S)$. That is, we associate to every loop, a distinct element, x_i , which is taken to be a generator of the free group and so has no relations on it. Being group elements, the x_i must be invertible, to incorporate this we give each loop a direction, anticlockwise from convention, we can then think of the inverse of an x_i to be an inversion of the direction of the loop it labels.

We can now talk about the operations in the motion group by referencing their action on the free group generators attached to the loops.

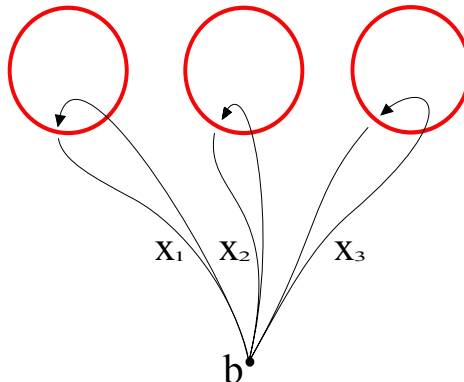


Figure 3.1: Pictorial representation of $\pi_1(M \setminus S)$ on three rings. With free group generators, x_i , labelling the loops.

Figure 3.1 shows the pictorial interpretation of the group $\pi_1(M \setminus S)$. We will see that elements of \mathfrak{Mot}_n can now be interpreted as simple operations on these loops. The generators of \mathfrak{Mot}_n fall into three separate types of motion, as defined by Dahm [40, 41]:

- *Exchanges*: Exchanges involve swapping the positions of two adjacent rings, as you would with point-like particles in three-dimensions. All possible exchanges are then contained in the symmetric group, \mathcal{S}_n . The presentation of \mathcal{S}_n was given in section 1.3 but we will reiterate it here for clarity. \mathcal{S}_n has generators, τ_i , which exchange the i^{th} and $(i + 1)^{th}$

rings and which obey the exchange relations:

$$\tau_i \tau_j = \tau_j \tau_i \quad \{|i - j| \geq 2\} \quad (3.1)$$

$$\tau_i \tau_{i+1} \tau_i = \tau_{i+1} \tau_i \tau_{i+1} \quad (3.2)$$

$$\tau_i^2 = 1 \quad (3.3)$$

The symmetric group, generated by the exchanges, is a finite group. It is important to note that this subgroup is not essential to the definition of the motion group, i.e. permutations of the rings may not be a symmetry of the system. This is the case if the rings are distinguishable.

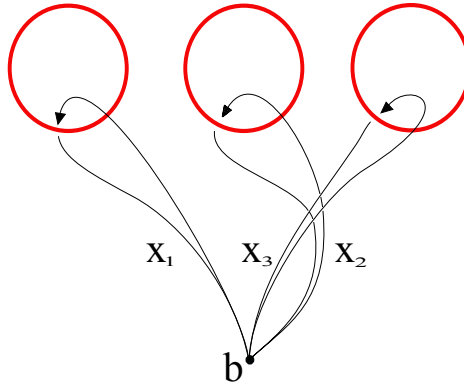


Figure 3.2: Exchange of the second and third rings, i.e. τ_2 .

- *Flips*: Flips involve rotating a ring through 180° , so if there is a direction associated with the ring, it is reversed. All flips are governed by the flip group, \mathfrak{F}_n , which has generators, f_i , which rotate the i^{th} ring and obey the flip relations:

$$f_i f_j = f_j f_i \quad \{i \neq j\} \quad (3.4)$$

$$f_i^2 = 1 \quad (3.5)$$

Given that the flips commute and are of order 2, we can say that $\mathfrak{F}_n = (\mathbb{Z}_2)^n$, i.e. the flip group is also a finite group. Similar to the symmetric group, the flip group is also not necessary for the definition of the motion group. If the flips are not symmetries of the system it means that different orientations of the rings can be distinguished from each other.

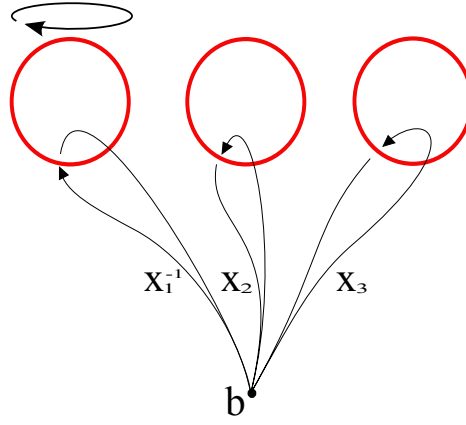


Figure 3.3: Flip of the first ring, i.e. f_1 .

- *Slides*: Slides involve shrinking one ring in size, pulling it through the centre of another ring and finally returning it to its original position, with its original size restored. All slides are governed by the slide group, \mathfrak{S}_n , with generators, σ_{ij} , which slide ring i through ring j and which obey the slide relations:

$$\sigma_{ij}\sigma_{kl} = \sigma_{kl}\sigma_{ij} \quad \{i, j, k, l \text{ all distinct}\} \quad (3.6)$$

$$\sigma_{ik}\sigma_{jk} = \sigma_{jk}\sigma_{ik} \quad \{j \neq k\} \quad (3.7)$$

$$\sigma_{ij}\sigma_{kj}\sigma_{ik} = \sigma_{ik}\sigma_{kj}\sigma_{ij} \quad \{i, j, k \text{ all distinct}\} \quad (3.8)$$

It can be seen that the slide group is infinite, the case for two rings is just the free group on the generators which must be infinite, and \mathfrak{S}_n will contain \mathfrak{S}_2 as a subgroup. Inclusion of the slide group is demanded by the definition of the motion group, the slide generators will be symmetries of the system even if the rings and their orientations are distinguishable.

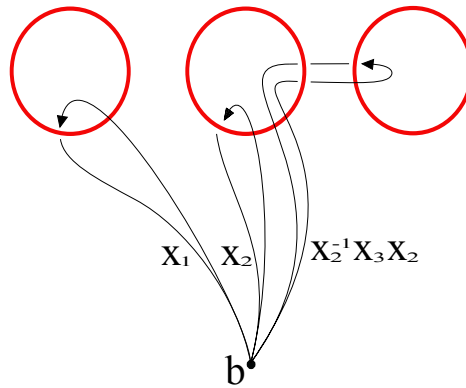


Figure 3.4: Sliding the third ring through the second, i.e. σ_{32} .

The three groups, \mathcal{S}_n , \mathfrak{F}_n and \mathfrak{S}_n are all subgroups of \mathfrak{Mot}_n . The motion of

the rings must obey relations (3.1) - (3.8) above and, in addition, the following cross relations which show how operators from the different subgroups act on each other:

$$\tau_k^{-1} f_i \tau_k = f_{\tau_k(i)} \quad (3.9)$$

$$\tau_k^{-1} \sigma_{ij} \tau_k = \sigma_{\tau_k(i), \tau_k(j)} \quad (3.10)$$

$$f_i \sigma_{jk} f_i = \sigma_{jk} \quad \{i \neq k\} \quad (3.11)$$

$$f_i \sigma_{ji} f_i = \sigma_{ji}^{-1} \quad (3.12)$$

where: $\tau_k(i)$ gives the index of the i^{th} ring after the permutation τ_k is applied to the system. We can now easily show the action of these operators just using the free group, i.e. we look at a set containing the labels of the loops, (x_1, x_2, \dots, x_n) , and show the action of the different operators on this set:

$$\tau_i(x_1, \dots, x_i, x_{i+1}, \dots, x_n) = (x_1, \dots, x_{i+1}, x_i, \dots, x_n)$$

$$f_i(x_1, \dots, x_i, \dots, x_n) = (x_1, \dots, x_i^{-1}, \dots, x_n)$$

$$\sigma_{ij}(x_1, \dots, x_i, \dots, x_j, \dots, x_n) = (x_1, \dots, x_j^{-1} x_i x_j, \dots, x_i, \dots, x_n)$$

3.2 Qubits Using Slides

We want to use these ring-shaped excitations to build qubits. Similar to chapter 2, we would like to examine the optimal way in which to design such a qubit which means calculating the maximum number of rings we can have in the qubit before the motion group on the rings becomes Abelian.

We can start by considering the slide group in isolation. As mentioned above, the slide group is the only subgroup which must be included in the motion group, we assume for the moment that permutations and flips of the rings are not symmetries of the system. As discussed at length in chapter 2, to examine the suitability of using the slides as qubit operations we will need to find all possible 2-dimensional representations of \mathfrak{S}_n .

We can choose a basis where σ_{12} is a diagonal matrix. If $\sigma_{12} = z\mathbb{1}_2$, i.e. some multiple of the identity, then this operation is trivial in all bases and we can move to a new basis where one of the other generators is diagonal (note that unlike the braid generators the slide generators aren't conjugate to each other

so can have different eigenvalues). We can keep doing this until we find a generator which is not trivial (assuming one exists), so we will assume we have labelled the rings in such a way that σ_{12} is a non-trivial operation if one exists in the group. We can then use equations (3.6) - (3.8) to try to find the full representation.

Relations (3.6) and (3.7) show that we can now simultaneously diagonalise all other generators except σ_{1k} (for $k \neq 2$) as they all commute with σ_{12} . We can obtain these other σ_{1k} by noting that they must obey the Yang-Baxter relation:

$$\begin{aligned}\sigma_{12}\sigma_{k2}\sigma_{1k} &= \sigma_{1k}\sigma_{k2}\sigma_{12} \\ [\sigma_{12}\sigma_{k2}]\sigma_{1k} &= \sigma_{1k}[\sigma_{12}\sigma_{k2}]\end{aligned}\tag{3.13}$$

Thus each σ_{1k} must commute with the matrix $[\sigma_{12}\sigma_{k2}]$ which is the product of two diagonal matrices. We then have two possibilities for each k :

1. $\sigma_{k2} = z\sigma_{12}^{-1}$: We then have $[\sigma_{12}\sigma_{k2}] = z\mathbb{1}$ which gives us no restrictions on σ_{1k} .
2. $\sigma_{k2} \neq z\sigma_{12}^{-1}$: This gives $[\sigma_{12}\sigma_{k2}] = D$, D being some diagonal, non-identity matrix. So σ_{1k} must itself be diagonal (as we have chosen $\sigma_{12} \neq z\mathbb{1}$).

If (2) is the case for all k then we get a completely trivial system, all generators commute with each other so the representation is Abelian. However, if some of the k 's obey case (1) then we can have non-diagonal generators and thus \mathfrak{S}_n has a non-Abelian representation.

Now consider a generator σ_{pq} , where $p \neq 1$, this will commute with σ_{12} and so must be diagonal. If we also have $q \neq k$, then σ_{pq} will also commute with σ_{1k} . Then, either σ_{1k} is a diagonal matrix (even if we have case (1) above) or $\sigma_{pq} = z\mathbb{1}$.

Such a σ_{pq} will always exist for any k provided $n \geq 4$. So if we have a non-diagonal representation of three rings, then any additional ring we add must act trivially when we slide any other ring through it. This means, though we can have as many rings as we wish inside the qubit, only three of the rings can produce non-trivial sliding operations or the representation will be Abelian.

Remember also that these calculations have only taken into account the slide subgroup of the motion group. If we add in the operations from \mathcal{S}_n and \mathfrak{F}_n the situation becomes even more restrictive. The issue arises due to the fact that, from equation (3.10), the slides become conjugate to each other under the exchange operations, i.e. $\sigma_{ij} = \tau^{-1}\sigma_{kl}\tau$, for some appropriate $\tau \in \mathcal{S}_n$. Thus, inclusion of \mathcal{S}_n ensures that the rings are indistinguishable and so all σ_{ij} must have equal eigenvalues. Then if any generator is a multiple of the identity all generators are a multiple of the identity and we cannot add rings which have trivial sliding operations to the system without making the representation of all slides trivial.

This is similar to the results we obtained in section 2.2.1 for qubits composed of point-like anyons, as we have a maximum of three objects with which non-trivial operations can be performed (if \mathcal{S}_n and \mathfrak{F}_n are omitted more operations can exist but they must all be trivial). This similarity stems from the fact that the braid group is actually contained within the motion group, as is evidenced by the presence of the spatially separate (equation (3.6)) and Yang-Baxter (equation (3.8)) relations in the presentation of the slide group. Specifically the braid group operators are equivalent to a slide operation followed by an exchange (the slide group alone contains the pure braid group).

Using similar methods to chapter 2 we could now calculate higher dimensional representations of the slide group. Due to eigenvalue multiplicity we would expect to find larger non-Abelian groups but as the group is so closely related to the braid group we would not expect to find any solutions which differ greatly from those calculated in the previous chapter.

3.3 Induced Representations of \mathfrak{Mot}_n

We have already mentioned that the slide group is an infinite group whereas the other two subgroups are finite. Thus there is an advantage to be gained from starting with a desirable representation of \mathfrak{S}_n and, using this, induce a compatible representation of the full motion group.

To start with we obtain a desirable, i.e. non-trivial, representation, π , of \mathfrak{S}_n as we have outlined in section 3.2. We then want to obtain a representation, $\text{IND}_{\mathfrak{S}}^{\mathfrak{Mot}}(\pi)$ of \mathfrak{Mot}_n which, when reduced to the subgroup \mathfrak{S}_n , contains the

representation π . If we take V_π to be the d_π -dimensional vector space on which the representation π acts, then we must first build the vector space, W , on which $\text{IND}_{\mathfrak{S}}^{\mathfrak{M}ot}(\pi)$ acts.

We can collect the elements of $\mathfrak{M}ot_n$ from the symmetric and flip groups together by taking the semidirect product these two subgroups, $\mathcal{S}_n \times \mathfrak{F}_n$, which has elements $g = (\tau, f)$, where $\tau \in \mathcal{S}_n, f \in \mathfrak{F}_n$. W can then be obtained by taking the tensor product of the group algebra of $\mathcal{S}_n \times \mathfrak{F}_n$ with the vector space V_π , i.e. $W = \mathbb{C}[\mathcal{S}_n \times \mathfrak{F}_n] \otimes V_\pi$. This means that the basis vectors of W have the form:

$$w_{g,i} = g \otimes v_i \quad (3.14)$$

where v_i is a basis vector of V_π and $g \in \mathcal{S}_n \times \mathfrak{F}_n$. We can then use equations (3.9) - (3.12) to calculate the representation acting on W . Firstly an element of $\mathcal{S}_n \times \mathfrak{F}_n$, acting on a basis vector, will simply permute it into another basis vector:

$$g'w_{g,i} = g'(g \otimes v_i) = g'g \otimes v_i = g'' \otimes v_i \quad (3.15)$$

A slide acting on a basis vector will act only on the vector, v_i , in the second tensor factor producing a representation, π , of some slide (not necessarily the same one) on the basis vector:

$$\sigma w_{g,i} = \sigma(g \otimes v_i) = g \otimes g^{-1}\sigma g v_i = g \otimes \pi(g^{-1}\sigma g)v_i = \pi(\sigma')(g \otimes v_i) \quad (3.16)$$

where $\sigma' = g^{-1}\sigma g$. Thus we can say in general if any element of $\mathfrak{M}ot_n$ can be written as $g\sigma$ then:

$$\text{IND}_{\mathfrak{S}}^{\mathfrak{M}ot}(\pi)(g\sigma) = \sum_{h,i} \pi(h^{-1}g\sigma g^{-1}h)g^{-1}h \otimes v_i \quad (3.17)$$

W then will have a basis vector for every element of $\mathcal{S}_n \times \mathfrak{F}_n$ combined with every basis vector of V_π , thus $\text{IND}_{\mathfrak{S}}^{\mathfrak{M}ot}(\pi)$ will be a $(n!2^n d_\pi)$ -dimensional representation. However, under certain conditions this representation will be highly reducible. This occurs if the centralizer of π is non-trivial which can arise as a result of the flips or exchange groups acting trivially. The centralizer of π is

defined as:

$$C_\pi := \{s \in \mathcal{S}_n \times \mathfrak{F}_n \mid \forall \sigma \in \mathfrak{S}_n : \pi(s^{-1}\sigma s) = \pi(\sigma)\} \quad (3.18)$$

Take a d_π -dimensional representation of the centralizer, i.e. states are given by a superposition of all centralizer elements; $\sum_{s \in C_\pi} s \otimes v_i$. Such a representation is invariant under the action of the centralizer elements and the slide operators. We produce new states by acting with elements of $\mathcal{S}_n \times \mathfrak{F}_n$ which are not elements of C_π , in general we get one state for each such element.

We have then found a subrepresentation of $\text{IND}_{\mathfrak{S}}^{\text{mot}}(\pi)$ whose dimension is smaller by a factor of the order of C_π , i.e. we have shown that we can easily reduce $\text{IND}_{\mathfrak{S}}^{\text{mot}}(\pi)$ to a representation of dimension: $d = \frac{n!2^n d_\pi}{|C_\pi|}$. This representation is not necessarily irreducible, the purpose here is merely to show that the induced representation can usually be reduced.

Generally the centralizer, C_π , contains only the identity element. In this case, using equations (3.10) and (3.12), we see that, for any s , there will be at least one σ for which $s^{-1}\sigma s \neq \sigma$. Reduction of $\text{IND}_{\mathfrak{S}}^{\text{mot}}(\pi)$ is not as simple and it may even be irreducible.

However, if we set the centralizer to contain the flip group, \mathfrak{F}_n , then from equation (3.12) we find that $\sigma_{ij} = \sigma_{ij}^{-1}$. Thus we can define a new representation which acts on a vector space, X_π , with basis states which are of the form $x_i = \sum_k f_k \otimes v_i$. These x_i states are invariant under \mathfrak{F}_n and get mapped into each other by elements of \mathcal{S}_n and \mathfrak{S}_n . So we get a reduced representation of dimension $d_X = \frac{n!2^n d_\pi}{2^n} = n!d_\pi$.

Similarly if we set the centralizer to contain the exchange group, \mathcal{S}_n , then from equation (3.10) we find that $\sigma_{ij} = \sigma_{kl}$. We then define a new representation acting on a vector space, Y_π , which has basis vectors $y_i = \sum_k \tau_k \otimes v_i$ which are invariant under the action of \mathcal{S}_n and which are mapped into each other by the elements of \mathfrak{F}_n and \mathfrak{S}_n . So we get a reduced representation of dimension $d_Y = \frac{n!2^n d_\pi}{n!} = 2^n d_\pi$.

Finally, we can take a combination of the above two cases and set the centralizer to contain the full semidirect product, $\mathcal{S}_n \times \mathfrak{F}_n$. We then have that all σ_{ij} are equal and are also equal to their inverses. Thus we can define a d_π -dimensional representation which acts on a vector space, Z , with basis vectors,

$z_i = \sum_{k,l} f_k \tau_l \otimes v_i$ which are invariant under the action of $\mathcal{S}_n \times \mathfrak{F}_n$ which are mapped into each other by \mathfrak{S}_n .

We have talked at length in chapter 2 about how higher dimensional representations yield more useful, efficient systems. When inducing representations of \mathfrak{Mot}_n , from a desired representation, π , of the slide group it will then be beneficial to have the order of the centralizer of π to be as small as possible. This is, however, related to physical characteristics of the system. If the centralizer encompasses all the elements of the flip or exchange groups it corresponds to the slides being equal under these operations.

3.4 Local Representations

The previous two sections showed that the efficiency of a qubit composed from anyonic rings, i.e. the number of independent operations available on the qubit, is limited by the requirement that the slide group has a non-Abelian representation. We would like to see if any alternative implementations of qubits can avoid this issue, allowing us to increase the number of possible logic gates without compromising the universality of the qubits.

To this end we consider a system in which each ring in the system has an internal d -dimensional vector space, V , associated with it. The Hilbert space of the system is then $V^{\otimes n}$, where n is the number of rings in the system, and has a dimensionality of d^n .

We can introduce local representations by defining the action of the motion group operators to be non-trivial only on the vector spaces associated with the rings which are involved in the motion. A given motion group operation, m_{ij} , acting on rings i and j (any motion group operation will act on at most two rings at a time) is then represented by a tensor product of d -dimensional matrices, m^i and m^j , acting on the vectors space corresponding to the i^{th} and j^{th} rings and the identity operator, $\mathbb{1}_d$, acting on all other vector spaces.

Specifically, the exchange operations, τ_i , acts by swapping the i^{th} and $(i+1)^{th}$ vector spaces inside the tensor product, i.e. it acts with some d^2 -dimensional exchange matrix, τ , on the i^{th} and $(i+1)^{th}$ tensor factors and acts

trivially on all other vector spaces:

$$\tau_i = \mathbb{1}^1 \otimes \mathbb{1}^2 \otimes \dots \otimes \tau^{i,i+1} \otimes \mathbb{1}^{i+2} \otimes \dots \otimes \mathbb{1}^n \quad (3.19)$$

It is important to highlight that we can define the exchanges such that they don't alter the local vector spaces of the rings, they simply exchange them. The flip operations, f_i , act with some orientation altering operation, f , on the i^{th} vector space only and act trivially on all other tensor factors:

$$f_i = \mathbb{1}^1 \otimes \mathbb{1}^2 \otimes \dots \otimes f^i \otimes \mathbb{1}^{i+1} \otimes \dots \otimes \mathbb{1}^n \quad (3.20)$$

The slide operators will act non-trivially on the two tensor factors with the slide operator, denoted \mathcal{R} (for reasons which will become clear later). However, unlike the exchanges, the tensor factors on which \mathcal{R} acts are not necessarily neighbouring. If we let $[r_p]^i$ be a d -dimensional matrix acting on the i^{th} vector space, then $\mathcal{R}_{ij} = \sum_p [r_p^1]^i \otimes [r_p^2]^j$ and:

$$\sigma_{ij} = \sum_p \mathbb{1}^1 \otimes \mathbb{1}^2 \otimes \dots \otimes [r_p^1]^i \otimes \dots \otimes [r_p^2]^j \otimes \dots \otimes \dots \otimes \mathbb{1}^n \quad (3.21)$$

If the exchange subgroup is included in the motion group, i.e. if the rings are indistinguishable, we can use the exchanges to give a slightly simpler form of σ_{ij} , we find a d^2 -dimensional matrix for \mathcal{R} acting on neighbouring sites, $\mathcal{R} = \sum_p [r_p^1]^i \otimes [r_p^2]^{i+1}$, then for any σ_{ij} we conjugate \mathcal{R} by the appropriate exchange operators in order to move the i^{th} and j^{th} tensor factors to neighbouring sites before we act with \mathcal{R} and then move them back to their original sites afterwards. We explained in the definition of the exchanges that the τ_i act trivially on the local vector spaces so this process will not affect the action of the \mathcal{R} matrix.

The representation of the motion group then consists of three independent operators, τ , f and \mathcal{R} . The generators of the motion group differ only by the vector spaces on which these operators act on. Finding local representations of a system then requires us to only find the representation of these three operators thus is less work compared to the methods in section 3.2 and 3.3. Also, under this definition of the operators many of motion group relations

are automatically simplified. This can be easily seen for equations (3.1), (3.4), (3.6) and (3.11) given the tensor product structure and for equations (3.2), (3.3), (3.9) and (3.10) from the permutation nature of the exchanges. We are then left with only four non-trivial relations, which can be expressed in terms of the operators τ , f and \mathcal{R} as:

$$f_i^2 = \mathbb{1}_2 \quad (3.22)$$

$$\mathcal{R}_{ik}\mathcal{R}_{jk} = \mathcal{R}_{jk}\mathcal{R}_{ik} \quad \{j \neq k\} \quad (3.23)$$

$$\mathcal{R}_{ij}\mathcal{R}_{kj}\mathcal{R}_{ik} = \mathcal{R}_{ik}\mathcal{R}_{kj}\mathcal{R}_{ij} \quad \{i, j, k \text{ all distinct}\} \quad (3.24)$$

$$f_j\mathcal{R}_{ij}f_j = \mathcal{R}_{ij}^{-1} \quad (3.25)$$

where the subscripts denote the tensor factors on which the f and \mathcal{R} operators act. This local representation approach presents us with an obvious advantage over the previously discussed methods, namely the dimension of the representation of the system will increase with the size of the Hilbert space. If an extra ring is added to the system, the representation of the operators of the smaller system changes only by the addition of a trivial tensor factor. This does not affect the form of the non-trivial f , τ and \mathcal{R} factors, it only increases the number of tensor factors each can act on, i.e. if the form of f , τ and \mathcal{R} allow for a non-Abelian representation of n rings, increasing the number of rings will not affect the non-Abelian nature of these operations on the n rings but it will add new operations to the system.

We can then increase the number of logic operation possible in the system, increasing the efficiency of our computations without adversely affecting the range of possible operations. However, it is expected that local representations will be reducible. Thus, even if the local representations are universal, there may be operations which we can never reach in a given irreducible subrepresentation.

We should mention that qudits are now defined locally on each ring. One qudit operations are then those which act solely on one local vector space, operations which involve multiple rings are then multi-qudit operations. As all states in the Hilbert space are included in the local representation, there is no longer any non-computational states in the system. Local operators

act within qudit spaces and all remaining states are accessible to multi-qudit gates, this means there we will not need to worry about leakage errors and all information remains within the computational space.

3.4.1 2 Dimensional Local Vector Spaces

We start with simplest nontrivial case, where the internal vector spaces are two dimensional. If f is not a multiple of the identity, we can think of this vector space as being spanned by the states which denote a direction associated with the ring. The flip operator is then a two dimensional matrix which acts only on a local vector space in a way which flips/changes between “forwards” and “backwards” directions. The exchange operator is a four dimensional matrix which exchanges two neighbouring vector spaces, specifically;

$$\tau = \begin{pmatrix} 1 & 0 & 0 & 0 \\ 0 & 0 & 1 & 0 \\ 0 & 1 & 0 & 0 \\ 0 & 0 & 0 & 1 \end{pmatrix} \quad (3.26)$$

We then need to find the representation of the \mathcal{R} and f matrices. From the slide group presentation, we can view \mathcal{R} as solutions of the Yang-Baxter relation, equation (3.8), which also obey equation (3.7). Considering \mathcal{R} in this way is beneficial to us as all four-dimensional solutions of the Yang-Baxter relation have been found and catalogued by Dye [47]. Thus we need only to check which of the solutions listed in this paper also obey equation (3.7) in order to find all possible representations of \mathcal{R} . We can then easily use relations (3.5) and (3.12) to calculate f .

Unitary Solutions to the Yang-Baxter Equation

Dye [47] identifies 5 families of solutions to the four-dimensional Yang-Baxter equation, we list them here for convenience. A solution to the Yang-Baxter equation can be written in the form:

$$\mathcal{R} = kAHA^{-1} \quad (3.27)$$

Where: $k = e^{i\phi}$ for arbitrary ϕ , A is of the form $Q \otimes Q$, with Q being a 2×2 , invertible matrix and H is some 4×4 matrix. Dye's five families of solutions, $\mathcal{F}_1 - \mathcal{F}_5$, are then given by different values of H and Q .

However for our purpose, i.e. using the slides to implement logic gates, we only care about solutions up to unitary equivalence. That is, if we can perform some basis change transformation, \tilde{U} , on any of these Yang-Baxter solutions, \mathcal{R} , to produce a different solution, \mathcal{R}' , then we say that they are equivalent; $\mathcal{R} \sim \tilde{U}\mathcal{R}\tilde{U}^{-1}$. Given the tensor product nature of our \mathcal{R} matrix we demand that this basis transformation is actually the tensor product of two equivalent 2×2 unitary matrices, $\tilde{U} = (U \otimes U)$. This ensures that two \mathcal{R} are considered equivalent only if they are related by performing the same basis transformation on the two vector spaces on which the slide operator acts. Therefore we will first classify Dye's solutions up to such a unitary equivalence.

Family 1, \mathcal{F}_1

$$H_1 = \begin{pmatrix} 1 & & & \\ & x & & \\ & & y & \\ 0 & & & z \end{pmatrix} \quad Q = \begin{pmatrix} a & b \\ c & d \end{pmatrix} \quad (3.28)$$

where: $|x| = |y| = |z| = 1$ and $a\bar{b} + c\bar{d} = 0$, i.e. the columns in Q are orthogonal. We can let U be a unitary matrix such that $Q = UD$, where D is some diagonal matrix. Then as $D \otimes D$ is a diagonal matrix it will commute with H :

$$\mathcal{R} = k(Q \otimes Q)H_1(Q \otimes Q)^{-1} = k(U \otimes U)H_1(U \otimes U)^{-1} \quad (3.29)$$

This shows that Family 1 just consists of matrices that are all unitarily equivalent to kH_1 . We rename it \mathcal{F}_1^U to highlight the fact that it is a family of unitary equivalent solutions.

Family 2, \mathcal{F}_2

$$H_2 = \begin{pmatrix} 0 & p \\ & 1 \\ & 1 \\ q & 0 \end{pmatrix} \quad Q = \begin{pmatrix} a & b \\ c & d \end{pmatrix} \quad (3.30)$$

where: $|pq| = 1$, $p = \frac{(|b|^2 + |d|^2)(\bar{a}b + \bar{c}d)}{(|a|^2 + |c|^2)(\bar{a}\bar{b} + \bar{c}\bar{d})}$, $q = \frac{1}{p}$ and $\bar{a}\bar{b} + \bar{c}\bar{d} \neq 0$. We can rewrite $H = h \otimes h$, where:

$$h = \begin{pmatrix} 0 & \sqrt{p} \\ \frac{1}{\sqrt{p}} & 0 \end{pmatrix} \quad (3.31)$$

The Yang-Baxter solution then becomes: $\mathcal{R} = k(QhQ^{-1})^{\otimes 2}$. The tensor product of a unitary matrix with itself is clearly also a unitary matrix, hence we can now look at the simpler case of QhQ^{-1} and if this is unitary then so will $\mathcal{R} = AH_2A^{-1}$. Let M be a matrix which diagonalises h , i.e.:

$$M = \begin{pmatrix} x\sqrt{p} & y\sqrt{p} \\ x & -y \end{pmatrix} \quad (3.32)$$

If we choose $\frac{y^2}{x^2} = p$ then QM^{-1} will be a unitary matrix, thus we can write $Q = UM$ for some unitary matrix U . \mathcal{R} then becomes:

$$\mathcal{R} = k(QhQ^{-1})^{\otimes 2} = k(UMhM^{-1}U^{-1})^{\otimes 2} = k(UDU^{-1})^{\otimes 2} \quad (3.33)$$

where D is a 2×2 diagonal matrix with eigenvalues ± 1 . Thus, family 2 consists of matrices which are unitarily equivalent to a diagonal matrix with eigenvalues $\pm k$. D is then a subset of the H_1 matrices, so the equivalence classes of Family 2 are the same as Family 1, thus \mathcal{F}_2 is contained within \mathcal{F}_1^U .

Family 3, \mathcal{F}_3

$$H_3 = \begin{pmatrix} 0 & p \\ & 1 \\ & 1 \\ q & 0 \end{pmatrix} \quad Q = \begin{pmatrix} a & b \\ c & d \end{pmatrix} \quad (3.34)$$

where: $a\bar{b} + c\bar{d} = 0$. Notice this is similar as Family 2 but here Q has orthogonal rows. This gives new restrictions on p and q , namely:

$$|pq| = 1 \quad |p| = \frac{|d|^2}{|a|^2} \quad |q| = \frac{1}{|p|} \quad (3.35)$$

We can use the same method as in Family 1 and write Q as the product of a unitary matrix, U , and a diagonal matrix, D ; $Q = UD$.

$$\mathcal{R} = (Q \otimes Q)H_3(Q \otimes Q)^{-1} = (U \otimes U)(D \otimes D)H_3(D \otimes D)^{-1}(U \otimes U)^{-1} \quad (3.36)$$

Therefore all of Family 3 are unitarily equivalent to $\tilde{H}_3 = (D \otimes D)H_3(D \otimes D)^{-1}$. To make things simpler we split Family 3 into two subfamilies; $\mathcal{F}_{3(i)}$ and $\mathcal{F}_{3(ii)}$. The difference between the two is that the members of $\mathcal{F}_{3(i)}$ have the restriction: $p = 1/q$, whereas $\mathcal{F}_{3(ii)}$ has only the less restrictive requirement $|p| = 1/|q|$.

Examining $\mathcal{F}_{3(i)}$ first, we have; $H_{3(i)} = H_2 = h \otimes h$, with h give by equation (3.31). Now choosing:

$$D = \begin{pmatrix} 1 & 0 \\ 0 & x \end{pmatrix} \quad \Rightarrow \quad \tilde{H}_{3(i)} = \begin{pmatrix} 0 & \frac{\sqrt{p}}{x} \\ \frac{x}{\sqrt{p}} & 0 \end{pmatrix}^{\otimes 2}$$

But conjugation by a unitary matrix cannot produce a unitary matrix from a non-unitary matrix. As \mathcal{R} is, by definition, a unitary matrix then DhD must also be unitary. Therefore we must have $x = \sqrt{|p|}e^{i\phi}$, for some phase factor ϕ , which gives:

$$\tilde{H}_{3(i)} = \begin{pmatrix} 0 & e^{-i\phi} \\ e^{i\phi} & 0 \end{pmatrix}^{\otimes 2} \quad (3.37)$$

This matrix can be easily diagonalized by a unitary transformation: $(U \otimes U)\tilde{H}_{3(i)}(U \otimes U)^{-1} = H_1$. So we see that $\mathcal{F}_{3(i)}$ is also a subset of \mathcal{F}_1^U .

$\mathcal{F}_{3(ii)}$ is not as easy to classify, we can no longer write H_3 as a tensor product of 2×2 matrices and so we have (by choosing D to be the same as in $\mathcal{F}_{3(i)}$):

$$\tilde{H}_{3(ii)} = \begin{pmatrix} 0 & \frac{p}{x^2} \\ & 1 \\ & 1 & \\ x^2q & & 0 \end{pmatrix} \quad (3.38)$$

We can bring \mathcal{R} into a nicer form by choosing an appropriate matrix for U ;

$$U = \begin{pmatrix} e^{i\gamma_1} & 0 \\ 0 & e^{i\gamma_2} \end{pmatrix} \quad (3.39)$$

$$\mathcal{R} = (U \otimes U)\tilde{H}_3(U \otimes U)^{-1} = \begin{pmatrix} 0 & \frac{p}{x^2}e^{2i(\gamma_1-\gamma_2)} \\ & 1 \\ & 1 & \\ x^2qe^{2i(\gamma_2-\gamma_1)} & & 0 \end{pmatrix} \quad (3.40)$$

In $\mathcal{F}_{3(i)}$ we showed that $x = \sqrt{|p|}e^{i\theta}$, this was a result of choosing an x which normalises Q , therefore, we can choose this value here too. We can rewrite p and q in a similar manner; $p = |p|e^{i\gamma_p}$ and $q = |q|e^{i\gamma_q} = \frac{e^{i\gamma_q}}{|p|}$. Finally we are free to choose the roots of unity in U , therefore can we set: $2(\gamma_1 - \gamma_2) = 2\theta - \gamma_p$ which allows us to express \mathcal{R} as:

$$\mathcal{R} = \begin{pmatrix} 0 & 1 \\ & 1 \\ & 1 & \\ e^{i\alpha} & & 0 \end{pmatrix} \quad (3.41)$$

where $\alpha = \gamma_q + \gamma_p$, note $e^{i\alpha} \neq 1$ as this corresponds to $p = 1/q$ which is part of $\mathcal{F}_{3(ii)}$. Thus $\mathcal{F}_{3(ii)}$ represents a distinct family of solutions which are unitarily equivalent to an off diagonal 4×4 matrix with eigenvalues 1 and $e^{i\alpha}$, for $\alpha \neq 0$.

We then get our second unitarily equivalent family; \mathcal{F}_2^U

Family 4, \mathcal{F}_4

$$H_4 = \frac{1}{\sqrt{2}} \begin{pmatrix} 1 & 0 & 0 & 1 \\ 0 & 1 & 1 & 0 \\ 0 & 1 & -1 & 0 \\ -1 & 0 & 0 & 1 \end{pmatrix} \quad Q = \begin{pmatrix} a & b \\ c & d \end{pmatrix} \quad (3.42)$$

Where: $a\bar{b} + c\bar{d} = 0$. Again we can use the $Q = UD$ trick and choose the same D as in the previous case to give:

$$\tilde{H}_4 = \frac{1}{\sqrt{2}} \begin{pmatrix} 1 & 0 & 0 & \frac{1}{x^2} \\ 0 & x & x & 0 \\ 0 & x & -x & 0 \\ -x^2 & 0 & 0 & 1 \end{pmatrix} \quad (3.43)$$

where $\tilde{H}_4 = DH_4D^{-1}$ and we must have $x = e^{i\frac{n\pi}{2}}$, with $n \in \mathbb{Z}$, for \mathcal{R} to be unitary. Family 4 then consists of matrices which are unitarily equivalent to \tilde{H}_4 . Note \tilde{H}_4 cannot be diagonalized by a unitary transformation, so it is not in \mathcal{F}_1 and the eigenvalues of \tilde{H}_4 are $\pm x, \frac{1}{\sqrt{2}}(1 \pm i)$ which are different to those of $\mathcal{F}_{3(ii)}$. Therefore, \mathcal{F}_4 is a new independent family of unitary equivalent solutions which we label; \mathcal{F}_3^U .

Family 5, \mathcal{F}_5

$$H_5 = \begin{pmatrix} 1 & 0 & 0 & 0 \\ 0 & 0 & 1 & 0 \\ 0 & 1 & 0 & 0 \\ 0 & 0 & 0 & 1 \end{pmatrix} \quad Q = \begin{pmatrix} a & b \\ c & d \end{pmatrix} \quad (3.44)$$

with no further restrictions on Q . Note that H_5 will commute with any $Q \otimes Q$ so we have $\mathcal{R} = kH_5$. H_5 cannot be diagonalised by a unitary transformation and its eigenvalues are ± 1 , therefore it is not in $\mathcal{F}_1, \mathcal{F}_{3(ii)}$ or \mathcal{F}_4 . So solutions constructed from H_5 are their own family of unitary solutions, \mathcal{F}_4^U

Unitarily Equivalent Families

The 5 families of Yang-Baxter solutions which Dye found then fit into the following 4 families of solutions up to unitary equivalence:

\mathcal{F}_1^U : Matrices of the form:

$$\mathcal{R} = k \begin{pmatrix} 1 & & & \\ & x & & \\ & & y & \\ 0 & & & z \end{pmatrix}$$

\mathcal{F}_2^U : Matrices of the form:

$$\mathcal{R} = k \begin{pmatrix} & & & 1 \\ 0 & & & \\ & 1 & & \\ & & 1 & \\ e^{i\alpha} & & & 0 \end{pmatrix}$$

\mathcal{F}_3^U : Matrices of the form:

$$\mathcal{R} = \frac{k}{2} \begin{pmatrix} 1 & 0 & 0 & e^{2i\beta} \\ 0 & e^{i\beta} & e^{i\beta} & 0 \\ 0 & e^{i\beta} & -e^{i\beta} & 0 \\ -e^{2i\beta} & 0 & 0 & 1 \end{pmatrix}$$

\mathcal{F}_4^U : Matrices of the form:

$$\mathcal{R} = k \begin{pmatrix} 1 & 0 & 0 & 0 \\ 0 & 0 & 1 & 0 \\ 0 & 1 & 0 & 0 \\ 0 & 0 & 0 & 1 \end{pmatrix}$$

where: $|x| = |y| = |z| = 1$, $0 < \alpha < 2\pi$, $\beta = n\pi/2$ for $n \in \mathbb{Z}$.

3.4.2 Representations of Slide and Flip Groups

We now impose our second condition on these Yang-Baxter solutions by seeing which of the \mathcal{R} 's listed above also satisfy the other relations of the motion group, i.e. equations (3.22), (3.23) and (3.25). To satisfy all these relations we must introduce the flip operator, f . Similar to the slide operator, we also require f to be unitary, therefore we can set it equal to some phase factor times a special unitary matrix:

$$f = e^{i\phi} \begin{pmatrix} a & b \\ -\bar{b} & \bar{a} \end{pmatrix} \quad (3.45)$$

But due to relation (3.22), we know that $\det(f) = \pm 1$, so; $e^{i\phi} = \pm 1$ or $\pm i$. If we test each of the families of solutions from section 3.4.1 we see that only the solutions in \mathcal{F}_1^U also satisfy relation (3.23). Therefore, from now on we shall

only consider solutions of the form:

$$\mathcal{R} = k \begin{pmatrix} 1 & & & \\ & x & & \\ & & y & \\ 0 & & & z \end{pmatrix} \quad (3.46)$$

where: $|x| = |y| = |z| = 1$. Finally we must check whether these remaining solutions satisfy relation (3.25). For simplicity we can assume the slide operates on neighbouring rings without loss of generality, we can then write:

$$\mathcal{R}(\mathbb{1}_2 \otimes f)\mathcal{R}(\mathbb{1}_2 \otimes f) = \mathbb{1}_4 \quad (3.47)$$

where we are concentrating only on the 4-dimensional space of the two rings which are acted on non-trivially by these operations. This gives the two following cases:

Case (i): $\mathbf{b} = \mathbf{0}$

When we have $b = 0$, we must necessarily have $a \neq 0$ and $|a|^2 = 1$. But from equation (3.22) we must also have $a = \pm e^{-i\phi}$, with $e^{i\phi} = \pm 1$ or $\pm i$ depending on the value of $\det(f)$. Equation (3.47) then gives; $k, x, y, z = \pm 1$. With these restrictions we then have the following form of $\mathcal{R}^{(1)}$ and $f^{(1)}$:

$$\mathcal{R}^{(1)} = \pm \begin{pmatrix} 1 & & & \\ & x & & \\ & & y & \\ 0 & & & z \end{pmatrix} \quad f^{(1)} = \pm \begin{pmatrix} 1 & 0 \\ 0 & \pm 1 \end{pmatrix} \quad (3.48)$$

Case (ii): $\mathbf{b} \neq \mathbf{0}$

Here we have $b \neq 0$, therefore $a = -x\bar{a}$ and $x = z/y$. From relation (3.22) we see that, if $b \neq 0$, then $a = -\bar{a}$. Therefore a is either zero or has no real part and $x = 1$. The same relation gives the equation:

$$e^{2i\phi}(a^2 - |b|^2) = 1 \Rightarrow e^{i\phi} = \pm i$$

So setting $b \neq 0$ restricts the determinant of f to only the $\pm i$ option. We can nicely parametrise a and b as: $a = \pm i \sin \theta$, $b = e^{i\psi} \cos \theta$. Note that $\theta \neq (2n+1)\pi/2$, for any $n \in \mathbb{Z}$, as this would correspond to $b = 0$. From equation (3.47) we get; $k = \pm 1$, $y = z = \pm 1$, this gives the following form for $\mathcal{R}^{(2)}$ and $f^{(2)}$, with $\theta \neq (2n+1)\pi/2$:

$$\mathcal{R}^{(2)} = \pm \begin{pmatrix} 1 & & 0 \\ & 1 & \\ 0 & z & z \end{pmatrix} \quad f^{(2)} = \begin{pmatrix} \sin \theta & ie^{i\psi} \cos \theta \\ -ie^{-i\psi} \cos \theta & -\sin \theta \end{pmatrix} \quad (3.49)$$

3.4.3 Canonical Flip Basis

It is interesting and helpful to move to the basis where the flip matrix is in the following canonical form;

$$\tilde{f} = \begin{pmatrix} 0 & 1 \\ 1 & 0 \end{pmatrix} \quad (3.50)$$

It now becomes obvious that, if the local states on the rings label the direction associated with the ring, the flip matrix exchanges between the “forwards” and “backwards” states.

If f is a multiple of the identity, as is a possibility for $f^{(1)}$, then it will be unchanged by any basis transformation and so we cannot put f (or \mathcal{R}) into the canonical flip basis form, given in equation (3.50). We deal then only with the subcases of relation (3.48) where f is diagonal, but not a multiple of the identity, i.e. those corresponding to $\det(f^{(1)}) = -1$. The following two cases then refer to the cases introduced in the previous section.

Case (i)

In this case we can change to the canonical flip basis via the following unitary transformation:

$$U_1 = \begin{pmatrix} 1 & 1 \\ 1 & -1 \end{pmatrix} \quad (3.51)$$

This will put f in the form of equation (3.50). We must then perform the same basis transformation on \mathcal{R} :

$$\tilde{\mathcal{R}} = (U_1 \otimes U_1)\mathcal{R}(U_1 \otimes U_1)^{-1} = \pm \frac{1}{4} \begin{pmatrix} \alpha & \beta & \gamma & \delta \\ \beta & \alpha & \delta & \gamma \\ \gamma & \delta & \alpha & \beta \\ \delta & \gamma & \beta & \alpha \end{pmatrix} \quad (3.52)$$

$$\left. \begin{array}{l} \alpha = 1 + x + y + z \quad \beta = 1 - x + y - z \\ \gamma = 1 + x - y - z \quad \delta = 1 - x - y + z \end{array} \right\} \text{ for } x, y, z = \pm 1$$

There is then 8 possible values for $\tilde{\mathcal{R}}$ depending on the combinations of ± 1 each of x, y, z take. If an even number of these values are -1 then we will be able to write $\tilde{\mathcal{R}}$ as a tensor product; $\tilde{\mathcal{R}}_{\text{even}(-1)} = \pm(\chi^1 \otimes \chi^2)$, where $\chi^i = \mathbb{1}_2$ or $\chi^i = f$. However if an odd number of the values are -1 then $\tilde{\mathcal{R}}$ has a slightly more complex form; $\tilde{\mathcal{R}}_{\text{odd}(-1)} = \pm^{1/2}[\chi^1 \otimes N \pm \chi^2 \otimes H]$, where χ^1 and χ^2 are the same as before but are always unequal, and H and N are given by:

$$H = \begin{pmatrix} -1 & 1 \\ 1 & -1 \end{pmatrix} \quad N = \begin{pmatrix} 1 & 1 \\ 1 & 1 \end{pmatrix} \quad (3.53)$$

Case (ii)

Now for the $\mathcal{R}^{(2)}$ and $f^{(2)}$ given in relation (3.49). By the definition of case (ii), $f^{(2)}$ can never be a multiple of the identity therefore we run into the same issue as for $f^{(1)}$. However, if $z = 1$, then $\mathcal{R}^{(2)}$ is a multiple of the identity and will not be affected by any basis change thus giving us a subcase of case (i), we will then only look at $z = -1$. First we move to the basis where $f^{(2)}$ is diagonal using the unitary transformation:

$$U_2 = \begin{pmatrix} \frac{ie^{-i\psi}(1-\sin\theta)}{\sqrt{2(1+\sin\theta)}} & \frac{1+\sin\theta}{\sqrt{2(1-\sin\theta)}} \\ \frac{ie^{-i\psi}\cos\theta}{\sqrt{2(1+\sin\theta)}} & \frac{\cos\theta}{\sqrt{2(1-\sin\theta)}} \end{pmatrix}$$

$$\Rightarrow f^{(2)'} = U_2 f^{(2)} U_2^{-1} = \begin{pmatrix} 1 & 0 \\ 0 & -1 \end{pmatrix} \quad (3.54)$$

We then have $f^{(2)}$ in the same form as in equation (3.48) (when $f^{(1)}$ is not a multiple of the identity), so we can again use the basis transformation U_1 to transform $f^{(2)}$ into the canonical form:

$$f^{(2)''} = U_1 U_2 f U_2^{-1} U_1^{-1} = \begin{pmatrix} 0 & 1 \\ 1 & 0 \end{pmatrix}$$

Performing the same basis transformation on \mathcal{R} gives:

$$\begin{aligned} \tilde{\mathcal{R}}^{(2)'} &= (U_1 \otimes U_1)(U_2 \otimes U_2)\mathcal{R}(U_2 \otimes U_2)^{-1}(U_1 \otimes U_1)^{-1} \\ \Rightarrow \tilde{\mathcal{R}}^{(2)'} &= \pm \begin{pmatrix} \cos \theta & \sin \theta \\ \sin \theta & -\cos \theta \end{pmatrix} \otimes \begin{pmatrix} 1 & 0 \\ 0 & 1 \end{pmatrix} \end{aligned} \quad (3.55)$$

Finally we can write down the families of unitary solutions to the relations of the motion group in the canonical flip basis. If the flip matrix, f , is a multiple of the identity then \mathcal{R} takes the form given in equation (3.46), otherwise we can move to the canonical flip basis where f is given by equation (3.50) and \mathcal{R} takes on one of the following forms:

$$\tilde{\mathcal{R}} = \pm(\mathbb{1}_2 \otimes \mathbb{1}_2), \quad \tilde{\mathcal{R}} = \pm(\mathbb{1}_2 \otimes f), \quad \tilde{\mathcal{R}} = \pm(f \otimes \mathbb{1}_2), \quad \tilde{\mathcal{R}} = \pm(f \otimes f)$$

$$\begin{aligned} \tilde{\mathcal{R}} &= \pm \begin{pmatrix} \cos \theta & \sin \theta \\ \sin \theta & -\cos \theta \end{pmatrix} \otimes \mathbb{1}_2 \\ \tilde{\mathcal{R}} &= \pm \frac{1}{2} \begin{pmatrix} -1 & 1 & 1 & 1 \\ 1 & -1 & 1 & 1 \\ 1 & 1 & -1 & 1 \\ 1 & 1 & 1 & -1 \end{pmatrix} \quad \tilde{\mathcal{R}} = \pm \frac{1}{2} \begin{pmatrix} 1 & -1 & 1 & 1 \\ -1 & 1 & 1 & 1 \\ 1 & 1 & 1 & -1 \\ 1 & 1 & -1 & 1 \end{pmatrix} \\ \tilde{\mathcal{R}} &= \pm \frac{1}{2} \begin{pmatrix} 1 & 1 & -1 & 1 \\ 1 & 1 & 1 & -1 \\ -1 & 1 & 1 & 1 \\ 1 & -1 & 1 & 1 \end{pmatrix} \quad \tilde{\mathcal{R}} = \pm \frac{1}{2} \begin{pmatrix} 1 & 1 & 1 & -1 \\ 1 & 1 & -1 & 1 \\ 1 & -1 & 1 & 1 \\ -1 & 1 & 1 & 1 \end{pmatrix} \end{aligned}$$

with $\theta \neq (2n+1)\pi/2$. \mathcal{R} then can have non-trivial action in this basis and so there is a potential for universality in the system. However, we will not be concerned in this thesis with testing the universality of such systems, we are only interested in showing that non-Abelian representations do exist.

3.5 Local Representations for $d > 2$

While successful in calculating the local two-dimensional representations of \mathfrak{Mot}_n , the method used in section 3.4.1 is not as useful if we want to go to higher dimensional local representations. This is due to the method relying heavily on known solutions to the Yang-Baxter equation, which we then specialised to suit our needs. In theory we could move forward using a similar method, however, Yang-Baxter solutions in higher dimensions are not as readily available and so we would have to calculate them ourselves, making the method extremely inefficient.

We can, however, show that the action of \mathcal{R} on the vector spaces of two rings is equivalent to the R -matrix of the quantum double of the group labelling the states in these vector spaces. We will start with the \mathcal{R} operator in the previously stated standard form: $\mathcal{R}_{ij} = \sum_p [r_p^1]^i \otimes [r_p^2]^j$. Equation (3.23) and the unitarity of \mathcal{R} then show that we can bring \mathcal{R} into the form of a controlled operation, $\mathcal{R} = \sum_i g_i \otimes e_i$ (where e_i projects onto the i^{th} basis vector), this allows us to label the basis vectors of the vector spaces by the projectors which act on them.

Using the Yang-Baxter relation (equation (3.24)) and the unitarity of \mathcal{R} again, we will see that the representation of \mathcal{R} decomposes into subrepresentations which act independently on the conjugacy classes of the \tilde{r}^1 . For each subrepresentation, we can then label the basis vectors according to the distinct matrix, g_k , and the copy, p , of that matrix to which the vector corresponds, $|e_i\rangle \rightarrow |g_k, p\rangle$.

By choosing an appropriate basis we then show that \mathcal{R} acts on the tensor product of two such states by conjugating the g -label of the first by the g -label of the second and by altering the copy number of the first by some matrix factor, α . The Yang-Baxter relation requires the α matrices to form a representation under conjugation of the centralizer of each conjugacy class. The action of \mathcal{R} is then seen to be equivalent to that of the R -matrix of the quantum double of the group composed of the g -matrices which label the basis states of the local vector spaces.

Linear Independence and Upper Triangular Form

We define some general matrix, \mathcal{R} , to be the non-trivial component of the slide operators. Given that the slide operators are conjugate under the exchanges which act trivially on the local vector spaces we can look exclusively at a single slide generator, say $\mathcal{R}_{i,i+1}$, the non-trivial component for this generator will be identical to that as for all other generators. We purposefully chose a generator which acts on adjacent rings so that \mathcal{R} is a d^2 -dimensional matrix which acts on neighbouring tensor factors, $\mathcal{R} = \sum_p [r_p^1]^i \otimes [r_p^2]^{i+1}$. The specific tensor factors that \mathcal{R} acts on is not important (i.e. we don't care about the value of i), if we then redefine \mathcal{R} to be a matrix acting on neighbouring tensor factors, we can drop the tensor factor labels allowing us to write the non-trivial slide component as: $\mathcal{R} = \sum_p r_p^1 \otimes r_p^2$.

We can safely assume that all the r^1 's and r^2 's are linearly independent, if not we can redefine them in such a way that they are. For example; say the r^1 's are not linearly independent, then there will be one r_p^1 (at least one but let's choose only one for simplicity) which can be given as a linear combination of the others, say $r_1^1 = \sum_{p \neq 1} c_p r_p^1$. Thus:

$$\begin{aligned} \mathcal{R} &= \left[\sum_{p \neq 1} c_p r_p^1 \right] \otimes r_1^2 + \sum_{p \neq 1} r_p^1 \otimes r_p^2 = \sum_{p \neq 1} \{ r_p^1 \otimes c_p r_1^2 + r_p^1 \otimes r_p^2 \} \\ &= \sum_{p \neq 1} r_p^1 \otimes (r_1^2 + c_p r_p^2) = \sum_{p \neq 1} r_p^1 \otimes \tilde{r}_p^2 \end{aligned}$$

Now \mathcal{R} does not contain r_1^1 so it is a sum of only linearly independent r 's. If there are more linearly dependent r 's we can repeat the above process to remove the dependent ones one by one until we are left with only linearly independent matrices.

We will now require \mathcal{R} to be a d^2 -dimensional representation of the slide operator. Firstly then, it must obey equation (3.23):

$$\begin{aligned} (\mathbb{1}_2 \otimes \tau)(\mathcal{R} \otimes \mathbb{1}_2)(\mathbb{1}_2 \otimes \tau)(\mathbb{1}_2 \otimes \mathcal{R}) &= (\mathbb{1} \otimes \mathcal{R})(\mathbb{1}_2 \otimes \tau)(\mathcal{R} \otimes \mathbb{1}_2)(\mathbb{1}_2 \otimes \tau) \\ \sum_{p,q} r_p^1 \otimes r_q^1 \otimes r_p^2 r_q^2 &= \sum_{p,q} r_p^1 \otimes r_q^1 \otimes r_q^2 r_p^2 \end{aligned} \quad (3.56)$$

But as all the r 's are linearly independent we must have: $r_p^2 r_q^2 = r_q^2 r_p^2$ for any

p and q (i.e. all r^2 matrices must commute with each other).

Any matrix can be brought into upper triangular form by a unitary transformation. It can also be shown that a set of commuting matrices can always be brought into upper triangular form simultaneously by the same unitary transformation [48]. So we can choose a basis such that all the r^2 matrices are upper triangular. Therefore, in the 2-dimensional case, for example, we have each r_p^2 in the following form:

$$r_p^2 = \begin{pmatrix} a & b \\ 0 & c \end{pmatrix} \Rightarrow \mathcal{R} = \sum_p \begin{pmatrix} [r_p^1]_{11} \begin{pmatrix} a_p & b_p \\ 0 & c_p \end{pmatrix} & [r_p^1]_{12} \begin{pmatrix} a_p & b_p \\ 0 & c_p \end{pmatrix} \\ [r_p^1]_{21} \begin{pmatrix} a_p & b_p \\ 0 & c_p \end{pmatrix} & [r_p^1]_{22} \begin{pmatrix} a_p & b_p \\ 0 & c_p \end{pmatrix} \end{pmatrix} \quad (3.57)$$

If we define e_{ij} as a matrix with all zero entries except for the $(i, j)^{th}$ entry which is 1, we can now easily write \mathcal{R} as:

$$\mathcal{R} = \sum_p \left\{ r_p^1 \otimes \sum_{j \geq i} c_p^{ij} e_{ij} \right\} = \sum_{j \geq i} \left(\sum_p c_p^{ij} r_p^1 \right) \otimes e_{ij} = \sum_{j \geq i} \tilde{r}_{ij}^1 \otimes e_{ij} \quad (3.58)$$

Note that, while the r_p^1 were taken to be all linearly independent, the $\tilde{r}_{ij}^1 = \sum_p c_p^{ij} r_p^1$ are not necessarily linearly independent.

Unitarity of \mathcal{R}

As we talked about in section 2.3.2, we only care about unitary representations. So \mathcal{R} should be unitary, meaning its rows and columns are orthonormal. Using equation (3.58), with an appropriate basis choice, we can write a general d^2 -dimensional \mathcal{R} as:

$$\mathcal{R} = \begin{pmatrix} \tilde{r}_{11}^1 & \tilde{r}_{12}^1 & \tilde{r}_{13}^1 & \cdots & \tilde{r}_{1d}^1 \\ 0 & \tilde{r}_{22}^1 & \tilde{r}_{23}^1 & \cdots & \tilde{r}_{2d}^1 \\ 0 & 0 & \tilde{r}_{33}^1 & \cdots & \tilde{r}_{3d}^1 \\ \vdots & \vdots & \vdots & \ddots & \vdots \\ 0 & 0 & 0 & \cdots & \tilde{r}_{dd}^1 \end{pmatrix} \quad (3.59)$$

where \tilde{r}_{ij}^1 are arbitrary $d \times d$ matrices. Looking at the first two columns of \mathcal{R} , $c^{(1)}$ and $c^{(2)}$, notice that all elements in these columns, which are not also

elements of \tilde{r}_{11}^1 , are zero. Therefore, in order for $c^{(1)}$ and $c^{(2)}$ to be orthonormal, the first two columns of \tilde{r}_{11}^1 must be orthonormal. This same argument can be used to show that, for the first d columns of \mathcal{R} to be orthonormal, all columns of \tilde{r}_{11}^1 must be orthonormal, i.e. \tilde{r}_{11}^1 must be unitary.

If \tilde{r}_{11}^1 is unitary, then its rows are also orthonormal. As the first row of \tilde{r}_{11}^1 is normalised, if any other elements along the first row of \mathcal{R} are non-zero then this first row of \mathcal{R} will not be normal. A similar argument can be made for the first d rows of \mathcal{R} . So, for \mathcal{R} to be unitary, all \tilde{r}_{1k}^1 , for $k \neq 1$, must be zero matrices.

Moving to the $(d+1)^{th}$ column of \mathcal{R} , we see that the only non-zero elements are those belonging to \tilde{r}_{22}^1 . We can use the same argument as above to say, that in order for columns $(d+1)$ through $(d+d)$ of \mathcal{R} to be orthonormal, \tilde{r}_{22}^1 must be unitary. Then, in order for rows $(d+1)$ through $(d+d)$ of \mathcal{R} to be normal, we must have that all \tilde{r}_{2k}^1 , for $k \neq 2$, must be zero matrices.

These unitary arguments can be easily extended to every column and row of \mathcal{R} to show that the only non-zero elements will be those which are elements of the submatrices \tilde{r}_{ii}^1 , for $1 \leq i \leq d$, all of which must be d -dimensional unitary matrices. The only non-zero entries are then those which correspond to the diagonal elements of r_p^2 . We then have $e_{ij} = 0$ unless $i = j$, so we can relabel the non-zero matrices as $e_i = e_{ii}$. \mathcal{R} is clearly block diagonal form, with each block being one of the r^1 matrices.

The e_i are projection operators which act non-trivially on only one basis vector of the second vector space, specifically the i^{th} basis vector. We can therefore label the states of this local vector space by the e_i matrix which acts on it, i.e. $V^{(2)} = \{e_1, \dots, e_d\}$.

Yang-Baxter Solutions

For notational ease we will rename $\tilde{r}_i^1 = g_i$, thus with \mathcal{R} from equation (3.58) and taking into account the results of the previous section we have;

$$\mathcal{R} = \sum_i g_i \otimes e_i \tag{3.60}$$

Now we can examine the effect of the Yang-Baxter relation (equation (3.8)) on these results:

$$\begin{aligned}
\mathcal{R}_{12}\mathcal{R}_{13}\mathcal{R}_{23} &= \mathcal{R}_{23}\mathcal{R}_{13}\mathcal{R}_{12} \\
\sum_{a,b,c} g_a g_b \otimes e_a g_c \otimes e_b e_c &= \sum_{a,b,c} g_b g_a \otimes g_c e_a \otimes e_c e_b \\
\sum_{a,b} g_a g_b \otimes e_a g_b \otimes e_b &= \sum_{a,b} g_b g_a \otimes g_b e_a \otimes e_b
\end{aligned} \tag{3.61}$$

The e_i are projectors so we have $e_i e_j = \delta_{ij} e_i$. We can ignore the sum over b and just focus on one single value, as linear independence of the e_i demands that any result obtained here must hold for all b . This also allows us to effectively ignore the final tensor factor, as before. So for all b we have:

$$\sum_a g_a g_b \otimes e_a g_b = \sum_a g_b g_a \otimes g_b e_a \tag{3.62}$$

We can examine the matrix elements of the g_a by multiplying on the left by a factor of $(\mathbb{1} \otimes e_m)$ and on the right by a factor of $(\mathbb{1} \otimes e_n)$ which gives:

$$\begin{aligned}
(\mathbb{1} \otimes e_m) \sum_a g_a g_b \otimes e_a g_b (\mathbb{1} \otimes e_n) &= (\mathbb{1} \otimes e_m) \sum_a g_b g_a \otimes g_b e_a (\mathbb{1} \otimes e_n) \\
g_m g_b \otimes e_m g_b e_n &= g_b g_n \otimes e_m g_b e_n \\
g_m g_b \otimes [g_b]_{mn} e_{mn} &= g_b g_n \otimes [g_b]_{mn} e_{mn}
\end{aligned} \tag{3.63}$$

where e_{mn} corresponds to the original definition of the e_{ij} above. So we then have our main result, that either of the following cases must be true:

$$\begin{aligned}
[g_b]_{mn} &= 0 \quad \text{or} \\
g_m g_b &= g_b g_n
\end{aligned} \tag{3.64}$$

Therefore if g_n is not conjugate to g_m by g_b (for any b), then there is no g_b with $[g_b]_{mn} \neq 0$. Therefore, if there exists some g_p which is not conjugate to any other g_q , then e_p projects onto an invariant vector. More generally, if the g 's divide into non-conjugate groups we get invariant vector subspaces.

Decomposing the Local Vector Spaces

We can show that the g matrices form a closed set under conjugation. We have already used the fact that the g 's are unitary matrices, therefore, for all b and m , there exists some n such that $[g_b]_{mn} \neq 0$ and, for all b and n , there exists some m such that $[g_b]_{nm} \neq 0$. Otherwise we would have that at least one g is a zero matrix and thus not unitary. This then implies:

$$\begin{aligned} \forall b, m \exists n : \quad g_n &= g_b^{-1} g_m g_b \\ \forall b, n \exists m : \quad g_m &= g_b g_n g_b^{-1} \end{aligned} \tag{3.65}$$

Thus the conjugate of any g by some other g' gives yet another g'' , so the g 's form a set which is closed under conjugation.

Let G be the group generated by the g -matrices. The set $\{g_1, \dots, g_d\}$ of g 's that occur in \mathcal{R} is then a union of conjugacy classes of G . We can order our basis by these conjugacy classes, by grouping basis vectors, e_i , together which have corresponding matrices, g_i , from the same conjugacy class. The e_i are then split into sets, A_j , where for any two elements, $e_a, e_b \in A_j$, their corresponding g -matrices are conjugate to each other, $g_a = X g_b X^{-1}$. The A_j then correspond to the conjugacy classes of G . We should note at this point that, as the g_i are not linearly independent, there can be multiple e_i corresponding to equivalent g -matrices.

Some features of the form of the g_i can now be deduced; we choose one such matrix, g_z . The condition from equation (3.64) means that the only non-zero elements of g_z will be those acting on basis elements whose corresponding g -matrix is conjugate to another g matrix by g_z . In short, there will only be non-zero elements between basis vectors from the same A_j set.

The basis has been ordered so that elements from the same A_j set are adjacent which means that g_z will take on a block diagonal form. The matrix, g_z , is then split into blocks of dimension d_{A_j} , where only blocks which correspond to the same A_j have non-zero elements.

For example; take a 7 dimensional local vector space where the g_i split into 3 conjugacy classes, $G = \{\{g_1, g_2\}, \{g_3, g_4, g_5\}, \{g_6, g_7\}\}$. We should reiterate that some of the g_i here may be equal, i.e. we have 7 basis vectors but not all

will correspond to a distinct g -matrix. The g -matrices then take the following form:

$$\begin{array}{c}
 A_1 \\
 A_2 \\
 A_3
 \end{array}
 \left\{
 \begin{array}{c}
 e_1 \\
 e_2 \\
 e_3 \\
 e_4 \\
 e_5 \\
 e_6 \\
 e_7
 \end{array}
 \left(
 \begin{array}{ccc}
 \begin{pmatrix} * & * \end{pmatrix} & 0 & 0 \\
 \begin{pmatrix} * & * \end{pmatrix} & & \\
 0 & \begin{pmatrix} * & * & * \\ * & * & * \\ * & * & * \end{pmatrix} & 0 \\
 0 & 0 & \begin{pmatrix} * & * \\ * & * \end{pmatrix}
 \end{array}
 \right)
 \right.
 \quad (3.66)$$

The block diagonal nature of the g 's lets us decompose the vector spaces, V , on which they act (i.e. the local vector spaces of the rings) into a direct sum of vector spaces containing basis vectors from the different conjugacy classes:

$$V = V^{A_1} \oplus V^{A_2} \oplus \dots \quad (3.67)$$

Any g will then act on V by acting individually with each of its submatrices, a_j , on the corresponding direct sum components, V^{A_j} . So the representation of \mathcal{R} acting on V decomposes into subrepresentations corresponding to the conjugacy classes of G .

It is worth noting that if all g_i are distinct, then the block matrices, a_j , will just be permutation matrices, with non-zero elements between basis vectors whose corresponding g -matrices are conjugate to each other under that particular g_i . However, as some of the g_i may be equivalent, more complicated forms of the a_j can occur.

The Copy Label

Assuming some of the g -matrices are equivalent, we look at one conjugacy class, A_j , where at least two distinct elements, g_a and g_b , have multiple copies. We can choose the order of the basis elements such that those corresponding to equivalent g 's are next to each other (equal g 's will obviously be in the same conjugacy class so the previous ordering is not affected).

Taking one matrix, g_d , we can look at one of its submatrices, a_j , which

corresponds to the conjugacy class, A_j , containing g_a , g_b and their copies. Assuming g_d is the matrix by which g_a and g_b are conjugate, there will be non-zero entries between any basis vectors whose g 's are equivalent. As the basis is ordered by those with equal g 's being adjacent, these non-zero elements will be grouped into block matrices with dimensions given by the number of copies of the g -matrices they relate. Thus the submatrix, a_j , is itself split up into submatrices, \hat{a}_k , which relate groups of equivalent basis vectors (but it is not necessarily block diagonal).

Earlier we saw how, in order for \mathcal{R} to be unitary, its submatrices, g_i , were required to be unitary. The same reasoning can be used to show that the submatrices of each g_i , a_j , must also be unitary and, furthermore, so must the submatrices of each a_i , \hat{a}_k . Thus we can safely say that the \hat{a}_k are square matrices, i.e. any groups of equivalent g 's must be the same size. Therefore, the elements of any conjugacy class, A_i , must all have the same number of copies. In our example the number of matrices that are equivalent to g_a must be the same as the number equivalent to g_b , as well as any other distinct g matrices in A_j .

This allows us to switch to a more convenient labelling of the basis vectors. Instead of using e_i , we will label such a vector by the distinct g -matrix to which it corresponds and also by an extra label which indicates which copy of that element which e_i corresponds to. While multiple basis vectors may then have the same g -label, their copy labels will differ. The subspace, V^{A_i} , can then be written as a tensor product of the form:

$$V^{A_i} = \mathbb{C}A_i \otimes V_\alpha \quad (3.68)$$

where $\mathbb{C}A_i$ is the algebra of the conjugacy class A_i , it has a basis of elements $|g_j\rangle$, with g_j in A_i . $V_\alpha = \mathbb{C}^{d_i}$ is a vector space with basis states $|p\rangle$, where p is an integer representing which copy of the element of A_i we are referring to. A state in this vector space then has the form;

$$|g_j, p\rangle = |g_j\rangle|p\rangle \quad (3.69)$$

Action of \mathcal{R}

Looking at the form of \mathcal{R} given in equation (3.60), we see that, while \mathcal{R} acts on two vector spaces simultaneously, it only alters the state of the first space. Specifically, the g -label of the state will be conjugated by the g -label of the state of the second vector space and the copy label will be changed by the action of some matrix, α , which depends on the g -label of both states. With the basis given in equation (3.69) for each of these vector spaces, this can be written as:

$$\mathcal{R}(|g_a\rangle|v\rangle \otimes |g_b\rangle|w\rangle) = |g_b g_a g_b^{-1}\rangle \alpha(g_a, g_b) |v\rangle \otimes |g_b\rangle |w\rangle \quad (3.70)$$

Now say we have two g -matrices, g_z and g_y , which both commute with a third, g_a . The vector spaces labelled by these g -matrices then form a (sub)system whose state is given by; $|g_a\rangle|a\rangle \otimes |g_y\rangle|y\rangle \otimes |g_z\rangle|z\rangle$. We can act on this system of three rings with \mathcal{R}_{12} , \mathcal{R}_{13} and \mathcal{R}_{23} , and this action must obey the Yang-Baxter relation (equation (3.24)):

$$\begin{aligned} \mathcal{R}_{12}\mathcal{R}_{13}\mathcal{R}_{23}(|g_a, a\rangle \otimes |g_y, y\rangle \otimes |g_z, z\rangle) &= \mathcal{R}_{23}\mathcal{R}_{13}\mathcal{R}_{12}(|g_a, a\rangle \otimes |g_y, y\rangle \otimes |g_z, z\rangle) \\ \alpha(g_a, g_z g_y g_z^{-1}) \alpha(g_a, g_z) |g_a, a\rangle \otimes \alpha(g_y, g_z) |g_z g_y g_z^{-1}, y\rangle \otimes |g_z, z\rangle &= \\ = \alpha(g_a, g_z) \alpha(g_a, g_y) |g_a, a\rangle \otimes \alpha(g_y, g_z) |g_z g_y g_z^{-1}, y\rangle \otimes |g_z, z\rangle \end{aligned}$$

In order for the Yang-Baxter relation to be satisfied we then must have:

$$\begin{aligned} \alpha(g_a, g_z g_y g_z^{-1}) \alpha(g_a, g_z) &= \alpha(g_a, g_z) \alpha(g_a, g_y) \\ \alpha(g_a, g_z g_y g_z^{-1}) &= \alpha(g_a, g_z) \alpha(g_a, g_y) [\alpha(g_a, g_z)]^{-1} \end{aligned} \quad (3.71)$$

This shows that, if c is an element of the centralizer of a conjugacy class, A_j , then $\alpha(c, A_j)$ is a representation of A_j under conjugation.

To give α a nicer form, we can choose for each conjugacy class, A , a special element g^A . For each $g_i \in A$, we then choose some element, x_{g_i} , of G such that; $x_{g_i} g^A x_{g_i}^{-1} = g_i$. The action of a particular x is; $x_{g_k} |g^A, p\rangle = \alpha(g^A, x_{g_k}) |g_k, p\rangle$. The basis vectors have already been ordered such that those corresponding to similar g -matrices are grouped together. Within these g -groups then, we can further order the basis vectors such that the x for a particular g -group maps each basis vector in the g -group to one with an equivalent copy number in the

g^A -group, i.e. we can choose our basis such that $\alpha(g^A, x_{g_k}) = \mathbb{1}$, for all g_k . The action of the x elements is then:

$$x_{g_k} |g^A, p\rangle = |g_k, p\rangle \quad (3.72)$$

Quantum Double Form

Now that we have completely fixed the basis of the local vector spaces (up to a phase) we can examine the action of some element, g_i , of the group G on this vector space:

$$\begin{aligned} g_i |g_k, p\rangle &= x_{g_i g_k g_i^{-1}} [x_{g_i g_k g_i^{-1}}]^{-1} g_i x_{g_k} [x_{g_k}]^{-1} |g_k, p\rangle = \\ &= x_{g_i g_k g_i^{-1}} [x_{g_i g_k g_i^{-1}}]^{-1} g_i x_{g_k} |g^A, p\rangle \end{aligned} \quad (3.73)$$

But we can easily see that $\left([x_{g_i g_k g_i^{-1}}]^{-1} g_i x_{g_k}\right)$ is an element of g^A 's centralizer:

$$\left([x_{g_i g_k g_i^{-1}}]^{-1} g_i x_{g_k}\right) g^A \left([x_{g_i g_k g_i^{-1}}]^{-1} g_i x_{g_k}\right)^{-1} = [x_{g_i g_k g_i^{-1}}]^{-1} g_i g_k g_i^{-1} x_{g_k} g^{-1} = g^A \quad (3.74)$$

where we have used the inverse of definition (3.72). Equation (3.73) then becomes:

$$\begin{aligned} x_{g_i g_k g_i^{-1}} [x_{g_i g_k g_i^{-1}}]^{-1} g_i x_{g_k} |g^A, p\rangle &= x_{g_i g_k g_i^{-1}} |g^A\rangle \alpha\left(g^A, [x_{g_i g_k g_i^{-1}}]^{-1} g_i x_{g_k}\right) |p\rangle = \\ &= |g_i g_k g_i^{-1}\rangle \alpha\left(g^A, [x_{g_i g_k g_i^{-1}}]^{-1} g_i x_{g_k}\right) |p\rangle \end{aligned} \quad (3.75)$$

But we have already seen that $\left([x_{g_i g_k g_i^{-1}}]^{-1} g_i x_{g_k}\right)$ is an element of g^A 's centralizer, therefore $\alpha\left(g^A, [x_{g_i g_k g_i^{-1}}]^{-1} g_i x_{g_k}\right)$ is a representation of this element.

For a group, H , with elements, $h \in H$, the quantum double, $D(H) = \mathbb{C}[H] \otimes F(H)$, is the group algebra generated by elements of the form $h \otimes e_h$, where F is some function of the group elements and $\mathbb{C}[H]$ is the group algebra associated with H [49, 50, 51]. By definition of the quantum double, there exists an element of $D(H) \otimes D(H)$ called the R -matrix given by:

$$R = \sum_{g,h} P_{hg} \otimes P_g \quad (3.76)$$

for $g, h \in H$. Taking these quantum double elements to label the states of some vector space we can look at the action of a single quantum double element, $P_h g \in D(H)$, on this space. Given the conjugate relationship between the group elements: $g P_h g^{-1} = P_{ghg^{-1}}$, we can order the basis such that conjugate elements are together to give invariant subspaces for each conjugacy class, A . The action of an element of the quantum double on one of these subspaces is then:

$$P_h g |h_i, v_j\rangle = \delta_{h, gh_i g^{-1}} |gh_i g^{-1}, \beta([x_{gh_i g^{-1}}]^{-1} g x_i) v_j\rangle \quad (3.77)$$

where: $h_i \in H$, v_j are the basis elements of a representation, β , of the centralizer of some special element, $A h$, of the conjugacy class and x_i is an element of H which relates h_i to this special element through conjugation. This action is easily seen to be equivalent to the action we have just derived for group elements acting on basis vectors of the representation of \mathcal{R} . Comparing equations (3.60) and (3.76), shows that \mathcal{R} is in fact the R -matrix of the quantum double of the group, G , labelling the basis states.

Thus, if the states of the local vector spaces of the rings are labelled by the distinct elements of a group, G , and the copy number of that element in G , then the representation of the slide operator, \mathcal{R} , will split into subrepresentations which act on subspaces corresponding to the conjugacy classes of G . Within a given subrepresentation, the action of \mathcal{R} is then equivalent to that of the R -matrix of the quantum double representation, $D(G) \otimes D(G)$. We have shown then that all local representations of the slide group are equivalent to representations of the quantum double of the group acting on the local vector spaces.

We must remember that this only gives us a representation of the slide group. However, once we have obtained such a representation of \mathfrak{S}_n , we can use it to induce a representation of the full motion group using the method outlined in section 3.3. This induced representation will usually not be irreducible but, given that it is induced from a non-Abelian representation of \mathfrak{S}_n , we know that there will be non-Abelian, irreducible subrepresentations within it.

3.5.1 6 Dimensional Example

A simple example is a 6^n -dimensional case. The loops of the fundamental group labelling each ring then take a 6-dimensional vector space with states labelled by the elements of some group of order 6 or higher (we could take a subgroup of a group with an order larger than 6).

The Dihedral Group

For this example we will choose the smallest such non-Abelian group, i.e. \mathcal{D}_3 , the dihedral group with two generators, $\{s, r\}$, and a presentation:

$$s^2 = e \quad r^3 = e \quad rs = sr^2 \quad (3.78)$$

This group then has 6 elements; $\{e, s, r, r^2, sr, sr^2\}$, which can be split into three conjugacy classes; $A_e = \{e\}$, $A_r = \{r, r^2\}$, $A_s = \{s, sr, sr^2\}$. Labelling the basis states by the elements of \mathcal{D}_3 , then gives us a 6-dimensional local vector space, V , for each ring. V will then naturally fall apart into a direct sum of three smaller vector spaces corresponding to the three conjugacy classes of \mathcal{D}_3 :

$$V = V^{A_e} \oplus V^{A_r} \oplus V^{A_s} \quad (3.79)$$

where $\dim(V^{A_e}) = 1$, $\dim(V^{A_r}) = 2$ and $\dim(V^{A_s}) = 3$. Each conjugacy class has only one copy of its elements so we can ignore the copy label for each state and the \mathcal{R} matrix becomes a direct sum of permutation matrices, up to phases, acting on the different vector spaces.

The Quantum Double Representation

As stated in the previous section, the representation of the R -matrix of the quantum double is given by (from equation (3.76)):

$$R = \sum_{h,g} P_h g \otimes P_g = \sum_g \left(\sum_h P_h \right) g \otimes P_g = \sum_g g \otimes P_g \quad (3.80)$$

for $g, h \in G$, $e_h g \in D(G)$, $R \in D(G) \otimes D(G)$ and P_j is a projection with $\sum_j P_j = \mathbb{1}$. We can see this directly matches our form for \mathcal{R} , as given in equation (3.60).

We can now act with \mathcal{R} separately on the subspaces associated with each of the conjugacy classes. V^{A_e} is a 1-dimensional vector space, on which \mathcal{R} acts trivially;

$$\mathcal{R}(V^{A_e} \otimes V^{A_e}) = \mathbb{1}_2(V^{A_e} \otimes V^{A_e})$$

V^{A_r} is a 2-dimensional space but, as the group elements labelling the basis vectors commute, we must have that \mathcal{R} acts trivially on this space too;

$$\mathcal{R}(V^{A_r} \otimes V^{A_r}) = \mathbb{1}_4(V^{A_r} \otimes V^{A_r})$$

For $q_i \in \{s, sr, sr^2\}$ we have, from the group relations in equation (3.78); $|q_1 q_2 q_1^{-1}\rangle = |q_3\rangle$. Thus, \mathcal{R} acts on V^{A_s} as a permutation matrix (up to a phase). We then have two trivial subrepresentations of \mathcal{R} and a non-Abelian subrepresentation acting on the vector space with states labelled by elements of A_s . However this non-Abelian, 3^n -dimensional local representation of the slide group is may still be reducible.

Reducing the non-Abelian Representation

For two rings, the 9-dimensional subrepresentation of \mathcal{R} acting on $V^{A_s} \otimes V^{A_s}$ can be reduced down into nine 1-dimensional representations and so the representation is Abelian. This can easily be deduced from the form of the two generators; \mathcal{R}_{12} will act only on the $V_1^{A_s}$ and \mathcal{R}_{21} will act only on $V_2^{A_s}$. The generators must therefore commute and so we can find a basis where both are represented by diagonal matrices.

We can now introduce the rest of the motion group generators, namely τ and f . The exchanges, τ , simply exchange the tensor factors; e.g. $\tau|s\rangle|sr\rangle = |sr\rangle|s\rangle$. The flips, f , act on a single tensor factor only but have no effect on these basis states; $f|s\rangle = |s^{-1}\rangle = |s\rangle$, $f|sr\rangle = |r^{-1}s^{-1}\rangle = |sr\rangle$, $f|sr^2\rangle = |r^{-2}s^{-1}\rangle = |sr^2\rangle$. Taking the full motion group into account, we will no longer have an Abelian representation. The states in the chosen basis now must be

invariant under τ and f operations as well as \mathcal{R} . We find that there will be five 1-dimensional subrepresentations which are Abelian but two 2-dimensional subrepresentations which can be non-Abelian.

For three rings, we can have a non-Abelian representation of the slide group alone. We now have generators, \mathcal{R}_{ij} , for $i, j \in \{1, 2, 3\}$, and, as in the previous case, we will have that \mathcal{R}_{ij} commutes with \mathcal{R}_{ji} , for all i, j . Also, from how we defined \mathcal{R} , we know that \mathcal{R}_{ik} will commute with \mathcal{R}_{jk} for all j, k . However, \mathcal{R}_{ij} and \mathcal{R}_{ik} will not necessarily commute, indeed we can find representations where they do not commute. We cannot, therefore, find a basis where all generators are simultaneously diagonal. Similar to the two ring case, we can now add in the other generators of the motion group which may add more interesting operations to the system.

Thus we are able to show that a system which can be described by such a local representation could possibly be utilized for non-Abelian computations, using the slide group alone as well as the full motion group. Note that it is known that the quantum double of D_3 is actually universal for anyonic braiding with a measure operation [52], and so we should expect these universality results to apply also for the $D(D_3)$ for the slide group of ring-shaped anyonic excitations. However, it is conjectured that such representations will never be universal for topological operations alone [45].

3.6 Conclusion

In this chapter we introduced the concept of (3+1)-dimensional anyonic excitations and showed that such quantum statistics are possible using ring-shaped anyons which are subject to the motion group. We saw that non-Abelian representations of such a system do exist and would be of potential use in topological quantum computation. The potential to increase the pool of possible systems in which to search for non-Abelian anyons presents a clear motivation for the study of these systems.

The bulk of the chapter focused on outlining three major procedures that can be used to obtain desired representations of a given system of rings; qubit representations of small numbers of rings, induced representations from non-Abelian slide group representations and local representations.

Qubit representations of the ring system were shown to have similar constraints to those found for the two-dimensional qubit models in chapter 2, with these results expected to continue to match for higher dimensional qudits.

We introduced the concept of local representations, which is defined by requiring the operators of the motion group to act non-trivially only on internal vector spaces associated with the rings which undergo the particular motion. Such representations were shown to provide a promising route to obtaining non-Abelian representations of a system of rings, presenting encouraging results for systems where increasing the number of rings did not alter the effect of the topological operations. This allows us to increase the number of possible logic operations on a qubit, potentially increasing efficiency, without compromising the universality of those operations. It also provides us with an easy way of producing many qubits.

Using results from ref. [47], we categorised all possible 2-dimensional local representations. For arbitrary dimension, we presented a proof showing how the local representation of the slide generator, \mathcal{R} , is related to the R -matrix of the quantum double of the group labelling the basis states of the vector spaces it acted on. With a representation for this operator, we showed how a representation of the full motion group could then be induced.

Chapter 4

Interacting Ising Anyons

The previous two chapters discussed the constraints imposed on a topological quantum computer by limitations placed on its constituent qubits due to the (abstract) mathematical laws they must obey (mainly the group-like nature of the operations). We were able to offer some guidelines on how to optimize the design of the computer within the confines of these laws.

However, in a real system these laws would not be the only constraints on the system. Although topological operations are robust against small perturbations of the system, unwanted topological changes which are out of our control may occur. Qubits should not be expected to exist in complete isolation and the inevitable interaction with their environment will have an effect on computations we perform.

This chapter focuses on one specific system where anyons are predicted to occur, we examine methods for creating qubits within this system and investigate how undesired interactions can affect the accuracy of calculations. By modelling these more realistic qubits, we hope similarly to the previous two chapters, to be able to provide some guidelines for how best to construct topological qubits in a physical system so as to minimize errors.

4.1 The Fractional Quantum Hall Effect

Fractional quantum Hall systems are currently among the most promising candidates for the physical realisation of topological qubits. When an electron gas is confined to a (2-dimensional) plane and subject to low temperatures and a strong, perpendicular magnetic field its Hall resistance, R_H , becomes

quantised [53];

$$R_H = \frac{1}{\nu} \frac{h}{e^2} \quad (4.1)$$

where e is the electron charge and h is Planck's constant. ν here is called the filling factor of the system, given by the ratio of electrons to magnetic flux quanta ($\Phi = hc/e$); $\nu = N_e/N_\Phi$, where N_Φ is the number of flux quanta. This quantisation of R_H is known as the quantum Hall effect. Semi-classically, the filling factor can take on non-integer values [54] giving rise to fractional quantum Hall systems.

At all integer values of the filling factor we would naively expect the Hall conductance, σ_H , to increase inversely to the magnetic field. However, experiments [53] show the presence of plateaus in the Hall conductance as the magnetic field is varied. Electrons moving in 2 dimensions in a perpendicular field have their kinetic energy quantised into Landau levels [55, 56]. The Landau levels for electronic systems have a degeneracy which is proportional to N_Φ , so if we decrease the magnetic field we decrease the degeneracy of the Landau levels and force electrons to occupy higher Landau levels (with higher kinetic energy) thus increasing the conductance.

When disorder is present in the system it splits the degeneracy of the Landau levels. The disorder potential allows electrons to take energy values between the Landau levels but these electrons are localised about equipotential contours and so do not contribute to the Hall conductance. Thus, when the magnetic field is decreased and some electrons are forced out of their Landau level, they may not reach the energy of the next Landau level and instead move to one of these localised states. Here they don't contribute to the current density and so the Hall conductance is not increased. We then don't see the proportional decrease in the Hall resistance we expect from the classical $R_H \propto B$ formula, rather plateaus appear where the localised states prohibit the Hall conductance from increasing with lower magnetic field. Such a plateau persists until an electron is excited to an extended state, this electron is not localised and so contributes to the conductance [57, 58, 59].

For certain fractional values of the filling factor the quantum Hall effect also displays plateaus, generally when ν is a simple, odd-denominator fraction. For

fractional filling of the lowest Landau level, $\nu < 2$ (for 2 spin directions), we see prominent plateaus at $\nu = 1/3, 1/7$, as well as $\nu = p/(2p \pm 1)$. In the first Landau level, $2 < \nu < 4$, we see new plateaus at $\nu = 5/2, 7/2$ and $12/5$.

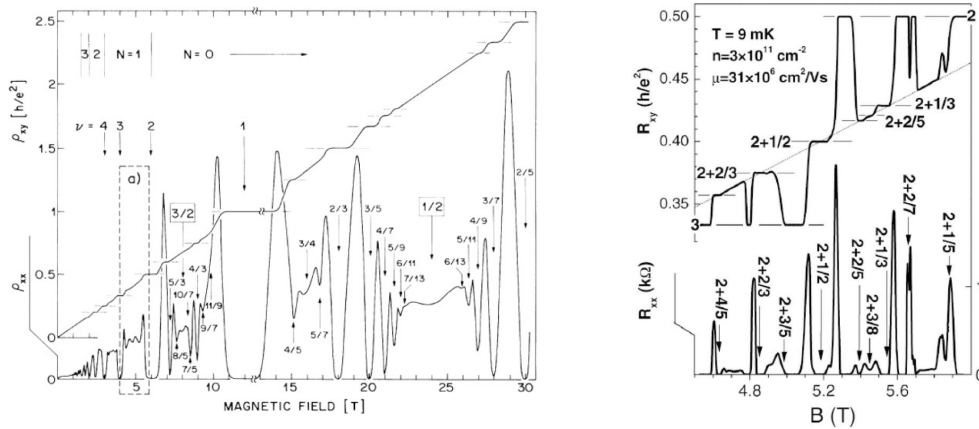


Figure 4.1: Quantised Hall states in the first (left) and second (right) Landau levels. R_{xy}, R_H are the Hall resistance and R, R_{xx} are the longitudinal resistance which goes to zero at the plateaus. Sources: refs. [60] and [61] respectively (reprinted with permission).

Trial Wavefunctions

The explanation behind these fractional quantum Hall states, however, is much more complex than the integer case. For filling fractions that are less than one, all electrons are in the lowest Landau level, meaning the kinetic energy is the same for all states and can be set to zero [62]. It is clear then, that the system is dominated by the interaction between the electrons. However, the specific underlying cause of the effect has not yet been fully determined, so we must rely on phenomenological descriptions in terms of trial wavefunctions or effective field theories, see for example refs. [63, 64]. From these approximations we can extrapolate some of the physics of the system, which can be compared to physical observations to determine the accuracy of the prediction, as well as using direct comparison with exact solutions from numerical models for small systems.

Trial wavefunctions have been proposed for a variety of fractional filling factors, including the Laughlin states at $\nu = 1/q$ ($q = \text{odd}$) [63] and the composite fermion / hierarchy states at $\nu = p/(2p \pm 1)$ [65, 66], and, while all studied states are predicted to exhibit anyonic excitations, for the most part these excitations are expected to be Abelian in nature [67].

The Pfaffian wavefunction proposed by Moore and Read [19] and its particle hole conjugate, the antiPfaffian state [68, 69], have been shown through numerical analysis to have a large overlap with the state at $\nu = 5/2$ [70, 71, 72, 73]. Though it is still unclear which best describes the state [74, 75] (recent results slightly favour the antiPfaffian [76]). This makes the $\nu = 5/2$ state of particular interest as the excitations of both the Pfaffian and antiPfaffian trial states carry non-Abelian statistics and so present a candidate system for topological quantum computation [77, 78]. While these statistics alone are not sufficient for universal quantum computation, methods have been devised to combine them with certain non-topologically protected operations in order to achieve universality [79, 80].

Non-Abelian statistics have also been predicted on the basis of other trial wavefunctions which have been shown to have good overlaps with certain fractional quantum Hall states, including the Read-Rezayi state [81, 82] at $\nu = 12/5$ and the Bonderson-Slingerland state [83, 84] at $\nu = 12/5$ and $\nu = 2 + 3/8$. However the Moore-Read state currently presents the best prospect for developing topological qubits, its larger gap to excitations means it can be seen at higher temperatures [61]. It is then more likely that experiments will observe and be able to manipulate this state than these other suggested states.

Qubits in FQH Liquids

Naturally the $\nu = 5/2$ state is under intense scrutiny at the moment and much effort has been made to address the question of how one might construct and operate on a qubit in the system. The interaction between quasiparticles in the bulk and the excitations on the edge of the system present a challenge to the construction of any qubit in the system.

In current proposals, qubits are imagined as collections of anyons in the bulk of the system. The state in which the qubit resides is determined by the fusion channels of the bulk anyons, as discussed in section 1.4. However, the integrity of the state may be compromised due to inevitable interactions between the qubit and edge excitations, as well as interactions between anyons in the bulk.

To be confident in the calculation performed by our topological computer,

we must then ensure to implement a design of the qubits which would minimize any compromising effects of the edge-bulk and anyon-anyon interactions, or at least we would like to understand these effects so that we can compensate for them in our calculations. To this end, this chapter focuses on modelling anyons in a $\nu = 5/2$ fractional quantum Hall sample in order to ascertain how exactly these interactions affect the state of the qubits. To do this, we must derive the eigenstates of the interacting system in order to calculate the time evolution of any information stored in the qubit.

4.2 The Ring Model

We take as our system a 2-dimensional electron gas subject to low temperatures and a strong, perpendicular magnetic field and we ensure that the ratio of electrons to magnetic flux quanta is appropriate to produce a fractional quantum Hall state at filling factor $\nu = 5/2$.

The incompressibility of a fractional quantum Hall fluid means it will try to maintain a constant density throughout. However, we will assume that the density would naturally decrease towards the edges, lowering the filling factor here and resulting in the creation of quasiparticle excitations in an attempt to keep the density constant [85]. Alternatively we can ensure that the quasiparticles will be created close to the edge by increasing the number of impurities here (as quasiparticles tend to be localised on impurities [86]) or by altering the magnetic field or electron density close to the edge.

For a circular droplet then, we can assume that these excitations approximate a circular ring close to the edge of the sample. This ring of bulk quasiparticles forms the qubit (or qubits) of the system, i.e. it is where we plan to store the information for quantum computations. For the predicted anyon model for this system (discussed more in the Ising anyon section), every pair of anyons has two possible fusion channels, forming a two-level system, so in a non-interacting system we would have $N/2 - 1$ qubits, for N anyons. The -1 factor here comes from choosing that the overall topological charge of the system to be the vacuum (this will actually depend on the number of the anyons in the system but we would expect excitations to be created in pairs which would fuse back to the vacuum).

The Chiral Edge

Being an incompressible liquid (see refs. [63, 87]), the fractional quantum Hall system has an energy gap to excitations in the bulk. The only low-lying excitations then, are surface waves along the edge of the liquid. At the boundary of the system there is a confining potential which pushes the energy of the Landau levels above the Fermi surface creating gapless excitations which are restricted to the 1-dimensional edge due to the bulk gap.

The Hall conductance and electric confinement generate a current which causes these excitations to propagate along the edge. With the direction of the propagation set by the magnetic field and backscattering suppressed by the necessarily strong nature of this field [88], these edge modes are chiral in nature.

The edge excitations can then be shown to be described by a $U(1)$ Kac-Moody algebra [89], for which the Hilbert space of the chiral boson theory forms a representation. By calculating the electron propagator it is found that the electrons are strongly correlated, with the electron correlator having an anomalous exponent. These states then resemble Luttinger liquids, where the electron correlator also bears an anomalous exponent [27]. Then, due to the unidirectionality of these edge modes, we can say that the edge can be thought of as a chiral Luttinger liquid. A series of papers by Wen and Lee [27, 90, 91, 89] show this in greater detail.

Most importantly for us, as we will see in later sections, the low energy excitations of a Luttinger liquid can be described by an appropriate conformal field theory [92, 93], and so the edge of a fractional quantum Hall liquid can be treated as a chiral conformal field theory.

Ising Anyons

The non-Abelian anyon species which are proposed to be present in the $\nu = 5/2$ state are of Ising type [19], meaning the edge is described by the Ising conformal field theory. The Ising CFT actually only describes the neutral excitations of the $\nu = 5/2$ state, for a full description of the $\nu = 5/2$ state we should tensor this Ising CFT with a $U(1)$ theory which describes the charged excitations. However, the charged excitations will only contribute Abelian phases to the

braiding representations [80], owing to the 1-dimensional nature of the $U(1)$ description. We will, therefore, largely ignore this part and concentrate solely on the neutral excitations.

This Ising CFT has three species of anyon; a topologically trivial particle, 1, a fermion, ψ , and an Ising anyon, σ , which have conformal weights; 0, 1/2 and 1/16 respectively and obey the Ising fusion rules:

$$\begin{aligned}
1 \times 1 &= 1, & 1 \times \psi &= \psi, & 1 \times \sigma &= \sigma \\
\psi \times \psi &= 1, & \psi \times \sigma &= \sigma \\
\sigma \times \sigma &= 1 + \psi
\end{aligned}
\tag{4.2}$$

along with their symmetric counterparts. Our model then consists of a ring of σ anyons excited close to the edge of a $\nu = 5/2$ fractional quantum Hall puddle, which interact with each other through the Ising fusion rules in equation (4.2) (a detailed Hamiltonian for this system will be given in section 4.3).

We can obtain the topological charge of the entire ring by looking at its fusion tree; we pick a particular σ and fuse it with a neighbouring σ , then fuse this product with the next σ and so on for all σ 's in the chain. A standard basis for such a chain is to label states by the possible labellings of the fusion tree, as shown in figure 4.2.

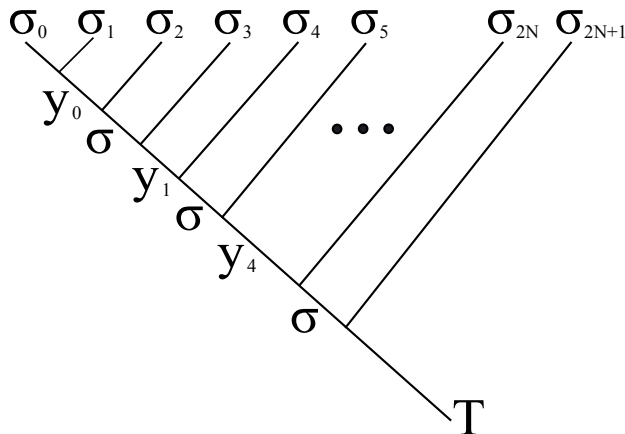


Figure 4.2: Fusion tree for a collection of interacting σ anyons. $y_i \in \{1/\psi\}$ labels the fusion of channel of all anyons to its left, i.e. $y_i \in \{\sigma_0 \times \sigma_1 \times \dots \times \sigma_{i+1}\}$ and T is the combined topological charge of all anyons in the system.

The links between even and odd numbered σ 's are fixed, due to the Ising fusion rules (equation (4.2)) all anyons to the left of any of these links must fuse to a σ charge. The links between odd and even numbered σ 's (labelled

by y 's in the figure), however, are variable, they can be labelled by either 1 or ψ . Each of these y -labelled links then has an associated 2-dimensional vector space, V , spanned by the states $\{|1\rangle, |\psi\rangle\}$.

However, as the chain is circular, the final fusion product must fuse back to the first σ . Due to translational invariance of the chain, we would expect the fusion between the N^{th} and zeroth anyons to behave in a similar fashion to all other fusions. This translational invariance is not apparent in our above basis choice, as each label is dependent on the fusions which preceded it and so different sites must be treated differently.

We will be interested in calculating the effect of anyons interacting with their nearest neighbours, it will therefore be useful to move to a more suitable basis which allows for a more simple interpretation of these interactions. We can perform an F -move on each of the (even, odd) links (i.e. those which must take a σ value) to produce a fusion tree in which each even numbered σ fuses with the odd numbered σ to its right, before combining with the fusion product of the anyons to the left of this pair. The F -move which performs this basis change is in fact trivial, $[F_{y'}^{y\sigma\sigma}]_{\sigma,y''} = 1$, for $y, y', y'' \in \{1/\psi\}$. So we can say this new basis, with (even, odd) pair fusing as shown in figure 4.3, is equivalent to the basis in figure 4.2.

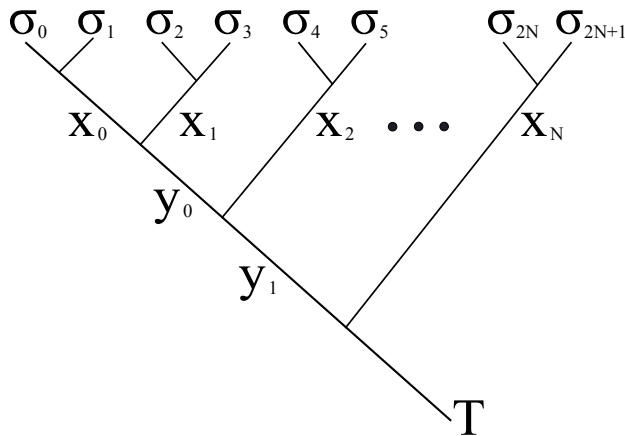


Figure 4.3: Fusion tree for σ anyons in an (even, odd) pairing basis. The $X_i \in \{1/\psi\}$ now label the fusion channel of only the individual pairs, i.e. $X_i \in \{\sigma_{2i} \times \sigma_{2i+1}\}$. The $y_i \in \{1/\psi\}$ labels on the main fusion branch are equivalent to the y labels in figure 4.2, they denote the fusion channel of all X 's (and hence all σ 's) to its left.

Clearly the basis in shown in figure 4.3 is only suitable for an even number of anyons, thus $T = 1/\psi$. For an odd number of anyons, we can still pair

them in a similar fashion, the only difference will be a single, lone anyon at the end of the tree, σ_{2N} . Thus for the odd case we must have $T = \sigma$. However, calculation of the interactions between neighbouring anyons is unaffected and can be carried out in the same manner as for the even case as we will see in the next section.

4.3 Anyon Ring Hamiltonian

An obvious place to start is by constructing the Hamiltonian for the ring of anyons, as done in ref. [94, 95, 86], this allows us to determine the dynamics of our qubits in isolation from any external interactions.

Firstly we look at an open chain of anyons. The Hamiltonian can be obtained by implementing an interaction between all neighbouring σ anyons which will be dependent on their fusion channel [24, 96, 97]. We then follow a similar procedure to the one outlined for Fibonacci anyons in ref. [94] and [95], to find the contribution of each site to the Hamiltonian.

We use the basis defined in figure 4.3 in the previous section, where anyons fuse together in (even, odd) pairings. An interaction is implemented by assigning some energy penalty to the fusion channels of the anyons, then, as each pair has two fusion channels, the interaction takes the form; $\Pi^J = J\sigma^z$ (σ^z is a Pauli matrix and is not associated with the σ anyons) where the sign of J will determine which channel is favoured (if $J > 0$ the ψ channel is favoured in this formulation).

We start by examining the interaction between these (even, odd) anyon pairs. In our chosen basis, this just involves applying the above interaction operator, Π^J , to the vector space associated with the fusion charge of each (even, odd) anyon pair. If we let Π_i and σ_i^z be operators which act trivially on the vector spaces of all X labels except for V_i , on which the Π or σ^z operators are applied respectively, then this interaction contributes a value of $\sum_{i=1}^N \Pi_i^J = -J \sum_{i=1}^N \sigma_i^z$.

We now need to account for the interaction between the (odd, even) anyon pairs. To do this, we must change to a basis where such anyons fuse together in this order. Take a subspace of 4 anyons, σ_{i-1} to σ_{i+2} , which, in our current basis, are fused with (σ_{i-1}, σ_i) giving a vector space, $V_{\frac{i-1}{2}}$, of their fusion

charges and $(\sigma_{i+1}, \sigma_{i+2})$ giving a vector space, $V_{\frac{i+1}{2}}$. For notational ease, we will label these two fusion charges as a and b respectively. The charge a then fuses with the total charge of all preceding anyons, $K \in \{X_0 \times \dots \times X_{\frac{i-3}{2}}\}$, giving $a \times K = L$, which then fuses with b to give $L \times b = M$ as the total charge of the first $i + 2$ anyons.

A trivial F -move allows us to move to a basis where a first fuses with b , giving a charge $y \in \{\sigma_{i-1} \times \sigma_i \times \sigma_{i+1} \times \sigma_{i+2}\}$ with $K \times y = M$ determining the values of y . Using another trivial F -move we can make a fuse with σ_{i+1} , to give a σ charge, before fusing with σ_{i+2} , to give y . Finally we must perform a non-trivial F -move on a , $[F_{\sigma}^{\sigma_{i-1}\sigma_i\sigma_{i+1}}]_{a,\tilde{a}}$, to move to a basis where σ_i and σ_{i+1} fuse together to give some charge, \tilde{a} .

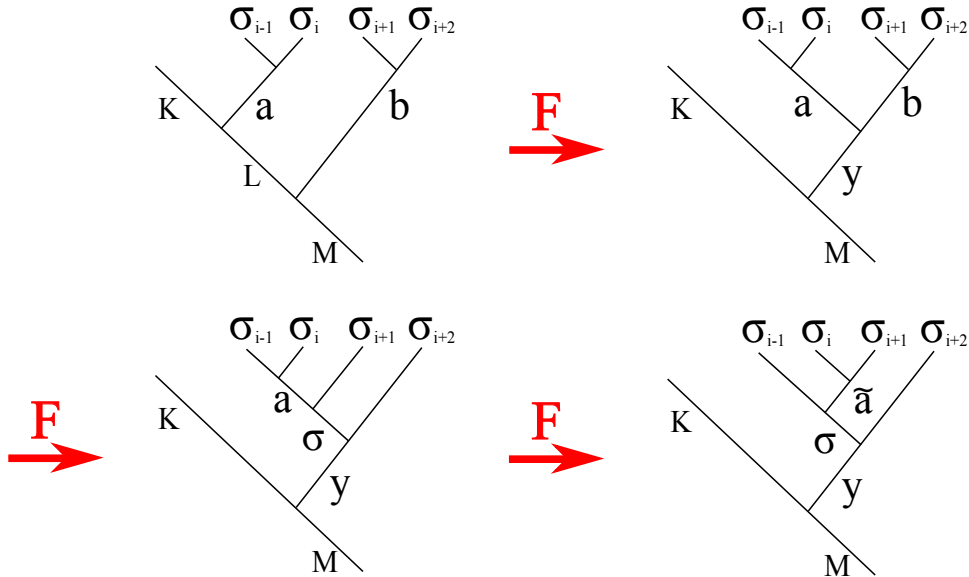


Figure 4.4: The process needed to move to a basis where an odd numbered anyon, σ_i , is paired with the even numbered anyon, σ_{i+1} , to its right. Only the final F -move shown is non-trivial.

As shown in figure 4.4, we now have a basis where σ_i is paired with σ_{i+1} , as desired. At this stage we implement the interaction as before, by applying the interaction operator, $J\sigma^z$, to the vector space associated with the charge of σ_i and σ_{i+1} , i.e. \tilde{a} .

Lastly we must reverse all of the operations performed to get to this basis, in order to return to our original basis of (even,odd) pairings. While inverting the various F -moves brings us back to our original basis, the entire process may result in a non-trivial action on our original vector spaces. The two spaces are then given new labels a' and b' , which are not necessarily the same as a

and b . However, while the vector spaces a and b may have been altered, the ultimate fusion of the four anyons cannot be affected by this process, i.e. we still must have $a' \times b' = a \times b = y$.

But a' is related to the original a by the following series of non-trivial operations;

$$a' = [F_{\sigma}^{\sigma_{i-1}\sigma_i\sigma_{i+1}}]_{\bar{a},a'} \Pi_{a'}^J [F_{\sigma}^{\sigma_{i-1}\sigma_i\sigma_{i+1}}]_{a,\bar{a}} a \quad (4.3)$$

and all F -moves of this form are equivalent, i.e. we have $a' = [F_{\sigma}^{\sigma\sigma\sigma}]^{-1} \Pi^J [F_{\sigma}^{\sigma\sigma\sigma}] a$, where;

$$F = [F_{\sigma}^{\sigma\sigma\sigma}] = \frac{1}{\sqrt{2}} \begin{pmatrix} 1 & 1 \\ 1 & -1 \end{pmatrix} \quad (4.4)$$

Thus with the value of Π^J given above, we have: $a' = \sigma^x a$ (σ^x is also Pauli matrix and is not associated with the σ anyons). So this process will ‘flip’ the state of a to the opposite fusion channel. Then for $a' \times b' = a \times b$ to hold we must also have $b' = \sigma^x b$. Thus the interaction between σ_i and σ_{i+1} causes the state of a to be flipped, which forces the state of b to also be flipped, in order for the total charge of the four anyons to remain unchanged.

We can perform a similar procedure for all (odd,even) pairings in the system, and so this interaction then contributes a factor of $J \sum_{i=1}^N \sigma_i^x \sigma_{i+1}^x$. Our resultant Hamiltonian is then a combination of the contributions from both the (even,odd) interactions and (odd,even) interactions:

$$H = J \sum_{i=1}^{N-1} \sigma_i^x \sigma_{i+1}^x + \sum_{i=1}^N \sigma_i^z \quad (4.5)$$

This is the Hamiltonian for a *chain* of interacting σ anyons. To describe the *ring* of anyons which features in our model, we need to close the chain by allowing the first and last anyons to interact. Due to translational invariance of the ring, we should be able to shift the numbering of the anyons without changing the physics, i.e. our choice of σ_0 is arbitrary and the system should behave the same regardless of this choice. The interaction between σ_N and σ_0 should then have an equivalent contribution to the other interactions in the system, i.e. we should get a $\sigma^x \otimes \sigma^x$ factor acting on the two vector spaces

involved, namely V_0 and V_N .

When obtaining Hamiltonians corresponding to interacting anyons, it is convention to set the energy assigned to one of the fusion channels to zero. This can be easily done by shifting the values assigned by interaction operator by J and setting $J = J/2$;

$$\Pi^{J/2} \mapsto \frac{J}{2} \mathbb{1}_2 - \Pi^{J/2} = J \begin{pmatrix} 0 & 0 \\ 0 & 1 \end{pmatrix} \quad (4.6)$$

where we have chosen to assign the zero energy to the 1 channel. This will have no effect on the Hamiltonian we have obtained; for each i we get an extra $-\mathbb{1}_i \otimes -\mathbb{1}_i = \mathbb{1}$ term from the $\sigma_i^x \sigma_{i+1}^x$ term and an extra $-\mathbb{1}_i$ term from the σ_i^z , which will obviously cancel. The only difference, is that now a positive J will penalize the ψ channel but we can add an overall negative sign to bring this in-line with our original formulation. According to ref. [98, 96] the ψ channel can have a lower energy, this is largely dependent on the distance between the anyons and can oscillate between positive and negative but the sign difference will not ultimately affect our results. We would like to choose J such that the ψ channel has an energy of $-J$, i.e. $J > 0$, this means we give an energy penalty to the 1 channel so that a given Ising link prefers to have a ψ charge. This finally gives the Hamiltonian as:

$$H = -J \sum_{i=1}^N \{ \sigma_i^x \sigma_{i+1}^x + \sigma_i^z \} \quad (4.7)$$

But equation (4.5) can be recognised as the Hamiltonian for the transverse field Ising model (TFIM) [99] at its critical point, with the magnetic field in the z direction.

The anyon ring described by this Hamiltonian is then coupled somehow to chiral edge modes described by an Ising conformal field theory. This coupling has been explored previously for the interaction between single bulk anyons and the edge [100, 85]. Before we examine the coupling in detail we first need to study the internal dynamics of the ring of bulk excitations.

4.3.1 The Transverse Field Ising Model

The method for diagonalising the above Hamiltonian (equation (4.7)) for the TFIM is well known, however, we will outline the procedure here to highlight some aspects which will be of particular importance when we move to our circular chain case. We will follow the derivations provided in ref. [101, 102, 103].

Open Chain

We start with the general form of the transverse field Ising Hamiltonian i.e. not at its critical point. With the magnetic field in the z direction this is written as:

$$H = -J \left\{ \sum_{i=0}^N \sigma_i^x \sigma_{i+1}^x + g \sum_{i=1}^N \sigma_i^z \right\} \quad (4.8)$$

Note in the finite, open chain case, the particles on the ends of the chain are nondynamical, their values are fixed by the boundary conditions. Therefore this calculation is done over a chain of length $N + 2$, where sites 0 and $N + 1$, the end sites, are fixed to be either equal or unequal. The first term in equation (4.8) gives the nearest neighbour interaction between the spins with an interaction energy of J , the second term gives the coupling to the perpendicular magnetic field, where Jg is the strength of the magnetic field. This model clearly reproduces equation (4.7) when $g = 1$, which also happens to be a quantum critical point between the ferromagnetic, $g < 1$, and paramagnetic, $g > 1$, phases of the TFIM.

Our first step is to move from a spin description of the model to a fermionic description wherein spin values on sites are reinterpreted as sites which are either occupied or unoccupied by a fermion. This is done using the following Jordan-Wigner transformation [104]:

$$\begin{aligned} \sigma_i^z &= 1 - 2c_i^\dagger c_i \\ \sigma_i^+ &= \frac{1}{2}(\sigma_i^x + i\sigma_i^y) = \prod_{j<i} (1 - 2c_j^\dagger c_j) c_i \\ \sigma_i^- &= \frac{1}{2}(\sigma_i^x - i\sigma_i^y) = \prod_{j<i} (1 - 2c_j^\dagger c_j) c_i^\dagger \end{aligned} \quad (4.9)$$

where: c_i^\dagger and c_i are fermionic creation and annihilation operators. Some algebraic manipulation then gives the fermionised Hamiltonian as:

$$H_f = -J \left\{ \sum_{i=0}^N [c_{i+1}c_i + c_{i+1}^\dagger c_i + c_i^\dagger c_{i+1} + c_i^\dagger c_{i+1}^\dagger] + g \sum_{i=1}^N [1 - 2c_i^\dagger c_i] \right\} \quad (4.10)$$

We can move to the momentum basis by introducing fermionic momentum operators, c_k , and then perform a Bogoliubov transformation [105], by switching to a description in terms of fermions which have creation operators;

$$\gamma_k^\dagger = u_k c_k^\dagger + i v_k c_{-k} \quad (4.11)$$

We choose the coefficients u_k and v_k so as to eliminate all terms which don't conserve fermion number:

$$u_k = \cos\left(\frac{\theta_k}{2}\right) \quad v_k = \sin\left(\frac{\theta_k}{2}\right) \quad \theta_k = \tan^{-1}\left(\frac{\sin(k)}{\cos(k) - g}\right) \quad (4.12)$$

Lastly, absorbing a constant term into the definition of H leaves us with the fully diagonalised Hamiltonian:

$$H = \sum_k \epsilon_k \left(\gamma_k^\dagger \gamma_k - \frac{1}{2} \right) \quad (4.13)$$

where $\epsilon_k = 2J\sqrt{1 + g^2 - 2g\cos(k)}$ is the excitation energy of a Bogoliubov fermion with momentum k . Inserting $g = 1$, to match up with our anyon model then leaves us with:

$$\epsilon_k = 4J \left| \sin\left(\frac{k}{2}\right) \right| \quad (4.14)$$

For appropriate values of N and J then, we can have arbitrarily small excitation energies, thus the system is gapless indicating that $g = 1$ is indeed a critical point of the TFIM. The possible momenta, k , will be restricted by the fixed boundary conditions on the finite chain, see for example refs. [99, 102] which give:

$$k = \frac{\pi}{N+1} \left(m + \frac{\theta_k}{\pi} \right) \quad \{\text{for integer } m\} \quad (4.15)$$

For $g \geq 1$ equation (4.15), with θ_k given in definitions (4.12), has N real solutions for $0 \leq k \leq \pi$. For $g < 1$ however, there are $N - 1$ real roots and one complex root of the form; $k_0 = \pi + i\lambda$ corresponding to a single localised Majorana mode. At the critical point, $g = 1$, the roots of equation (4.15) take on the simplified form:

$$k = \frac{(2m + 1)\pi}{2N + 1} \quad \{\text{for: } m = 0, \dots, N - 1\} \quad (4.16)$$

If g is not restricted to the critical point, we can use the result to describe a model with paramagnetic ($g > 1$) and ferromagnetic ($g < 1$) sections. One dimensional wires, with such paramagnetic and ferromagnetic sections, contain Majorana fermions on the critical boundary between them and have been used in another proposed TQC model [106, 3]. Many of our results will then have relevance to this TQC implementation also.

We have assumed in the above calculations that the interaction between each pair of anyons is of the same strength (implying that all anyons are evenly spaced throughout the ring). However, it is likely that this will not be the case in reality and the interaction between the anyons will vary. This can be accounted for by implementing a per site interaction strength, J_i , and field strength, g_i . We should then reformulate the Hamiltonian as:

$$H' = \sum_i \{J_i \sigma_i^z \sigma_{i+1}^z + g_i \sigma_i^x\} \quad (4.17)$$

We can use a Jordan-Wigner transformation to fermionise the system in a similar fashion to before but, as the system is no longer translationally invariant, we cannot diagonalise the Hamiltonian in the momentum basis to obtain momentum dependent energies of the form in equation (4.14). Nonetheless it will prove useful to keep this model in mind as a comparison to our “evenly spaced, homogeneous field” model and we will periodically return to this alternative model as we proceed through this chapter.

Closed Chain

Now we need to reintroduce the fact that this chain is actually a closed ring, which will have an effect on the the outcome of the diagonalisation, specifically

on the permitted momenta.

Firstly, into the original Ising chain Hamiltonian, equation (4.7), we insert an extra term which accounts for the Ising interaction between the last and first σ anyons, as discussed earlier:

$$H_c = -J \left\{ \sum_{i=0}^{N-1} (\sigma_i^z \sigma_{i+1}^z + \sigma_i^x) + \sigma_N^z \sigma_0^z \right\} \quad (4.18)$$

Performing a similar Jordan-Wigner transformation and basis change, as was outlined above in equation (4.9), gives:

$$H_c = -J \left\{ \sum_{i=0}^{N-2} (c_i^\dagger + c_i)(c_{i+1}^\dagger - c_{i+1}) - P(c_{N-1}^\dagger + c_{N-1})(c_0^\dagger - c_0) + \sum_{i=0}^{N-1} (1 - 2c_i^\dagger c_i) \right\} \quad (4.19)$$

This is similar to equation (4.10) except we have an extra term accounting for the closed nature of the chain. It is not immediately clear how we would diagonalise this Hamiltonian, so we would like to express it in a more familiar form. To this end we introduce the parity operator, P :

$$P = \prod_{j < N+1} (1 - 2c_j^\dagger c_j) = (-1)^F \quad (4.20)$$

Note $(-1)^F$ will give -1 if F is odd and $+1$ if F is even, where we have used the fact that $1 - 2c_j^\dagger c_j = -1$ if a fermion is present and $+1$ if not. As the product in the above formula is over all sites, F simply counts the number of sites which are occupied by a fermion. Hence, P gives ± 1 depending on whether there is an even or odd number of fermions present in the chain, it is then referred to as the parity term.

We see that, if there is an odd number of occupied sites, $P = -1$, then the extra term is of the same form as the first term and so this term can be absorbed into the first sum. We know that the N^{th} site must be identified with the 0^{th} site in order to close the chain into a ring, so we relabel $c_0 = c_N$ and the Hamiltonian is then in the same form as in equation (4.10), i.e. $H_c = H_f$, but with periodic boundary conditions.

However, if there is an even number of occupied sites, $P = +1$, then the parity operator term has the wrong sign and so cannot be absorbed into the

sum of the first term. To remedy this, we introduce antiperiodic boundary conditions, $c_0 = -c_N$. Again this puts equation (4.19) in the same form as equation (4.10) but now with antiperiodic boundary conditions.

Thus we are separating the Hilbert space into two subspaces according to the parity of the number of occupied sites. We then consider the Hamiltonian, H_f , acting on each subspace separately.

From here, we can just follow the same procedure as in the open chain case, meaning we obtain a similar result for the closed Hamiltonian:

$$H_c = \sum_k \epsilon_k \left(\gamma_k^\dagger \gamma_k - \frac{1}{2} \right) \quad (4.21)$$

We must now say something about the restrictions on the values of the momentum k which arise from the discretisation of a finite chain with periodic or antiperiodic boundary conditions. We obtain different restrictions for the two Hilbert subspaces:

$$k = \begin{cases} \frac{2m\pi}{N} & \text{If } P = -1 \\ \frac{(2m+1)\pi}{N} & \text{If } P = +1 \end{cases} \quad (4.22)$$

for $-\frac{N}{2} \leq m \leq \frac{N}{2} - 1$ if N is even and $-\frac{N-1}{2} \leq m \leq \frac{N-1}{2}$ if N is odd. It is important to remember that N here is the number of fermionic sites in the chain, i.e. the number of spins in the transverse field Ising model, but as the chain sites refer only to every second link in the anyon fusion tree the number of anyons in the chain will actually be $2N$.

Summarising; if there is an odd number of occupied sites, then the momenta of the Bogoliubov fermions (i.e. the fermions created by application of the γ_k^\dagger operators) are restricted to integer multiples of π/N and, if there is an even number of occupied sites, then the momenta are restricted to half-integer multiples of π/N .

The Ground State

The ground state of a system described by the Hamiltonian in equation (4.21) is of the form of the BCS ground state [107, 108]. It is a product of the Bogoliubov annihilation operators acting on the vacuum, $|gs\rangle = |BCS\rangle = \prod_k \gamma_k |0\rangle$. It

is important to calculate the contribution to the ground state energy of the $k = 0$ and $k = \pi$ modes. As these both satisfy $k = -k$, their omission from the ground state could, depending on the phase, lower its energy, see ref. [109]. At the critical point, $\epsilon_0 = 0$, so the $k = 0$ mode contributes nothing to the energy of the groundstate. Its inclusion in the product then makes no difference to the ground state energy but we must omit it as $\gamma_0 = c_0$ which would give; $|gs\rangle = \prod_{k \neq 0} \gamma_k \gamma_0 |0\rangle = 0$. For $k = \pi$ we have $\epsilon_\pi = 4J$, its inclusion then increases the energy of the ground state and so we should also omit this mode from the product. Normalising, we then get the ground state in the following form:

$$|gs\rangle = \prod_{0 < k < \pi} (u_k + iv_k c_k^\dagger c_{-k}^\dagger) |0\rangle \quad (4.23)$$

However, the range of k values will be different depending on which parity sector we are in, thus we get two separate states which we label $|gs_{even}\rangle$ and $|gs_{odd}\rangle$. Note that this is just for notational ease, it is not clear yet which one of these is the actual ground state. Also $|gs_{odd}\rangle$ is not the ground state of the odd sector, in fact it is not even an eigenstate of the system as valid odd sector states must be given by a product of an odd number of γ_k^\dagger acting on $|gs_{odd}\rangle$. It can be easily checked that any γ_k will annihilate the appropriate ‘‘ground’’ state. We can obtain the energy of either state with by acting on it with H_c . For $|gs_{even}\rangle$ we get:

$$H_c |gs_{even}\rangle = - \sum_k \frac{\epsilon_k}{2} |gs_{even}\rangle = -2J \sum_{m=0}^{N-1} \sin \left[\frac{(2m+1)\pi}{2N} \right] |gs_{even}\rangle \quad (4.24)$$

We write the sin term in exponential form and use $\sum_{j=0}^{L-1} x^j = \frac{1-x^L}{1-x}$ to get:

$$E_{gs}^{even} = -2J \frac{1}{\sin \left(\frac{\pi}{2N} \right)} \quad (4.25)$$

For $|gs_{odd}\rangle$ we get:

$$H_c \gamma_0^\dagger |gs_{odd}\rangle = - \sum_k \frac{\epsilon_k}{2} \gamma_0^\dagger |gs_{odd}\rangle = -2J \sum_{m=0}^{N-1} \sin \left[\frac{2m\pi}{N} \right] \gamma_0^\dagger |gs_{odd}\rangle \quad (4.26)$$

Using similar methods to those which produced equation (4.25) above, we get:

$$E_{gs}^{\text{odd}} = -2J \frac{\cos\left(\frac{\pi}{2N}\right)}{\sin\left(\frac{\pi}{2N}\right)} \quad (4.27)$$

In general $\frac{\cos\left(\frac{\pi}{2N}\right)}{\sin\left(\frac{\pi}{2N}\right)} < \frac{1}{\sin\left(\frac{\pi}{2N}\right)}$, so $E_{gs}^{\text{even}} < E_{gs}^{\text{odd}}$, meaning the lowest even sector state is the true ground state of the system, $|gs_{\text{even}}\rangle = |gs\rangle$. However, in the thermodynamic limit all states will become degenerate, as their energies are proportional to $1/N$.

Given the excitation energy, equation (4.14), and the property of our system that $J > 0$, it is clear that, in the odd parity sector, single particle excitations will contain the lowest energy state. As the energy of a state is proportional to its momentum, we easily identify the lowest energy state in the odd sector to be $\gamma_0^\dagger |gs_{\text{odd}}\rangle$. While it can be shown that $|gs_{\text{odd}}\rangle$ and $\gamma_0^\dagger |gs_{\text{odd}}\rangle$ have the same energy, as stated earlier, $|gs_{\text{odd}}\rangle$ is not an eigenstate of the system and so does not have a well-defined energy. The energy of the true state is given by adding the excitation of a zero momentum Bogoliubov fermion to E_{gs}^{odd} :

$$H_c \gamma_0^\dagger |gs_{\text{odd}}\rangle = \left[\epsilon_0 \gamma_0^\dagger - \sum_k \frac{\epsilon_k}{2} \gamma_0^\dagger \right] |gs_{\text{odd}}\rangle = 0 - 2J \sum_{m=0}^{N-1} \sin\left[\frac{2m\pi}{N}\right] \gamma_0^\dagger |gs_{\text{odd}}\rangle \quad (4.28)$$

The zero momentum excitation is then a Majorana fermion with zero energy, giving the lowest state of the odd sector an energy of:

$$E_0 = -2J \frac{\cos\left(\frac{\pi}{2N}\right)}{\sin\left(\frac{\pi}{2N}\right)} \quad (4.29)$$

We also want to calculate the energy of first excited state in the even sector, i.e. the energy of exciting two fermions with the lowest possible total momentum available in the even sector, the reason for this will become clear later. The lowest possible total momentum is $K = 0$ and the lowest energy

state with $K = 0$ is $\gamma_{\pi/N}^\dagger \gamma_{-\pi/N}^\dagger |gs\rangle$:

$$\begin{aligned}
H_c \gamma_{\pi/N}^\dagger \gamma_{-\pi/N}^\dagger |gs\rangle &= \left[\epsilon_{\pi/N} + \epsilon_{-\pi/N} - \sum_k \frac{\epsilon_k}{2} \right] \gamma_{\pi/N}^\dagger \gamma_{-\pi/N}^\dagger |gs\rangle \\
&= \left[4J \left| \sin \left(\frac{\pi}{2N} \right) \right| + 4J \left| \sin \left(-\frac{\pi}{2N} \right) \right| + E_{gs} \right] \gamma_{\pi/N}^\dagger \gamma_{-\pi/N}^\dagger |gs\rangle \\
&\Rightarrow E_{-\pi/2, \pi/2} = 8J \sin \left[\frac{\pi}{2N} \right] - 2J \frac{\cos \left(\frac{\pi}{2N} \right)}{\sin \left(\frac{\pi}{2N} \right)} \tag{4.30}
\end{aligned}$$

We now rescale the zero energy so that $E_{gs} = 0$ and recalculate E_0 and $E_{-\pi/2, \pi/2}$ relative to this new ground state energy. Further simplification can be achieved using $\sin(1/N) \approx 1/N$ for $N \gg 1$. Finally we can make the results a little clearer by setting the scaling energy $J = \frac{N}{4\pi}$, leaving us with:

$$\begin{aligned}
E_{gs} &= 0 \\
E_0 &= 1/8 \\
E_{-\pi/2, \pi/2} &= 1 \tag{4.31}
\end{aligned}$$

in the $N \rightarrow \infty$ limit. These energies will prove useful for identifying the appropriate conformal field theory to describe the model.

4.3.2 TFIM - Ising CFT Correspondence

We have indicated previously that our model is described by the transverse field Ising model at its critical point, we therefore expect it to have some equivalent description in terms of conformal field theory. We then need to deduce which conformal field theory corresponds to the critical TFIM, of course this is well known [28] but it is useful show it explicitly (which we will do by comparing the Lagrangian of the system with that of a conformal field theory with $c = 1/2$).

We can write the Hamiltonian in the continuum limit, where the lattice spacing, a , goes to zero, we follow the procedure outlined in ref. [101]. We define the continuum fermion field as:

$$\psi(x_i) = \frac{1}{\sqrt{a}} c_i \quad \{\psi(x), \psi^\dagger(x')\} = \delta(x - x') \tag{4.32}$$

Inserting this into the position basis Hamiltonian, equation (4.10), and writing $\psi(x_i)$, using a Taylor expansion, as; $\psi(x_{i+1}) = \psi(x_i) + a\partial_x \psi(x_i) + \mathcal{O}(a^2)$, we

get:

$$H = -J \sum_i \left\{ g + 2a(1-g)\psi^\dagger(x_i)\psi(x_i) + a^2 [\psi^\dagger(x_i)\partial_x\psi^\dagger(x_i) - \psi(x_i)\partial_x\psi(x_i)] + \mathcal{O}(a^3) \right\} \quad (4.33)$$

We can then move to the continuum limit by replacing a by an infinitesimal distance in the x direction, dx :

$$H = \text{const.} - \int \left\{ 2J(1-g)\psi^\dagger(x)\psi(x) + Ja [\psi^\dagger(x)\partial_x\psi^\dagger(x) - \psi(x)\partial_x\psi(x)] \right\} dx \quad (4.34)$$

We are interested in the critical point, setting $g = 1$ means the first term in the integral will be zero. Note the second term in the integral implies that as $a \rightarrow 0$ we must take $J \rightarrow \infty$, the constant term is dependent on J and so will tend to ∞ in the continuum limit. At the critical point the Hamiltonian density can then be expressed as; $\mathcal{H} = \psi\partial_x\psi - \psi^\dagger\partial_x\psi^\dagger$ which has a corresponding Lagrangian density:

$$\mathcal{L} = 2i (\psi\bar{\partial}\psi + \bar{\psi}\partial\bar{\psi}) \quad (4.35)$$

where $\partial = 1/2(\partial_t - i\partial_x)$ is the holomorphic differential operator and $\psi^\dagger = \bar{\psi}$ in one dimension. This \mathcal{L} is the Lagrangian density for massless free Dirac fermions in one dimension. To see this, note that fermions which are solutions to the Dirac equation have the following Lagrangian density:

$$\mathcal{L}_{ff} = i\Psi^\dagger [\gamma^\mu\partial_\mu - m] \Psi \quad (4.36)$$

where: $\Psi = (\psi \quad \bar{\psi})^T$ is a Dirac spinor field and m is the mass. For massless fermions in the x and t dimensions only, this can be rewritten as:

$$\mathcal{L}_{ff} = i \begin{pmatrix} \bar{\psi} & \psi \end{pmatrix} \begin{pmatrix} 0 & \partial_t - i\partial_x \\ \partial_t + i\partial_x & 0 \end{pmatrix} \begin{pmatrix} \psi \\ \bar{\psi} \end{pmatrix} = 2i (\psi\bar{\partial}\psi + \bar{\psi}\partial\bar{\psi}) \quad (4.37)$$

We see that this is identical to \mathcal{L} . Thus we can say that the TFIM at its critical point can be described by the same conformal field theory which describes

massless free fermions.

This is known to be the Lagrangian of a conformally invariant field theory with central charge $c = 1/2$, see ref. [29]. This corresponds to $m = 3$ in equation (1.9) which gives three primary fields with conformal dimensions, $h_{1,1} = 0$, $h_{2,1} = 1/2$ and $h_{2,2} = 1/16$ (where $\bar{h} = h$ for all fields).

We can derive this directly by setting the Hamiltonian corresponding to this Lagrangian density to be the energy-momentum tensor, which can then be expressed in terms of the Virasoro operators, as described in section 1.5. This shows the $h_{2,1}$ primary field to be the fermion field, ψ , and the $h_{1,1}$ field to be the topologically trivial field, i.e. the identity, 1. The $h_{2,2}$ field is a little more complex, it is found to relate to a field σ called the twist field, see for example ref. [31], which is an interpretation of the boundary conditions of the ψ field, rotating the ψ field about the σ field changes its boundary conditions from periodic to antiperiodic.

Returning to our original formulation in terms of Ising anyons, the three fields correspond directly to the vacuum, the fermion and the Ising anyon. The interpretation of the twist field is now more obvious as inclusion of an extra Ising anyon will increase the number of sites in the chain by one, thus requiring us to change the boundary conditions of the chain. Indeed the fusion rules produced by the CFT confirm these comparisons. For the Ising model, $m = 3$, equation (1.11) gives us the appropriate fusion between the primary fields as:

$$\begin{aligned} \phi_{1,1} \times \phi_{a,z} &= \phi_{a,z} & \phi_{2,1} \times \phi_{2,1} &= \phi_{1,1} \\ \phi_{2,1} \times \phi_{2,2} &= \phi_{2,2} & \phi_{2,2} \times \phi_{2,2} &= \phi_{1,1} + \phi_{2,1} \end{aligned} \quad (4.38)$$

(for $a, z \in \{1, 2\}$) which match exactly with the fusion rules listed earlier in the chapter for the Ising anyon model (equation (4.2)).

This correspondence then explains our results in section 4.3.1, here we showed that the three lowest lying, zero momentum states of the system had, in the thermodynamic limit, relative energies of 0, $1/8$ and 1. Due to the non-chiral nature of the ring we would expect, in the CFT description, the primary fields to occur in holomorphic and antiholomorphic pairs, $(\bar{\phi}, \phi)$. The action of the three primary fields of the Ising model, $(1, 1)$, (ψ, ψ) and (σ, σ) , will then

produce highest weight states $|0, 0\rangle$, $|1/2, 1/2\rangle$ and $|1/16, 1/16\rangle$ (pairs of fields with different conformal dimensions are forbidden, this will be explained further in the next section).

This shows that these three lowest lying, zero momentum states can be interpreted as the lowest weight states of the $(1, 1)$, (ψ, ψ) and (σ, σ) representations of the Virasoro algebra for $c = 1/2$. Using the Virasoro operators, we can then build towers of descendant states from these primary states which should produce the (low-energy) spectrum of our model.

Spectra Comparison

We can understand this correspondence between the fermionic operator and CFT pictures more accurately if we examine the spectra for the low-lying states in both cases. For the fermionic operator case we will have two separate spectra, one for the even sector and one for the odd sector.

Even sector: If we take the thermodynamic limit and set $J = N/4\pi$ as above, we get: $\epsilon_k \approx |k/2|$, with $k \in \frac{(2m+1)\pi}{N}$. We can approximate the spectrum by simply calculating the possible excitations which can produce a given energy. For example:

- $\epsilon = 0$: This energy can only be achieved by a state with no excitations thus the total momentum, K , of the state is also zero.
- $\epsilon = 1/2$: This energy is only achievable in a state with one excitation but such states are not in the even sector, so we do not include any states at this energy level. For a similar reason we ignore all energies which are an odd multiple of $1/2$.
- $\epsilon = 1$: We produce this energy from a state with two excitations, one with $k_1 = \pi/N$ and the other with $k_2 = -\pi/N$, so the total momentum is $K = 0$. We denote such an arrangement as:

$$\left(-\frac{\pi}{N}, +\frac{\pi}{N}\right) \rightarrow K = 0$$

- $\epsilon = 2$: There are four possible states with this energy:

$$\left(\pm \frac{\pi}{N}, \pm \frac{3\pi}{N} \right) \rightarrow K = \pm \frac{2\pi}{N}, \pm \frac{4\pi}{N}$$

We continue on in this fashion and obtain the plot in figure 4.5.

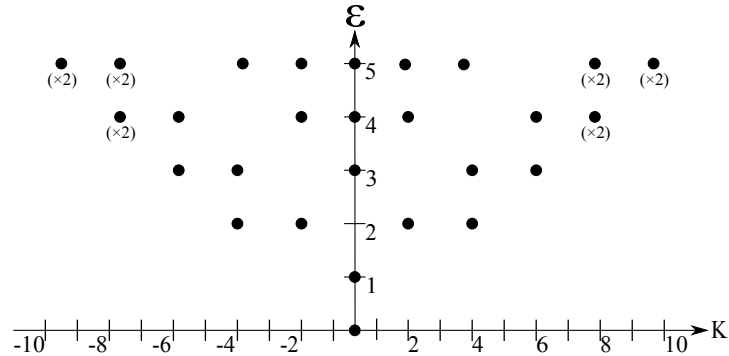


Figure 4.5: Low energy spectrum for the $P = +1$ sector. The $(\times 2)$ labels represent the fact that two states are represented here.

Odd sector: We can do a similar calculation for the odd sector, where we will have $\epsilon_m \approx \frac{2m\pi}{N} + \frac{1}{8}$, the $\frac{1}{8}$ contribution coming from the ground state energy of the odd sector. This then gives us the spectrum shown in figure 4.6.

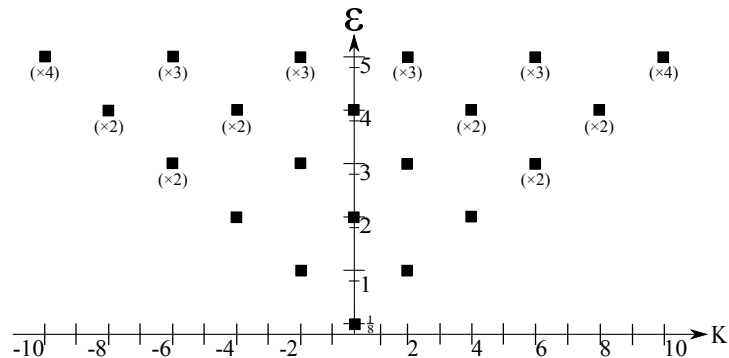


Figure 4.6: Low energy spectrum for the $P = -1$ sector. The $(\times n)$ labels represent the fact that n states are represented here.

From the Ising CFT, we can use the representation of the Verma module of each field to plot the spectrum. By acting on the states produced by the ladder operators with $(L_0 + \bar{L}_0)$ and $(L_0 - \bar{L}_0)$, we can obtain their energy and momentum. Doing this separately for the three fields then yields the following spectra:

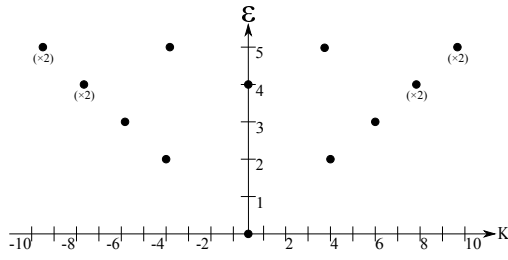


Figure 4.7: 1 sector.

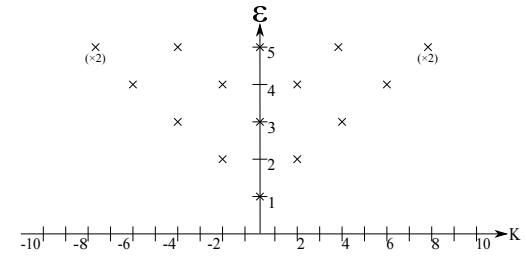


Figure 4.8: ψ sector.

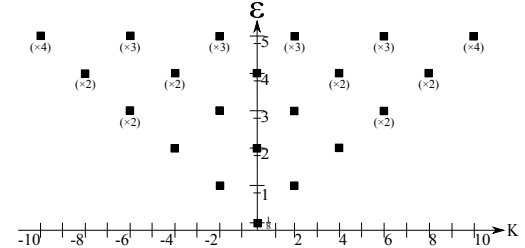


Figure 4.9: σ sector.

It can be seen that the σ spectrum, figure 4.9, exactly matches the odd sector spectrum, figure 4.6. None of the above spectra match the even spectrum, figure 4.5, however, if we combine the 1 and ψ spectra, figures 4.7 and 4.8, we see that together these exactly reproduce it, as follows:

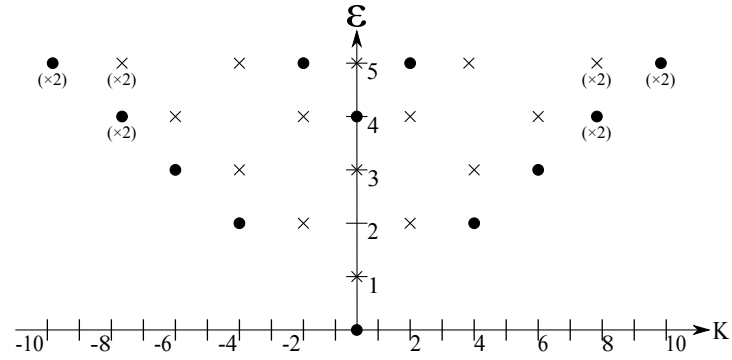


Figure 4.10: Composite spectrum produced by combining the spectra for the 1 and ψ sectors.

The even sector then contains two CFT particle towers, the $(1,1)$ and (ψ, ψ) . These can be differentiated by noting that states in the $(1,1)$ sector have an even number of right-moving (if we take the convention that holomorphic operators create positive momentum states) and an even number of left-moving (negative momentum) fermions excited, whereas states in the (ψ, ψ) sector have an odd number of left-moving and an odd number of right-moving fermions excited, hence the (x_L, x_R) notation of the fields which show the left and right moving channels. The fermionic operators, γ_k , being the modes of

the fermionic field, have a relation to the modes, L_n , of the energy-momentum tensor of the field [29]:

$$L_n = \frac{1}{2} \sum_{k=-\infty}^{\infty} \left(k + \frac{1}{2} \right) : \gamma_{n-k} \gamma_k : \quad (4.39)$$

Here the notation of the fermionic operators follows that of the Virasoro generators, i.e. $\gamma_{-k} = \gamma_k^\dagger$ and $\bar{\gamma}_k = \gamma_{-k}$, and the colon brackets represent normal ordering of the fermionic operators, i.e. annihilation operators are always moved to the right. We see then, that the L_{-n} operators will always create or destroy an even number of right-moving fermions, similarly the \bar{L}_n create or destroy an even number of left-moving fermions. Application of these operators to any state will then always conserve the parity of the number of left and right moving fermions, thus states in a particular tower will all have the same parity of left and right moving fermions.

For states in the odd sector, the parity of the number of right-moving fermions can be even or odd but the parity of the number of left-moving fermions must be the opposite. Again the L_n and \bar{L}_n operators conserve the parity of the number of both right and left-moving fermions, so they always create valid odd sector states.

We can now see why pairs of fields with different conformal dimensions are disallowed. A pair such as $(\psi, 1)$ would correspond to a state with an odd number of right-moving and even number of left-moving excitations, thus an odd number of excitations overall. This puts the state in the odd sector but the momentum of the state is still determined by the allowed momenta of the 1 and ψ fields, i.e. it has even sector momentum, which is not allowed in the odd sector. Similar results are found for other combinations of dissimilar conformal fields. More generally this constraint comes from the modular invariance of the theory, i.e. the requirement that the theory makes sense when defined on the torus restricts the combinations of the Verma modules which can possibly occur, see ref. [29]. Thus pairs of fields with different conformal dimensions correspond to states with a momentum which is not permitted in the parity sector of the particle number. These are not valid eigenstates of the Hamiltonian and are, in fact, not even part of the Hilbert space of the system.

Finally, it is important to remember that the spectra in figures 4.5 and

4.6 are only an approximation of the energy spectrum of the Hamiltonian in equation (4.21), which is only accurate provided the angle $k/2$ is small. Figure 4.11 shows a direct comparison between the spectrum obtained from exact diagonalisation of the Hamiltonian and that from our approximation for a finite sized chain.

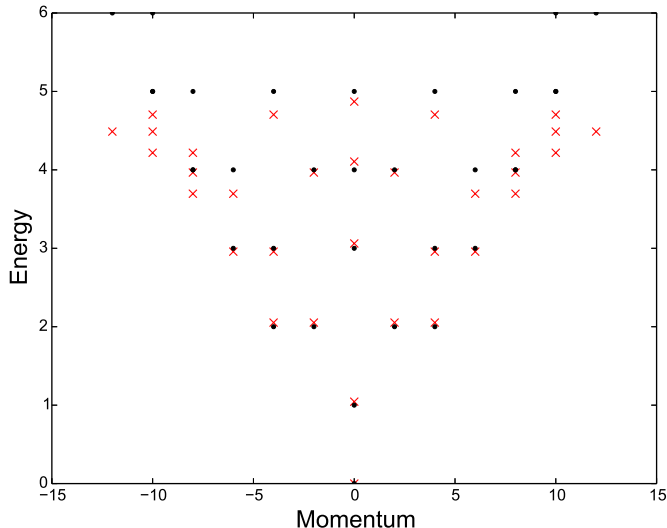


Figure 4.11: Low energy spectrum for the $(1, 1)$ and (ψ, ψ) sectors with $N = 12$. Dots represent approximate, CFT spectrum values, crosses represent exact spectrum values.

The approximate spectrum, and hence the conformal field theory description, is then clearly only good for the low momenta, and consequently low energy, states of the spectrum. Assuming the system is big enough, this will not be a problem as such low lying states will be sufficient for our purposes.

4.3.3 Qubit Definition

In order to achieve our ultimate goal of using this system to implement topological quantum computation, we will need to decide in what way the qubits of the computer will be encoded. For TQC, we would like to choose states which are topologically degenerate [9]. Only topological operations in this degenerate subspace can alter the state of the qubit thus protecting it from local perturbations.

In the $J \rightarrow 0$ limit, the anyons are all far apart and essentially isolated from each other, there is then no chain interpretation. The energy difference between the fusion channels of two anyons disappears, i.e. all states become

degenerate, and we get a system of N “ideal” qubits, with the degenerate fusion channels of each pair of anyons taken as the qubit states.

This is clearly an idealised system. In reality we would expect some interaction between at least some of the anyons. Returning to $J \neq 0$, we recover our ring model where the interactions between the anyons in the ring then lifts the degeneracy of the states in the spectrum. At low energies we then get bands of degenerate states arising from the CFT description of the chain, as seen in figures 4.5 and 4.6. The energy difference between the states then introduces a time scale for the dephasing of states in the system, related to the gap between the bands.

It is then no longer obvious which states should be chosen as the qubit states. States which are degenerate are in the same parity sector and are thus not topologically distinct, i.e. they will correspond to a similar labelling of the fusion tree for the anyon ring. However, since the energies of the spectra are in units of $4J\pi/N$, we can choose a system large enough so that the bands in the two sectors become close in energy.

Looking at the lowest “band” in each sector, i.e. just the $|gs\rangle$ and $\gamma_0^\dagger|gs\rangle$ states, figure 4.12 shows how they become more degenerate at higher N . Other degenerate bands in the system can be shown to behave in a similar manner and any pair of states from these quasi-degenerate bands can then be considered a good choice for qubit states.

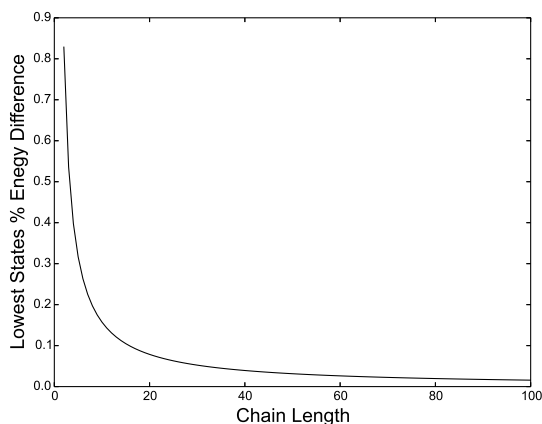


Figure 4.12: Energy difference between $|gs\rangle$ and $\gamma_0^\dagger|gs\rangle$ as the system size, N , grows (for $J = 1$, i.e. we keep the same distance between the anyons at all N , thus there is a lower 2-dimensional density of anyons at higher N).

Note that, in a real system, increasing the number of anyons forces the

separation between the anyons to decrease, thus increasing J and lifting the degeneracy again. However, J decays exponentially with distance, so we would expect it to grow at a slower rate than N . $(-1)^F$ will remain a protected quantum number for large N so, if these quasi-degenerate states are close enough in energy, they will produce a good approximation of the ideal qubits.

Assuming the anyon-anyon interaction remains significant, the band structure within each parity sector will still cause dephasing of any qubit states we choose. Any information stored in the qubit will then become corrupted after a certain time, as we can no longer be confident of its state.

We will focus on one possible solution to this problem. The parity of a state should not be affected by the dephasing, i.e. states will only dephase into other states within their own parity sector. Thus we take the anyon ring to be single qubit, with the qubit states defined to be the parity of the state of the ring. These states will remain good qubit states regardless of the values of N or J , thus any information stored in the qubit will not be corrupted by the dephasing of the specific state of the ring.

However, this choice of qubit will limit the number of operations that can be performed on the qubit, certain topological operations exist which alter the state of the qubit but not its parity, phase change for example. Thus, while information can be reliably stored in this parity sector qubit, it may not be practical for quantum computation. We will not, however, assess the practicality of the system in this thesis, so this implementation of a qubit will be sufficient for our purposes.

Another solution to this qubit definition issue can be uncovered by returning to the alternative system discussed in section 4.3.1. Here we allowed the distance between anyons in the chain to vary, resulting in a site-dependent interaction energy, J_i , with a description of the system given by Hamiltonian in equation (4.17). Moving to the continuum limit shows the the Lagrangian for this system to be:

$$\mathcal{L}' = 2(J(x) - G(x))\psi^\dagger(x)\psi(x) + J(x)a [\psi^\dagger(x)\partial_x\psi^\dagger(x) - \psi(x)\partial_x\psi(x)] \quad (4.40)$$

where the interaction energy and the magnetic field coupling are now a function of space, $J_i, G_i \mapsto J(x), G(x)$. Since, in general, these two functions will not

be equal everywhere, this prevents the cancellation of the mass term. Thus letting the anyons space differently in the chain alters the description of the model from massless to massive free fermions. The mass term introduces a gap to excitations for the ground states of both parity sectors which protects them from perturbations of the system. The ground states of the parity sectors may then represent good qubit states.

It should be noted however, that these excitations occur within the energy gap of the incompressible fractional quantum Hall state and so this “new” mass gap must be smaller than the original gap, in which our system has been created. If one is relying on this smaller gap to define qubits, then it must be first ensured that the topological operations performed on the qubit can be done within the time-scale set up by this smaller energy difference. It is also clear that the inclusion of this mass term means that the Lagrangian density is no longer conformally invariant, and so the CFT correspondence breaks down for this model.

Now that some regimes for the computational states of the system have been suggested we need to examine how interactions between the qubit and the edge of the fluid will influence the integrity of the various qubit implementations.

4.4 Edge Interaction

As stated in section 4.2, the neutral sector of the edge of the $\nu = 5/2$ quantum Hall fluid is described by a chiral Ising conformal field theory. The energy spectra for such a system can be easily pictured as similar to those shown above in figures 4.7, 4.8 and 4.9 except, due to the chiral nature of the edge, we only consider those descendant states which arise from the application of holomorphic Virasoro operators on the primary fields, as antiholomorphic operators must annihilate the primary fields; $\bar{L}_{-m}|p\rangle = 0$ [29]. More simply only states which have momentum which is both in the direction permitted by the orientation of the magnetic field and proportional to the energy of the state (i.e. states with a constant velocity, $k/E_k = const$) are kept.

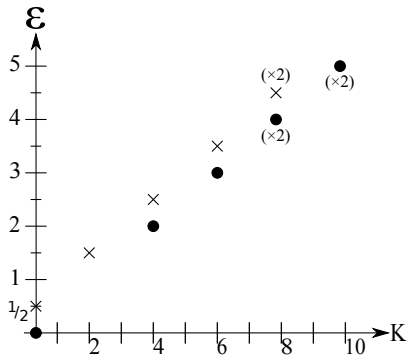


Figure 4.13: Chiral even sector spectrum.

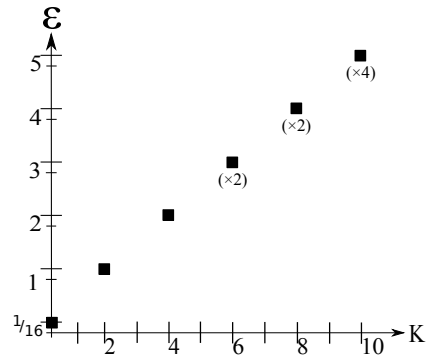


Figure 4.14: Chiral odd sector spectrum.

Comparing these edge spectra with the bulk ring spectra given by figures 4.5 and 4.6, one notices that not only are many states missing in the chiral case, but some of those which remain are at different energies to the non-chiral case. This is because, as detailed in section 4.3.2, primary fields for the non-chiral case are, in fact, a composite of a field with its anti-holomorphic counterpart thus they have double the energy, i.e. $E(1, 1) = 0$, $E(\psi, \psi) = 1$ and $E(\sigma, \sigma) = 1/8$ in the bulk ring but $E(1) = 0$, $E(\psi) = 1/2$ and $E(\sigma) = 1/16$ on the edge.

The purpose of this chapter is to study the interaction between the edge and the anyon ring in the bulk. To this end, we need to introduce some coupling between the anyon ring, described by the spectra in figures 4.5 and 4.6, and the edge modes, described by the spectra in figures 4.13 and 4.14. We can then write the Hamiltonian for the full system as:

$$H = H_R + H_E + H_I \quad (4.41)$$

where H_R is the contribution to the Hamiltonian from the interaction between the anyons in the bulk ring, given by equation (4.21), H_E is the contribution from the chiral CFT on the edge and H_I accounts for the interaction between the bulk ring and the edge.

The fundamentally different way we have treated the bulk ring and the edge up to this point makes it difficult to think about how an interaction between the two would affect the system. The simplest interactions would involve an exchange of fermionic modes between the edge and the ring which conserves momentum [100], thus changing the state of both subsystems, however the energy separation between states in the two spectra are different so it is unclear

what states the interaction would force each subsystem into. On top of this, the most likely interactions would naturally involve the exchange of only a single excitation, but this would change the parity sector of both subsystems causing them both to enter into a sector where the momenta of the exchanged excitation is not permitted. We can solve these issues by allowing states with momenta in either direction on the edge, i.e. we remove the chiral condition, the edge is then of a similar form to the bulk ring and so the interaction is easier to calculate.

4.4.1 Double Chain System

The correspondence between the description of the ring spectrum in terms of fermions and in terms of conformal field theory, mentioned in section 4.3.2, shows that we can think of the ring as being composed of two chiral edges, an inner and outer edge, on which particles flow in opposite directions, thus giving us the holomorphic and antiholomorphic descendant states seen in figures 4.5 and 4.6.

We want to use this comparison to make a simplification to our calculation; instead of examining the interaction between the edge chiral CFT and the ring transverse Ising chain, we instead model the edge as another non-chiral chain. We then perform the much simpler calculation of the interaction between two identical, concentric, periodic chains. The inner chain represents the ring of anyons in the system and so we call it the *ring chain*, the outer chain represents the edge of the system and is therefore named the *edge chain*, we use R and E respectively to label elements from the different chains.

To reproduce an approximation of the actual system, after the interaction term is calculated we simply project onto a subspace of the Hilbert space of this system which contains only those states from the edge chain which contain no negative momentum modes. More simply we treat the edge as a full, non-chiral chain but after the calculation is completed we reduce back to the chiral case by eliminating states produced by application of antiholomorphic operators.

There are, however, some subtleties, most importantly, in the even sector we must still include the lowest negative momentum mode, $\gamma_{-\pi/N}^\dagger$, in order to obtain the states in the ψ tower. This may seem arbitrary but we can consider

it a mathematical trick necessary to obtain states which would be physically present. We justify this trick by claiming that the operation $\gamma_{-\pi/N}^\dagger \gamma_{\pi/N}^\dagger$ is actually a different type of operation to the fermion creation operators and should instead be considered some sort of topological operator, T_0 . In section 4.3.2 we mentioned that the $(1, 1)$ and (ψ, ψ) towers were distinguished by the parity of their number of right (and left) moving fermions, with states in both sectors having an overall even number of fermions. For the chiral case we would expect the tower with an odd number of right movers, the ψ tower, not to exist as any of its states cannot have an odd number of left movers to ensure an overall even fermion number. However, such states are physically present. T_0 is then essential as it introduces a single left moving fermion, $\gamma_{-\pi/N}$, which is necessary to produce states in the ψ tower.

We must also consider the energy of the states in the edge chain. Remember the chiral spectrum shows that the primary fields of the ψ and σ towers, and the descendant states created from these, have a lower energy than their counterparts in the non-chiral spectrum. This is an important consideration as the energy difference between two states will dictate how likely the system is to jump between those two states when perturbations (such as edge/bulk interactions) are introduced. Thus we must implement a lowering of the energy of the states in the ψ and σ sectors of the edge chain (by $\frac{E_2}{2}$ and $\frac{E_1}{2}$ respectfully), but not the 1 sector.

In our simplified system we then have two copies of the Hamiltonian from equation (4.21):

$$H_0 = H_E + H_R = \sum_k \epsilon_k \left(\gamma_k^\dagger \gamma_k - \frac{1}{2} \right) + \sum_l \zeta_l \left(\delta_l^\dagger \delta_l - \frac{1}{2} \right) \quad (4.42)$$

where: $\delta_l = u_l d_l - i v_l d_{-l}^\dagger$, the d_i^\dagger being fermion creation operators on the edge chain. Using exact diagonalisation, we can easily produce the spectrum for such a system (if the chains are relatively small) as can be seen in figure 4.15.

Now we need to consider how these chains interact with each other. We can introduce a coupling between the chains at each site, producing a closed ladder model (see for example refs. [110, 111]) where, due to the varying distances between the chains, the inter-chain couplings will be site-dependent. We can reasonably assume that in an actual system neither chain will be per-

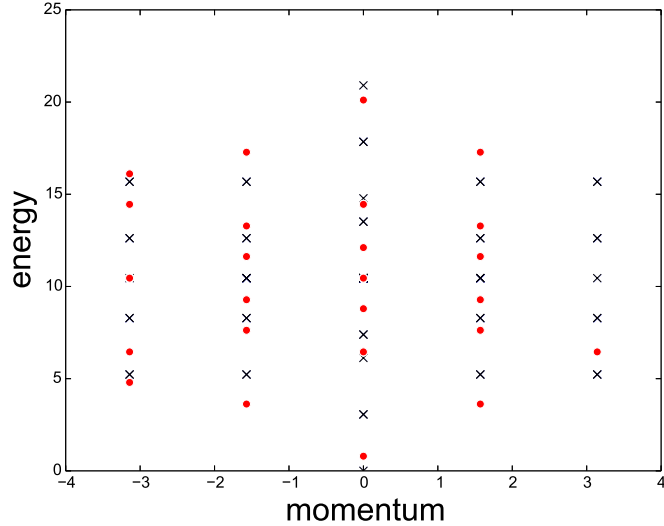


Figure 4.15: Spectrum for two noninteracting rings of 8 σ anyons.

factly circular, thus we would expect for there to be a point where both chains are closest together. Any interaction between the two chains would obviously be strongest at this point. We note that the interaction strength decays exponentially with distance between the anyons, so in our model we will make the assumption that the inter-chain coupling is negligible except at the point where the chains are closest.

We then have two closed chains which are coupled to each other at one point only. The chains are composed of the same species of anyon, so the interaction between two anyons from separate chains should be the same as that between two anyons from the same chain, though with potentially a different coupling strength. We will choose the numbering of the anyons so that the non-negligible interaction occurs between the zeroth anyon on each chain, i.e. σ_0^E and σ_0^R .

In the current basis these anyons are paired with their respective neighbouring anyons, we must therefore use F -moves to break this pairing and pair them together before applying the interaction operator Π^{J_I} , we then unpair them and return to the original basis pairings. From section 4.3, we see that this is equivalent to the process for obtaining the interaction between an (odd, even) pair of anyons. We know then that the result will be a factor of $J_I(\sigma^x \otimes \sigma^x)$ applied to the tensor product of vector spaces; $V_0^E \otimes V_0^R$.

Thus the extra term, H_I , which is added to H_0 (from equation (4.42)) to

account for this inter-chain interaction, is given by;

$$H_I = J_I \sigma_{0,E}^x \sigma_{0,R}^x \quad (4.43)$$

where J_I is dependant on the distance between the two chains at their closest point. We now need to express this term in the same basis as the base Hamiltonian, H_0 , from equation (4.42). We use the procedure from section 4.3, first performing a Jordan-Wigner transformation on H_I , then switching to the momentum basis leads to:

$$H_I = \frac{J_I}{\sqrt{N_R N_E}} \sum_{k,l} \left\{ (c_k + c_k^\dagger) (d_l + d_l^\dagger) P_{\text{even}}^R P_{\text{even}}^E + (c_k + c_k^\dagger) (d_l + d_l^\dagger) P_{\text{even}}^R P_{\text{odd}}^E \right. \\ \left. + (c_k + c_k^\dagger) (d_l + d_l^\dagger) P_{\text{odd}}^R P_{\text{even}}^E + (c_k + c_k^\dagger) (d_l + d_l^\dagger) P_{\text{odd}}^R P_{\text{odd}}^E \right\} \quad (4.44)$$

where the $P_{\text{even/odd}}^{E/R}$ are projections onto the even and odd parity sectors of the two rings. These projections just ensure that the correct momenta values are summed over, i.e. if it is understood that k and l should be summed over the momenta values appropriate to the sector of the particular state H_I is acting on, then we can express this more simply as:

$$H_I = \frac{J_I}{\sqrt{N_R N_E}} \sum_{k,l} (c_k + c_k^\dagger) (d_l + d_l^\dagger) \quad (4.45)$$

Here, similar to H_0 , the momenta values which k and l take are those from the particular sector in which the Hamiltonian is acting. One could now perform a Bogoliubov transformation to put H_I in the exact same form as the base Hamiltonian but it will often be more useful to keep the interaction term in this form, i.e. in terms of c_k operators rather than γ_k operators. The interaction is then described by a fermion of momentum, k , on the ring chain being annihilated and a superposition of fermions of all available momenta, l , being created on the edge chain, or vice versa. The effect of the interaction on the system will be nontrivial as it mixes certain states together, specifically now each momentum state, $|k\rangle$, on one chain is coupled to all momentum states, $|l\rangle$, in the sector the other chain is in.

4.4.2 Computing Elements of H_I

Due to the addition of the interaction term, the full Hamiltonian, $H = H_0 + H_I$, is no longer diagonal in the basis of eigenstates of H_0 . We then need to find a method to diagonalise this interacting Hamiltonian to find the eigenstates and energies of the interacting system.

Firstly, we will need to be able to write down the interaction matrix, i.e. we need to see how H_I acts on the eigenstates of H_0 . The matrix elements of H_I in our basis are obtained by computing expectation values of the form; $\langle A^{(0)} | H_I | Z^{(0)} \rangle$. Here $|A^{(0)}\rangle$ and $|Z^{(0)}\rangle$ are states of the non-interacting, double chain system (occasionally we will refer to such states as “bare” system states) which have the form:

$$\prod_{i,j} \gamma_i^\dagger \delta_j^\dagger |g_{S_R}, g_{S_E}\rangle = \gamma_i^\dagger |g_{S_R}\rangle \delta_j^\dagger |g_{S_E}\rangle \quad (4.46)$$

with γ_i^\dagger representing excitations of the ring chain and δ_i^\dagger representing excitations of the edge chain. Given the form of H_I from equation (4.45), this allows us to write matrix elements of H_I as:

$$\begin{aligned} \langle A | H_I | Z \rangle &= \frac{J_I}{\sqrt{N_R N_E}} \sum_{k,k'} \langle \alpha, \beta | \left(c_k e^{ik} + c_k^\dagger e^{-ik} \right) \left(d_{k'} e^{ik'} + d_{k'}^\dagger e^{-ik'} \right) | \omega, \psi \rangle \\ &= \frac{J_I}{\sqrt{N_R N_E}} \langle \alpha | \sum_k \left(c_k e^{ik} + c_k^\dagger e^{-ik} \right) | \omega \rangle \langle \beta | \sum_{k'} \left(d_{k'} e^{ik'} + d_{k'}^\dagger e^{-ik'} \right) | \psi \rangle \\ \Rightarrow \langle A^{(0)} | H_I | Z^{(0)} \rangle &= J_I \frac{1}{\sqrt{N_R}} \langle A_R^{(0)} | H_{I,R} | Z_R^{(0)} \rangle \frac{1}{\sqrt{N_E}} \langle A_E^{(0)} | H_{I,E} | Z_E^{(0)} \rangle \quad (4.47) \end{aligned}$$

Thus allowing us to reduce such expectation values to the product of two simpler expectation values, each containing operators which only act on one of the chains. We can then calculate the expectation values for each chain separately and combine the results to obtain the matrix elements of H_I .

Another point of note is that, due to the linear nature of H_I (linear in terms of the action on single ring), the action of H_I on a particular bare state is to produce a superposition of states all of which have the opposite parity to the initial state. For all states in this superposition, the momentum of the excited fermions will not be allowed in the parity sector defined by the number of excited fermions e.g. a state with an odd number of even momentum

excitations. Physical interpretation of the states in the superposition is then difficult as they are not eigenstates of the system (fortunately, evaluation of the expectation values does not require a physical meaning for them).

These states will only have a non-zero overlap with states of equal parity, thus the only non-zero expectation values will come from those from the opposite parity sector to the initial bare state on which H_I acted. Evaluation of these expectation values is then complicated as the commutation relations between operators from different parity sectors are not the usual fermionic anticommutation relations, i.e. $\{c_k, c_{k'}\} \neq \delta_{k,k'}$.

Opposite Parity Operators

To progress any further then, we must find the commutation relations for operators from different parity sectors. Using the definitions of the fermionic momentum operators:

$$c_k = \frac{1}{\sqrt{N}} \sum_j c_j e^{-ikj} \quad (4.48)$$

we see that, if a is a momentum value from the even sector and z is a momentum from the odd sector, i.e. $a = \frac{(2n+1)\pi}{N}$, $z = \frac{2m\pi}{N}$ for $n, m \in [-\frac{N}{2}, \frac{N}{2} - 1]$ if N is even or $n, m \in [-\frac{N+1}{2}, \frac{N-1}{2}]$ if N is odd, then:

$$\{c_a, c_z\} = \{c_a^\dagger, c_z^\dagger\} = 0 \quad \{c_a, c_z^\dagger\} = \frac{1}{N} \sum_j e^{i(z-a)j} = \frac{1}{N} \sum_j e^{\frac{2i\pi}{N}(m-n)j} e^{-i\frac{\pi j}{N}} \quad (4.49)$$

Similarly, using definition (4.11) we get:

$$\{\gamma_a, \gamma_z\} = \{\gamma_a^\dagger, \gamma_z^\dagger\} = 0 \quad \{\gamma_a, \gamma_z^\dagger\} = \frac{1}{N} \sum_j e^{i(z-a)j} [u_a u_z + v_a v_z] \quad (4.50)$$

In the case of equal parity states these relations simplify to the delta functions we are more familiar with;

$$\begin{aligned} \{c_a, c_z\} &= \{c_a^\dagger, c_z^\dagger\} = 0 & \{c_a, c_z^\dagger\} &= \delta_{a,z} \\ \{\gamma_a, \gamma_z\} &= \{\gamma_a^\dagger, \gamma_z^\dagger\} = 0 & \{\gamma_a, \gamma_z^\dagger\} &= \delta_{a,z} \end{aligned}$$

It is quite clear from these commutation relations that any term in a matrix element calculation, of the form in equation (4.47), that contains states, $|\alpha\rangle$, $|\omega\rangle$ or $|\beta\rangle$, $|\psi\rangle$, which have equivalent parity, will be zero. Each expectation value is obtained by summing a number of state overlaps and each of these overlaps will contain a H_I contribution. Acting on a state with H_I gives a superposition of states of the opposite parity, as each term in H_I is linear (that is, in its action on a single chain). An overlap between states of different parities will always have an odd number of raising and lowering operators which, by the commutation relations above, must always annihilate the state.

From here on then we will only ever consider the overlaps between opposite parity states, i.e. we will deal exclusively with matrix elements of H_I between even and odd sector states, the rest of the overlaps are always zero.

Approximations

The nature of the states of the system is dependent on the number of sites on the chain, N , as this dictates the number of possible excitations and their allowed momentum values. We can say then that the matrix elements of H_I will be difficult to evaluate analytically for general N as, from the definition of the states (equations (4.46) and (4.23)) and the commutation relations for the momentum operators (equation (4.49)), we will obtain an infinite series of products over u_k factors and sums over v_k factors.

It is beyond the scope of this project to try to obtain analytic solutions for such terms but for relatively small chains we can solve these overlaps. However, as the following quick approximation of the quantity of necessary calculations shows, this problem is intractable by hand for even the smallest systems.

To compute the matrix elements of H_I we must evaluate expectation values of the form; $\langle n|H_I|x\rangle$, where $|n\rangle$ is the state which is the initial, bare state of the system. For each state $|x\rangle$, then we will have to calculate a large number of factors, giving us a superposition of overlaps inside the sum. We would like to work with the momentum space operators, c_k, c_k^\dagger , so for each γ^\dagger excitation in each state there will be two terms. Now we must include the terms from the ground states, we will have one even parity state, whose excitations act on $|gs_{even}\rangle$, and one odd parity state, whose excitations act on $|gs_{odd}\rangle$. These

“ground states” (remember $|gs_{odd}\rangle$ is not actually a ground state of the system but the state on which odd parity sector excitations act) contain 2 factors for each momentum value from the appropriate sector which is between zero and π . Finally, we have to account for H_I which contains a creation operator and an annihilation operator for every possible momentum value in the sector of $|n\rangle$. In total, for each state $|x\rangle$, then there will be:

$$N_x = 2 \times N_\gamma^x + 2 \times N_\gamma^n + 2 \times N_{(0 < k < \pi)}^{\text{even}} + 2 \times N_{(0 < k < \pi)}^{\text{odd}} + 2 \times N_k^{\text{even/odd}} \quad (4.51)$$

where: N_γ^a is the number of γ^\dagger operators in the state $|a\rangle$ and N_k is the number of possible momenta values. We then must calculate N_x factors for every state, $|x\rangle$, which produces a non-zero results for a given $|n\rangle$, of which there are 2^{N-1} .

For example, let us look at the elements corresponding to the bare ground state for $N = 2$. There are 4 possible states in the system, 2 of which are the opposite parity to $|gs\rangle$ and so give a non-zero overlap. Each of the odd parity states have only a single excitation, $|gs_{odd}\rangle$ has a single term (there is no odd sector momenta between 0 and π so $|gs_{odd}\rangle = |0\rangle$) and H_I contains 4 operators. This gives $N_x = 16$, with only 2 possible odd sector states this means, in order to obtain the elements of H_I corresponding to the bare ground state, we must calculate 32 separate overlaps.

This is only for the ground state which is the simplest state, we will also need to calculate 3 more similar terms, one for each of the other bare eigenstates. The overlaps in these terms will get progressively more complicated as the number of excitations in the state increases. Note also, that this is only considering one ring, there is also the overlap on the other ring to consider.

Solving computationally is clearly the only option for involved calculations, however the calculations will still be computationally expensive for large N . It will be useful therefore, to examine if there are any approximations we can make which will reduce the number of terms that need to be computed while not deviating too far from the exact result.

We have already mentioned how any overlap of states we will come across must be evaluated using the commutation relations from equation (4.49). Due to the dependence of these commutations on $1/N$ we may then expect, for

large enough systems, a small contribution from overlaps which require a large number of commutations to evaluate. Naively then, we could expect a good approximation of an overlap by expanding it in terms of the commutation factors and eliminating any terms above an order of $1/N$.

However we must be careful, each of the commutation factors also contains a sum over N values of j ; $0 \leq j \leq N - 1$. The sum factors are all roots of unity, so the magnitude of the sum will then be $< N$, meaning the commutation term is < 1 . It's exact magnitude then depends on the difference between the momentum values of the operators being commuted, if this is large then the commutation term will be small, $\sim 1/N$, but in general this will not be the case. This results in a similar situation to the usual equal parity operator commutation relations.

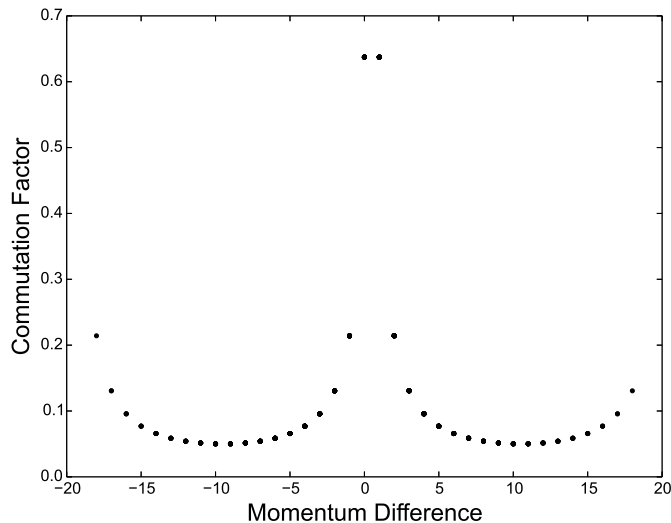


Figure 4.16: Evaluation of the commutation factor $\{c_a, c_z^\dagger\}$, where $a = \frac{2m\pi}{N}$, $z = \frac{2(n+1)\pi}{N}$. The system size is $N = 20$, and we calculate this term on all: $-\frac{N}{2} \leq m, n \leq \frac{N}{2} - 1$.

A simple plot of the commutation terms dependence on the difference between the momenta values, figure 4.16, shows that there will be many momenta values for which this factor cannot be considered negligible, for small system sizes. It is apparent then that the order of $1/N$ for a term is not indicative of the magnitude of that term, terms of high order in $1/N$ cannot be assumed to be negligible and so we must find another approximation method.

Instead we can expand a given state, $\prod_p \gamma_p^\dagger |gs\rangle$, in terms of c_p, c_p^\dagger operators, which gives a superposition of states of the form $A(c_a \cdots c_z)(c_a^\dagger \cdots c_z^\dagger)|0\rangle$

(where A is some constant which is a product of u_p and v_p factors). From the definitions of γ_k^\dagger and $|gs\rangle$ it is clear that, if we calculate the total number of u_k and v_k factors in A , then this number will be the same for each term in the superposition, i.e. the total number of u_k and v_k factors remains constant, though their ratio will vary between terms. A plot of u_k and v_k , figure 4.17, over all possible momentum values shows that for any given k ; $|u_k| > |v_k|$.

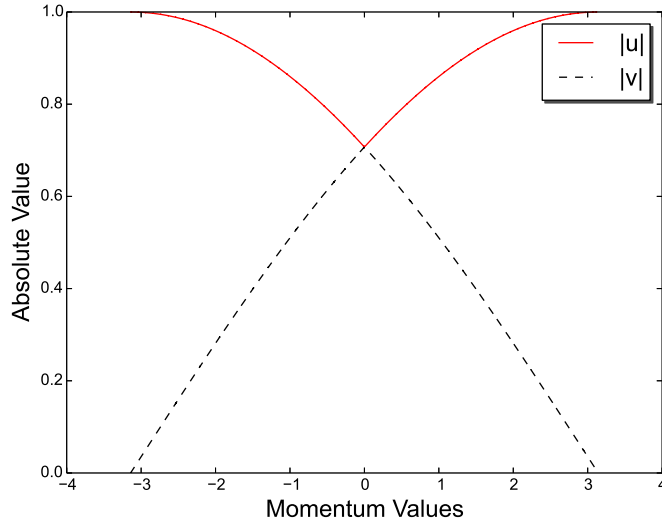


Figure 4.17: Plot of $|u_k|$ and $|v_k|$ for all k values. Note that at $k = 0$; $|u_k| = 1$, $|v_k| = 0$, we have omitted this point as the behaviour of the functions here is not clear in the plot.

Replacing a u_k factor with a v_k factor for any A will then clearly always result in decreasing the magnitude of A . We can then say that terms in the superposition which have a higher number of v_k factors will give a less significant contribution to any overlap.

We can then write a given expectation value as a sum of terms with increasing order of v_k factors. To get an idea of what order of v_k terms will be significant to the evaluation of the expectation value, we can perform some numerical simulations for small system sizes. States with higher momentum excitations will have more accurate results for a given order of v_k (as the v_k terms at large k are smaller) therefore we examine the expectation value with the lowest momentum excitations; $\langle gs_{even} | H_I \gamma_0^\dagger | gs_{odd} \rangle$ (the notation $|gs_{even}\rangle$ and $|gs_{odd}\rangle$ was explained in section 4.3.1). For small values of N we can compute this expectation value exactly and compare it to approximations to various orders of v_k .

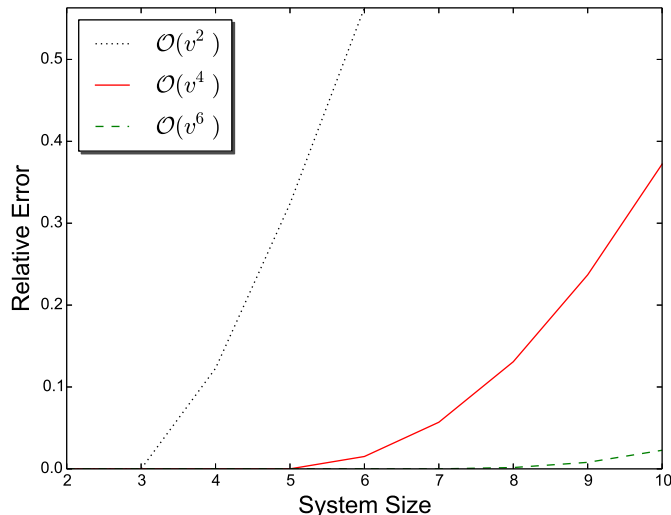


Figure 4.18: Difference between exact and approximate results for $\langle gs_{even} | H_I \gamma_0^\dagger | gs_{odd} \rangle$ as a percentage of the exact overlap value for increasing values of N .

We find, see figure 4.18, that calculating the overlap up to fourth order in v_k gives a good approximation for small system sizes. We can then justify ignoring all terms which are $\mathcal{O}([v_k]^5)$ and higher in expectation value calculations.

We write a given state, $\prod_p \gamma_p^\dagger |gs\rangle$, as a superposition of states in terms of momentum space fermion operators, c_k^\dagger . Examining the form of the ground state, equation (4.23), it is clear that the order of v_k factors in any of the superposition states is related to the number of excited fermions of the state. By lowering the maximum order of v_k we allow in our computation, we are restricting the calculation to states with lower numbers of excitations. Overlaps of states with large numbers of excitations will take many commutations to evaluate, each of which lowers the magnitude of the overlap (see equation (4.49)). These would then be expected to contribute less to the expectation value than the overlaps from states with less excitations.

4.4.3 Reintroducing Chirality

As stated in section 4.4.1, we have been using the two interacting rings as a simplified model of our actual system. In the real system the edge ring is in fact chiral in nature, thus we must account for this at some point.

After obtaining the energies and eigenstates of two non-chiral, interacting rings we can simply alter our methods to fit the more complicated chiral system

by projecting out all states of the edge chain which are not present if only one direction of momentum is permitted.

The excitations on the chiral edge chain can only propagate in one direction, which we choose to be the $+k$ direction. If we look at the energy spectrum, figures 4.5 and 4.6, we want to eliminate any states which contain negative momentum excitations. We do this by projecting onto the space of positive-only momentum states, i.e. we only consider states which are created by γ_{+k}^\dagger operators (except for the T_0 operator mentioned in section 4.4.1).

The interaction Hamiltonian (equation 4.45) also must be altered, as it is it can hop any excitations from one chain to the other but now certain excitations, i.e. those with negative momentum, are no longer allowed on the edge chain. Expressing the portion of the interaction Hamiltonian which acts on the edge ring, $H_{I,E}$, in terms of Bogoliubov operators then we have:

$$\begin{aligned} H_{I,E} &= \sum_k \left\{ u_k \gamma_k + i v_k \gamma_{-k}^\dagger + u_k \gamma_k^\dagger - i v_k \gamma_{-k} \right\} = \\ &= \sum_{k \geq -\pi/N} \left\{ (u_k + i v_k) \gamma_k + (u_k + i v_k) \gamma_{-k}^\dagger + (u_k - i v_k) \gamma_k^\dagger + (u_k - i v_k) \gamma_{-k} \right\} \end{aligned} \quad (4.52)$$

Now, as with the base states, we remove any terms containing negative momenta operators.

$$H_{I,E} = \sum_{k \geq -\pi/N} \left\{ (u_k + i v_k) \gamma_k + (u_k - i v_k) \gamma_k^\dagger \right\} \quad (4.53)$$

The states on the inner ring remains unchanged so we don't need to worry about altering $H_{I,R}$. Thus the full Hamiltonian now looks like:

$$\begin{aligned} H &= \sum_{k \geq -\pi/N} \epsilon_k \left(\gamma_k^\dagger \gamma_k - \frac{1}{2} \right) + \sum_l \zeta_l \left(\delta_l^\dagger \delta_l - \frac{1}{2} \right) + \\ &+ \frac{J_I}{\sqrt{N_E N_R}} \sum_{k \geq -\pi/N}^{\text{all } l} \left\{ (u_k + i v_k) \gamma_k + (u_k - i v_k) \gamma_k^\dagger \right\} \left\{ u_l \delta_l + i v_l \delta_{-l}^\dagger + u_l \delta_l^\dagger - i v_l \delta_{-l} \right\} \end{aligned} \quad (4.54)$$

4.4.4 Scaling Interaction Energies

There are three separate interaction energies in this problem, remember these are the energy penalties assigned to the $1/\psi$ fusion channel splitting and so they describe how favourable the ψ fusion channel is due to the distance between the anyons. For the interaction between σ anyons on the edge, we have the energy J_E , on the ring we have J_R (collectively we will call these the in-chain interaction energies) and for the interaction between the ring and the edge we have J_I (often referred to as the inter-chain interaction energy).

As the interactions are all between the same species of anyons ($\sigma - \sigma$ interactions) it would seem reasonable to assume that all of the interaction energies are equal, i.e. $J_E = J_R = J_I$. However the locations of the two σ particles in any interaction will be different for interactions involving different J 's. Along with the differencing behaviour between the edge and the bulk, this will cause the different interaction energies to scale differently.

The ring is composed of σ anyons in the bulk, thus the strength of an interaction between any two such anyons scales as a function of the distance between them. For a fixed number of anyons, N_E , the distance between any two particles is proportional to the length of the chain, L_R , for a constant linear density of anyons. We would expect the distance between anyons in the ring to then be $\Delta_R \sim L_R/N_R$. Thus the energy splitting, J_R , decays exponentially with an increase in the chain length, for fixed N_R we have; $J_R \sim e^{-L_R/l}$ for some characteristic length, l , of the system (usually taken to be the magnetic length). This scaling is described further in section 1.5 and ref. [101].

The edge however, is described by a conformal field theory. Its critical nature requires the interactions to scale linearly with the length, L_E , for fixed N_E we have; $J_E \sim l/L_E$. Previously we have described the edge as a chiral chain, so it may be expected that the interaction strength should scale similar to that of the ring. However, we should always keep in mind that the chain description of the edge (and similarly the CFT description of the ring) is only an approximation of the system, in reality the edge is described more precisely by the Ising CFT, so the interaction strength must scale linearly. To compensate for this, in the anyon chain model of the edge, the number of anyons in the chain must grow proportional to the length of the chain so the

scaling remains linear.

Lastly, the strength of the interaction between the rings themselves is determined by the distance, d , between the two at their closest point, i.e. between $\sigma_{0,E}$ and $\sigma_{0,R}$. From how we have defined our model, the ring will always stay “close” to the edge with the two lengths growing in tandem as the system is scaled. The distance between the two then grows proportional to their length and we would expect an exponential scaling of the interaction energy, $J_i \sim e^{-d}$, where d does not have any obvious dependence on N_R or N_E .

There are, however, many possibilities for the physical realisation of the anyon ring. We will explore just two interesting regimes of the system arising from some of these possible realisations.

- **Regime 1:** *The number of quasiholes is proportional to the length of the ring.* When the size of the system is increased the number of anyons increases in proportion to it, meaning that the interaction strength in the ring is now a linear function of length, similar to the edge, $J_R \sim l/L_R$. This describes the creation of anyons along the edge necessary to maintain constant linear density in the liquid as the system grows. For larger systems there will then be more potential qubits present in the system.
- **Regime 2:** *The number of quasiholes in the ring is fixed.* This is the situation we have described above, the number of σ anyons in the system does not change as we increase the size of the system, so as the length of the ring increases the interaction strength falls off as $J_R \sim e^{-L_R/l}$. This best describes a ring of a set anyon number which we wish to place in systems of various sizes. For larger systems the anyons in the bulk interact less and so the qubits are better protected.

Both of these regimes will be explored in more detail in the numerical simulations section (section 4.6).

4.5 Perturbation Theory

Now that we have outlined exactly how to obtain the elements of the interaction matrix, H_I , we can move forward with diagonalising it. Given the size of the

system, $2^{N_E+N_R}$ for the non-chiral case, direct diagonalisation of H_I will require extensive computational time for large systems.

If H_I is small in comparison to H_0 , then we can consider it a small perturbation to a fully diagonalised system. This allows us to use perturbation theory as an alternative method to calculate the eigenstates and eigenvalues of the interacting system under this weak perturbation, see for example ref. [112] for an introduction to perturbation theory. The potential advantage of this method comes from expanding interacting eigenstates in terms of the small parameter of H_I , we can then save computing time by omitting terms of high order in this parameter.

The $(N_E N_R)^{-1/2}$ factor in H_I would certainly qualify as a small parameter (for large enough systems) and indicates that perturbation theory is appropriate but we must be careful as the inter-chain coupling, J_I , must also be taken into account. If $J_I \approx J_{E/R}$ then the use of perturbation theory can be justified but, given that the anyons composing the ring are created close to the edge, this cannot be argued to be true in general and there may be regimes of the system where J_I is considerably larger than the in-chain couplings.

However, it will prove fruitful to examine the perturbation theory regardless, not only for its potential speed up in diagonalising large/weakly-interacting systems but, more importantly, because it can provide us with an approximation for the general form of an interacting eigenstate (and its energy) for such systems. This general form would give an insight into the effect the interaction has on non-specific systems and may let us make some more universal predictions for the how this will influence the information in the qubit.

Therefore, assuming $J_I(N_E N_R)^{-1/2}$ is small, perturbation theory offers a good approximation for the eigenvalues and eigenvectors of the interacting system. Specifically, it allows us to express the perturbed eigenvalues and eigenstates of the system in terms of the more simple bare eigenvalues and

eigenstates. To second order in $J_I(N_E N_R)^{-1/2}$ we have:

$$E_n = E_n^{(0)} + \langle n^{(0)} | H_I | n^{(0)} \rangle - \sum_{m \neq n} \frac{|\langle m^{(0)} | H_I | n^{(0)} \rangle|^2}{E_m^{(0)} - E_n^{(0)}} \quad (4.55)$$

$$\begin{aligned} |n\rangle = & |n^{(0)}\rangle - \sum_{m \neq n} \frac{\langle m^{(0)} | H_I | n^{(0)} \rangle}{E_m^{(0)} - E_n^{(0)}} |m^{(0)}\rangle + \\ & + \sum_{m, m' \neq n} \left[\frac{\langle m^{(0)} | H_I | m'^{(0)} \rangle \langle m'^{(0)} | H_I | n^{(0)} \rangle}{(E_m^{(0)} - E_n^{(0)})(E_{m'}^{(0)} - E_n^{(0)})} - \frac{\langle m^{(0)} | H_I | n^{(0)} \rangle \langle n^{(0)} | H_I | n^{(0)} \rangle}{(E_m^{(0)} - E_n^{(0)})^2} \right] |m^{(0)}\rangle \end{aligned} \quad (4.56)$$

where the bracketed superscripts indicate the order of the correction of that value, i.e. $X^{(0)}$ is the unperturbed, bare system value of the quantity X .

More Approximations

Notice in equations (4.55) and (4.56) that the matrix elements of H_I all appear with an energy denominator, related to the difference in energy between the two states in the expectation value of the element. If the states in a given expectation value have a large difference, then they will always appear with a large denominator rendering their contribution to the perturbation theory effectively negligible. The most significant contributions to a perturbed state, $|n^{(0)}\rangle$, will then be from states which are “close” in energy to $|n^{(0)}\rangle$. Perturbation theory then offers a further saving on computational resources by enabling us to also omit from our calculation those expectation values which contain states with large energy differences.

We first need to find, for a given state, which of the other states have a large enough energy difference to justify removing them from our calculation, this is not as straight forward as it may first seem. Naively, we can assume that the energy of a state depends largely on the number of excitations in that state, we can easily count the number of excitations in each of the states in the expectation value and if they are above a set limit we can exclude this term. However, there is a larger number of states with high numbers of excitations (for large enough systems) thus, though the energy difference between states with low and high numbers of excitations will be large and so contributes little to the overall calculation, the number of such terms in the sum is also large and so their combined contribution may be significant. Before we rule out all

states with a certain number of excitations, we should examine how many such states exist to determine if their combined effect will still be negligible.

For the perturbed energy value of a given state, it is then useful to compare the combined contribution to the perturbation from states of differing excitation numbers. In figure 4.19 we look at four sample states from a particular system, each with a different number of excitations. We then calculate the perturbed energy value for each of these states where, for each term, we note the excitation difference between the states appearing in that term along with the terms contribution. We then collect together the contributions from expectation values with equal excitation number differences and compare their total contribution to the overall perturbed energy. Doing this for the perturbed value of states with differing excitation numbers, allows us to see a trend of the type states which will have the most profound effect on the perturbed energy.

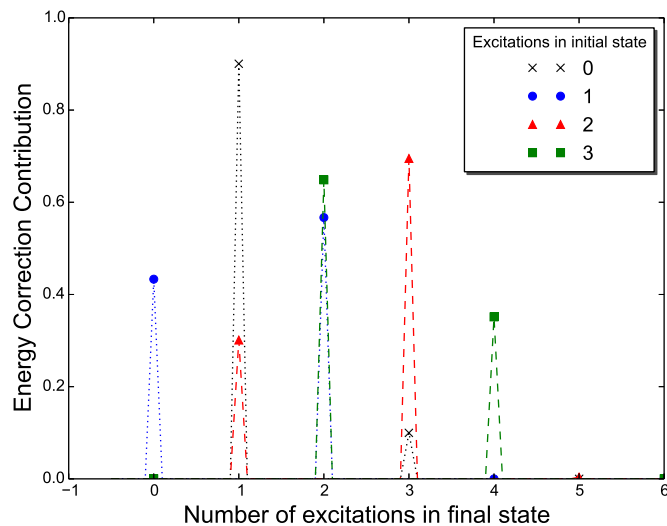


Figure 4.19: Comparison between expectation values with various final state configurations as the number of excitations in the initial state grows (for system size $N = 6$).

The plot in figure 4.19 clearly shows that the most significant states for the perturbed energy are those which have an excitation number which is one greater or one less than the number of excitations in the state being perturbed, i.e. the states closest in excitation number but which don't contribute zero due to being equal parity to the perturbed state.

Combining the low v_k order and close excitation number approximations together will enable us to calculate the perturbed eigenstates and eigenvalues

more quickly, while ensuring the result will be to a good approximation.

Degeneracies

Equations (4.55) and (4.56) will work only if the states in the system are non-degenerate. If degenerate energy levels exist, there will be energy denominators which are zero and so the perturbation theory breaks down. According to the spectra in figures 4.5 and 4.6, we should expect quite a few degenerate energy levels in our model. The perturbation of states corresponding to these degenerate energies must be handled carefully due to singularities which will arise.

Terms containing singularities must be solved directly, i.e. by diagonalisation of the portion of the Hamiltonian which acts on the degenerate subspace, before perturbation theory is applied to the other states in the system. How to handle these states is dependent on the parity sectors to which the degenerate states belong.

If any states are at the same energy but in opposite parity sectors, then the first order term in the eigenstate calculation (equation (4.56)) contains singularities. Projecting the matrix $H_0 + H_I$ onto the degenerate subspace we obtain the eigenvectors of this degenerate subspace through exact diagonalisation. No opposite parity states appear in the second order term as this gives only overlaps between equal parity states and the expectation value of H_I between states from the same parity sector is always zero, as discussed in section 4.4.2, thus any singularities are cancelled by zeros in the numerator. The eigenvectors of the degenerate subspace can then be taken as the unperturbed states, substituting them into the non-degenerate formula (equation (4.56)), with the sums therein taken over only states in the non-degenerate subspace, gives the perturbed states we are looking for.

Conversely, if the states are in the same parity sector, then there is no first order contribution from degenerate states, again due to overlaps between non-equal parity states equalling zero and H_I changing the parity of the states it acts on. There is, however, a contribution to second order states, singularities can then arise because the grouping of the terms in the energy difference denominator does not match with the grouping in the numerator's overlaps.

Therefore, we project the second order matrix $H_0 + H_I(H_0 - E_d)^{-1}\mathcal{P}_{nd}H_I$ (where E_d is the degenerate energy and \mathcal{P}_{nd} is a projection onto the non-degenerate subspace) onto the degenerate subspace and diagonalise to obtain its eigenvectors. Again if the eigenvectors of this matrix are taken as the unperturbed states, using the non-degenerate theory with them (and sums taken only over non-degenerate states) produces the interacting states.

Occasionally an energy level will contain multiple states from both parity sectors (in the $N \rightarrow \infty$ limit). We then have equal parity degeneracy and opposite parity degeneracy together. To tackle this we simply combine the two above approaches, we project onto the degenerate subspace and diagonalise the matrix $H_0 + \mathcal{P}_s H_I \mathcal{P}_s + \mathcal{P}_o H_I (H_0 - E_d)^{-1} \mathcal{P}_{nd} H_I \mathcal{P}_o$, where \mathcal{P}_s and \mathcal{P}_o are projections onto the equal parity degenerate space and the opposite parity degenerate space respectively.

For the eigenvalues we only need to worry about opposite parity states. The first order correction contains no singularities (it is always zero as it must be an overlap of equal parity states) and the second order term is only non-zero for opposite parity states. Then, if there is only equal parity states in the degenerate subspace, there will only be corrections to the energy from non-degenerate states but, if there is opposite parity states, we obtain the corrections to the energy by calculating the eigenvalues of the matrix mentioned above.

The presence of degeneracies then forces us to directly diagonalise parts of H_I corresponding to the degenerate subspace. We saw in section 4.3.3, that the number of degenerate states depends on the system size and for the large systems to which perturbation theory can be applied there will be a large number of degenerate states. Therefore, in the very systems we expected perturbation to help speed up our calculations, we find that it cannot be applied to the majority of the states, thus we may lose a lot of the computing time we would have hoped to have saved.

Also in the implementation of the numerical simulations it was found that the calculation of the many overlaps required to compute the matrix elements of H_I was a much bigger drain on computational resources than its subsequent diagonalisation (this is discussed further in section 4.6). Thus any speed up offered by the perturbation theory was not at the point of the calculation where

it could be really effective. As a computational tool then, perturbation theory does not offer much help, however, its ability to produce a general form of the interacting eigenstates warrants its continued use.

4.5.1 Interacting System Eigenstates

Using equations (4.55) and (4.56), the eigenvalues, Δ_k , and eigenstates, $|k^I\rangle$, of the interacting system can now be expressed in terms of the noninteracting eigenvalues, E_k , and eigenstates, $|k^N\rangle$.

Firstly the interacting energies, note that the first order terms will be zero as they are all of the form $E_n^{(1)} = \langle k^N | H_I | k^N \rangle$, i.e. an overlap of equal parity states. Thus we are left with;

$$\Delta_n^I = E_{n,R} + E_{n,E} - \frac{J_I^2}{N_E N_R} \sum_{p(m) \neq p(n)} \frac{|\langle m_R^N | H_{I,R} | n_R^N \rangle \langle m_E^N | H_{I,E} | n_E^{(0)} \rangle|^2}{(E_{m,R} - E_{n,R})(E_{m,E} - E_{n,E})} \quad (4.57)$$

where $p(k) \neq p(n)$ means the sum is over states $|k^N\rangle$ where the parity of $|k_R^N\rangle$ and $|k_E^N\rangle$ are the opposite parity to those of $|n_R^N\rangle$ and $|n_E^N\rangle$ respectively. The eigenstates of the interacting system are then;

$$\begin{aligned} |n^I\rangle = & |n_R^N n_E^N\rangle - \frac{J_I}{\sqrt{N_E N_R}} \sum_{p(m) \neq p(n)} \frac{\langle m_R^N | H_{I,R} | n_R^N \rangle \langle m_E^N | H_{I,E} | n_E^N \rangle}{E_{n,R} - E_{m,R} \quad E_{n,E} - E_{m,E}} |m_R^N m_E^N\rangle + \\ & + \frac{J_I^2}{N_E N_R} \sum_{p(m)=p(n)}^{p(k) \neq p(n)} \sum_{m_R \neq n_R}^{m_E \neq n_E} \left\{ \frac{\langle m_R^N | H_{I,R} | k_R^N \rangle \langle k_R^N | H_{I,R} | n_R^N \rangle}{(E_{m,R} - E_{n,R})(E_{k,R} - E_{n,R})} \times \right. \\ & \left. \times \frac{\langle m_E^N | H_{I,E} | n_E^N \rangle \langle k_E^N | H_{I,E} | n_E^N \rangle}{(E_{m,E} - E_{n,E})(E_{k,E} - E_{n,E})} \right\} |m_R^N m_E^N\rangle \end{aligned} \quad (4.58)$$

Again notice that the last second order term from equation (4.56) drops out as it contains an overlap of equal parity states.

We can now talk generally about the interacting eigenstates and energies. It is clear the energies in particular will only be slightly perturbed from their original values in the absence of a first order correction. Most importantly we see that the most significant perturbations to a given state/energy come from states which are close in energy to the non-interacting state and from the opposite parity sector to it.

Naively we would expect the most probable outcome from an interaction which hops single fermions between chains to be states which are closest in

energy and in the opposite parity sector, i.e. states which require little extra energy to excite. The above result enforces these expectations.

4.5.2 Time Evolution

We discussed in section 4.3.3, that we will be interested in using the parity sectors of the anyon ring as the qubit states. Assuming we can manipulate the anyons in the ring, then we can force the system to be in any particular eigenstate of the noninteracting system we wish. However the eigenstates of the noninteracting system, i.e. those composing the qubit states, are not eigenstates of the interacting system. This becomes an issue if we look at how the state behaves over time.

The evolution of eigenstates, $|\chi_j\rangle$, of the system over time can be easily obtained from Schrödinger's equation as:

$$|\chi_j(t)\rangle = e^{-\frac{iE_j t}{\hbar}} |\chi_j(0)\rangle \quad (4.59)$$

where E_j is the eigenvalue corresponding to $|\chi_j\rangle$. If the system is placed in one of its eigenstates then the probability of finding the system in that same eigenstate after a time t will always be 1:

$$P_{\chi_j}(t) = |\langle \chi_j(0) | \chi_j(t) \rangle|^2 = \left| \langle \chi_j(0) | e^{-\frac{iE_j t}{\hbar}} \chi_j(0) \rangle \right|^2 = \left| e^{-\frac{iE_j t}{\hbar}} \right|^2 |\langle \chi_j(0) | \chi_j(0) \rangle|^2 = 1 \quad (4.60)$$

States which are not eigenstates of the system have a slightly more complicated time evolution. Firstly, to see how such a state evolves, we express it in terms of a superposition of the eigenstates of the system. Let $|s\rangle$ be a state which is not an eigenstate of the system, then:

$$|s\rangle = \sum_j |\chi_j\rangle \langle \chi_j | s \rangle = \sum_j a_j |\chi_j\rangle \quad (4.61)$$

where $a_j = \langle \chi_j | s \rangle$ is just a constant. We can now time evolve each of the eigenstates separately to find how $|s\rangle$ evolves.

$$|s(t)\rangle = \sum_j a_j |\chi_j(t)\rangle = \sum_j a_j e^{-\frac{iE_j t}{\hbar}} |\chi_j(0)\rangle \quad (4.62)$$

Each eigenstate then oscillates at a different frequency, determined by its eigenvalue, so the probability of finding the system in a state $|s\rangle$ after a time t is not always 1 if $|s\rangle$ is not an eigenstate of the system.

For our system then, the noninteracting eigenstates are not eigenstates of the interacting system. Therefore, if we place the system in one of these noninteracting states, the system will oscillate out of that state over time. This in turn, means that at a certain time the probability of finding the system in the state we started with may be lower than the probability of finding it in some other state.

In short, the interaction between the edge and the ring introduces a time scale for how long the information in the qubit remains uncorrupted. Operations on the qubit will have to be done within this time frame in order for us to be confident in the validity of the results.

Applying this time evolution to the general form of the interacting eigenstates, given in the previous section (equations (4.58)), allows us to see how a general interacting state will behave over time for weakly interacting systems. For the system we are dealing with we will call an eigenstate of the noninteracting system, $|n^N\rangle$, we place our qudit in this state by manipulating the fusion channels of the σ anyons appropriately. The eigenstates of the actual system are the interacting eigenstates, $|n^I\rangle$, given by perturbing the non-interacting eigenstates using equation (4.56):

$$|n^I\rangle = |n^N\rangle + \sum_{m \neq n} \frac{\langle m^N | H_I | n^N \rangle}{E_n - E_m} |m^N\rangle \quad (4.63)$$

where the zeroth order term is the noninteracting state and the E_i are the energies corresponding to the noninteracting states. We can then expand $|n^N\rangle$ in terms of these eigenstates:

$$|n^N\rangle = \sum_k |k^I\rangle \langle k^I | n^N \rangle = \sum_k |k^I\rangle \left\{ \langle k^N | n^N \rangle + \sum_{m \neq k} \frac{\langle k^N | H_I | m^N \rangle}{E_k - E_m} \langle m^N | n^N \rangle \right\} \quad (4.64)$$

But the noninteracting eigenstates are orthonormal, $\langle a^N | b^N \rangle = \delta_{a,b}$:

$$\begin{aligned} |n^N\rangle &= \sum_k |k^I\rangle \left\{ \delta_{k,n} + \sum_{m \neq k} \frac{\langle k^N | H_I | m^N \rangle}{E_k^N - E_m^N} \delta_{m,n} \right\} \\ |n^N\rangle &= |n^I\rangle + \sum_{par(k) \neq par(n)} \frac{\langle k^N | H_I | n^N \rangle}{E_k - E_n} |k^I\rangle \end{aligned} \quad (4.65)$$

where the sum is only over states with the opposite parity to $|n^N\rangle$. We can now time evolve the interacting eigenstates as they are the eigenstates of the system, if Δ_j is the energy corresponding to the interacting eigenstate $|j^I\rangle$ then we get:

$$|n^N(t)\rangle = e^{-\frac{i\Delta_n t}{\hbar}} |n^I\rangle + \sum_{par(k) \neq par(n)} \frac{\langle k^N | H_I | n^N \rangle}{E_k - E_n} e^{-\frac{i\Delta_k t}{\hbar}} |k^I\rangle \quad (4.66)$$

Note that the Δ 's are interacting eigenvalues, they can also be expressed in terms of the noninteracting eigenvalues, using equation (4.55).

$$\Delta_k = E_k - \sum_{par(m) \neq par(k)} \frac{|\langle m^N | H_I | k^N \rangle|^2}{E_m - E_k} \quad (4.67)$$

The interaction energy, J_I , enters into the equations through the perturbation term, H_I . From equation (4.66), we see then that this energy quantity influences how much the evolution of a state depends on interacting eigenvectors which are obtained by perturbing the other noninteracting states.

If the interaction energy is very weak, the state can be approximated by just the interacting eigenstate coming from perturbing itself, $|n^N\rangle \approx |n^I\rangle$, which means there will be very little oscillation and the probability of staying in that state remains high. As J_I is increased, a greater dependence on other interacting eigenstates comes into play, with the state expressed as a superposition of more than one eigenstate then it will start to oscillate more wildly as each of the eigenstates rotates at a different rate. As stated earlier, the perturbation theory only holds for small values of J_I but this at least gives us an idea of how the system can be expected to behave in general and we will see later that these predictions are actually quite useful, even at large J_I .

Equation (4.67) shows that the interaction energy influences how large the eigenvalues of the interacting eigenstates will be, specifically increasing J_I will

decrease the magnitude of the eigenvalue (assuming the second order term is smaller than the zeroth order term which will be true unless J_I is large). As would be expected then, we find that the strength of the interaction between the anyon ring and the edge of the fractional quantum Hall puddle directly affects how reliable the qudit is.

The probability that the system has moved from its initial state, $|n^N\rangle$ to some alternative state of the non-interacting system, $|m^N\rangle$, can be found by measuring the overlap of the two states at after a particular time t . Keeping to second order we obtain:

$$|\langle n^N(t)|m^N(0)\rangle|^2 = \left| \frac{\langle n^N(0)|H_I|m^N(0)\rangle}{(E_n - E_m)} \left(e^{\frac{i\Delta_n t}{\hbar}} - e^{\frac{i\Delta_m t}{\hbar}} \right) \right|^2 \quad (4.68)$$

This probability will clearly depend heavily on the value of J_I and so the states of a strongly interacting system will have a greater probability of moving into a different state of the noninteracting system through time evolution.

4.6 Numerical Simulations

We have stated previously that an analytic solution to this problem for general N is beyond the scope of the project and is potentially not possible. Though the perturbation theory provides us with some general impressions of how the system's time evolution can be expected to depend on the interaction strength, these perturbation results will not be applicable to all types of systems we wish to examine, as J_I is not always small.

Instead we use numerical simulations to understand how the system is behaving. For set values of J_E and J_R we can vary J_I and monitor how this affects the time evolution of the system. This allows us to compare the regimes defined in section 4.5.1. Such simulations can then be used to shed some light on which regimes would be most beneficial to an actual implementation of TQC in this system.

It is important to note at this point that the simulations in this section consider all regimes for only a single system size, i.e. only one value of N_E and N_R is examined. While the effects of increasing the number of anyons (or decreasing the size of the system) can be approximated by changing the

in-chain interactions appropriately, this approximation is only exact in the thermodynamic limit. A large system modelled by increasing the interaction values of a smaller system will inherit the finite size effects of the smaller system, causing a deviation from the true spectrum of that system.

It must be stressed then, that a much deeper study of these regimes for larger system sizes is needed before it is possible to say anything definitive about the nature of the model in the thermodynamic limit. With these simulations then we aim only to glimpse some distinguishing features of the model and draw attention to areas which warrant closer examination.

System Size

Our first step is to find the eigenstates of the interacting system, i.e. we need to diagonalise H_I . Diagonalisation is computationally expensive for large matrices and so this will limit the size of systems we can simulate in a reasonable time frame. For weakly interacting systems, one may consider using the results of perturbation theory (equations (4.55) and (4.56)) to more quickly evaluate a good approximation of the interacting eigenstates. However, as discussed in section 4.5, the large number of degenerate states present in large systems (where these results would be most accurate) indicate that we will still have to use exact diagonalisation to obtain a number of the eigenstates.

Further, it was shown in section 4.4.2 that the number of terms within expectation values of H_I grows rapidly with increasing system size. Due to this, it is found that the calculation of these expectation values of H_I are, in fact, the most intensive part of the calculation. Thus, with large sums over such expectations values, the perturbation theory method is actually quite slow. It is then more efficient to calculate the eigenvectors by exact diagonalisation of H_I , where the expectation values are used only to calculate the matrix elements. This method is also not restricted to the weakly interacting systems the perturbation theory applies to, and so it can be used for all values of J_I .

With the complexity of the matrix elements of H_I as the limiting factor, we find a system size of $N_R = N_E = 4$ as an upper limit for systems that we could simulate in a reasonable time. Note that this relatively small system, with a Hilbert space of dimension $2^{N_E} \times 2^{N_R}$, could be diagonalised much

quicker in a real space description. However, for the analysis of this model it is required to formulate the problem in momentum space as we need to be able to distinguish the direction of the momentum of the states on the edge ring in order to project onto the chiral subsystem. Thus, the states of the system and the interaction term take on a more cumbersome form which causes a severe escalation of the computation time for larger systems.

It is also noteworthy that, at this system size, the $\mathcal{O}(v^4)$ approximation, which we introduced in section 4.4.2 for the calculation of overlaps between states, becomes exact as there will be no terms of higher order in v . Thus, all matrix elements of H_I are calculated exactly in the following numerics.

Hilbert Space

With a specific value for the size of the chains, we can easily calculate the allowed momentum values and write down states of the noninteracting system.

Remember that only certain combinations of edge and ring states are permitted. For the topological charge of the full system to be 1, the topological charge of the ring and the edge must be equal. For an odd number of anyons on both chains, the charge of each chain will be σ and so we can always choose the 1 fusion channel of the two chains. Thus we get no extra restrictions on the states and the Hilbert space will be $(2^{N_E} \times 2^{N_R})$ -dimensional. However, for a chain with even anyon number, the topological charge will be 1 or ψ . For two such chains to fuse to 1 then we must require that they both have the same charge which restricts the number of allowed states.

The labelling conventions used so far may cause some confusion at this point. The topological charge, 1, ψ or σ , of a chain depends on the number of σ anyons on the chain and their combined fusion channel. But regardless of its topological charge, the states in the spectrum of the chain can be split between conformal sectors, also labelled 1, ψ and σ , which are dependent on the momenta of the excitations in the states. For a set charge of the chain, the number of anyon pairs fusing to ψ then gives the number of fermions in the system, which, in turn, dictates the momentum parity sector of the spectrum. For an odd number of ψ fusings, the chain is in the σ momentum sector and, for an even number of ψ fusings, the chain is in the 1 or ψ momentum sector

(the exact sector in the even case depends on how many of these ψ fermions are left and right moving which is not obvious in the anyon fusion-tree picture).

For an (even, even) ring and edge chain system, like the one we will be simulating, the chains must either both be in the odd momentum sector or both in the even momentum sector. The possible conformal sector combinations are then; $(\sigma, \sigma), (1, 1), (1, \psi), (\psi, 1), (\psi, \psi)$. We then must eliminate the combinations which give an undesired total charge, namely states in the $(\sigma, 1/\psi)$ or $(1/\psi, \sigma)$ conformal sectors. For each individual chain, the number of states in each parity sector is 2^{N-1} , thus the dimension of the Hilbert space will be given by:

$$d_{\mathcal{H}} = n_{\text{odd}}^E \times n_{\text{odd}}^R + n_{\text{even}}^E \times n_{\text{even}}^R = 2(2^{N_E-1} \times 2^{N_R-1}) \quad (4.69)$$

For the $N_E = N_R = 4$ system we wish to simulate then we have a 128-dimensional Hilbert space.

Time Evolution

For our simulation, the system is set in a particular initial state of the noninteracting system, $|n\rangle$. We will choose this to be the ground state for simplicity and speed but the same methods can be applied to any state.

This initial state is then expanded as a superposition of interacting eigenstates, as shown in section 4.5.1, in which form we can easily time evolve the initial state, using the method outlined in section 4.5.2. For each time step, we measure the probability of the system being in the same state it was at $t = 0$, $P_n(t) = |\langle n(0)|n(t)\rangle|^2$. The probability that the system has remained in its initial state can then be plotted as a function of time.

Finally, for each time step we also measure the probability that the system has moved into any one of the other non-interacting eigenstates of the system, $|k\rangle$; $P_k(t) = |\langle k(0)|n(t)\rangle|^2$. We can then produce a number of plots showing how the likelihood of the system being in each of the states of the noninteracting system changes over time. As outlined in section 4.3.3, we are not actually concerned with the individual state that the system is in but rather the fermion number parity of this state. We can then combine the probabilities to make the plots more legible. Note in all plots time will be given in units of $1/\hbar$.

As mentioned earlier, the initial state is always chosen to be the ground state, i.e. an even sector state. If the parity sectors are considered to be the states of a qubit, then $\sum_{k=odd} P_k(t)$ will give a measure of the reliability of the qubit at a given time, t .

4.6.1 Non-Chiral System

Firstly we examine time evolution in the simplified, non-chiral system described in section 4.4.1.

We would first like to examine the effect of the interaction on the base system by comparing the energy spectra of the two systems. However, the interacting eigenstates do not have a well-defined momentum, as translational invariance is broken when the interaction is introduced. This makes a direct comparison between the two spectra, beyond their eigenvalues, quite difficult.

Instead, for set values of J_E and J_R , we can look at the spread of the non-interacting states in terms of energy, then follow their evolution for small changes in the interaction energy. The extent to which the spread of the spectrum has changed from the non-interacting case (figure 4.15) will give an indication of how strongly J_I will affect the time evolution of a non-interacting state subject to this interaction.

Regime 1

We first consider the case where J_E and J_R scale similarly, the scaling for J_I has not been determined and it will likely not relate to J_E and J_R in any obvious way. Fixing J_E and J_R to be equal, we can look at a range of values of J_I to analyse how it affects the system.

This can be considered part of regime 1 (see section 4.4.4), describing a system where the linear density of the anyons in the ring chain scales with the system size thus giving J_R a similar linear scaling to the scaling of J_E , from the CFT describing the edge chain. Note, however, that this could also refer to the case where J_E and J_R both scale exponentially with size. This may be a more useful interpretation as, by its definition, the non-chiral case more accurately describes two similar chains. The double ring case then may be more relevant to modelling systems where the anyons in each ring behave very

similarly, i.e. two rings of bulk anyons, rather than our proposed system where the ring chain scales differently to the edge and the similarity is achieved by scaling the linear anyon density on the ring to compensate.

Figure 4.20 shows the change in the spread of the spectrum for $J_E = J_R = 1$. Note that the $J_I = 0$ point describes the spread of the non-interacting spectrum in figure 4.15.

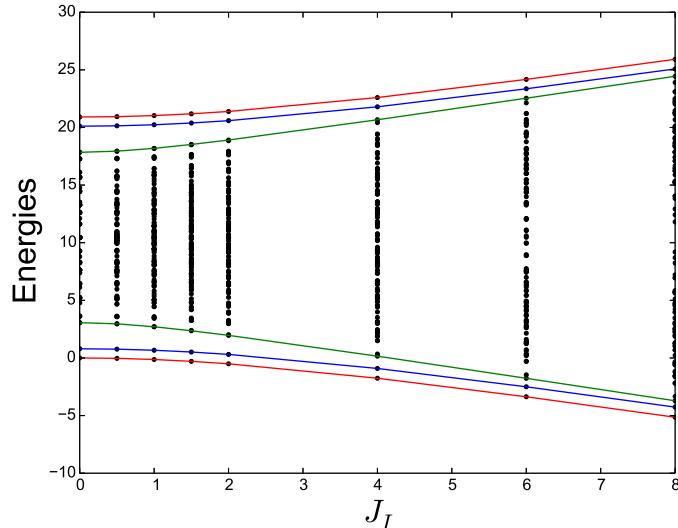


Figure 4.20: Change in the spread of the eigenvalues of the systems as J_I is increased. With guides to the eye shown to highlight the evolution of the 3 lowest and highest energy states.

With a lower interaction energy the states are less disturbed from their non-interacting energies, thus a larger interaction between the edge and the chain will disorder the system more, relative to the non-interacting spectrum. For a large J_I then, we expect a given non-interacting state to have a bigger overlap with a large number of interacting eigenstates. As outlined in section 4.5.1, this will cause the expected value of the state to change more dramatically over time. We would expect the time evolution plots to reflect this and show that a greater probability of the system changing to an opposite parity state as J_I is increased.

In figures 4.21 - 4.24 we plot the time evolution of the non-interacting ground state for increasing values of J_I , with J_E and J_R remaining constant.

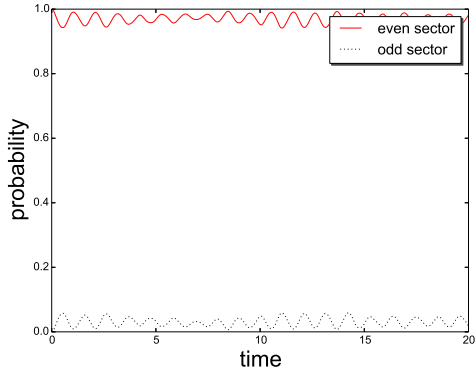


Figure 4.21: $J_E = J_R = 1, J_I = 1$

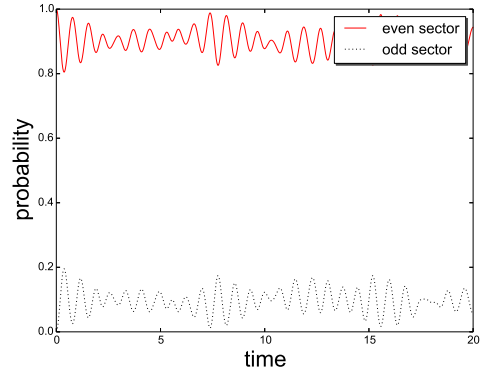


Figure 4.22: $J_E = J_R = 1, J_I = 2$

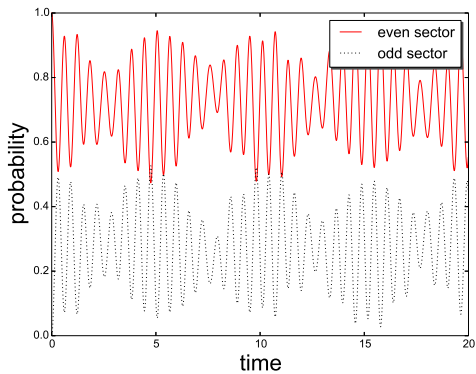


Figure 4.23: $J_E = J_R = 1, J_I = 4$

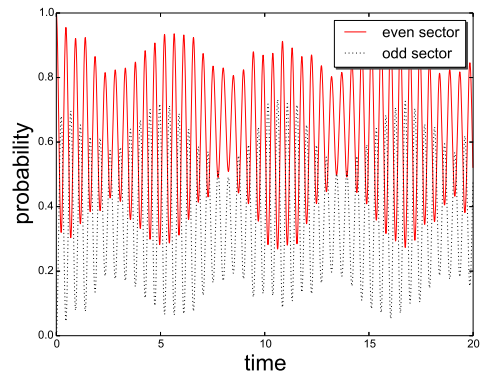


Figure 4.24: $J_E = J_R = 1, J_I = 6$

It is clear that, if $J_I > 4$, then for this system there is a significant probability of the system moving into an opposite parity state ($P_{\text{opp}} > 0.5$). Figure 4.23 shows that the possibility of the system changing to an opposite parity state starts to become more probable than it remaining in the initial state for $J_I = 4$. For larger interaction energies than this, the information stored in the qubit is likely to be corrupted.

We have two options to reduce the chances of this occurring, first we could try to perform any calculations within the time frame where the state is unlikely to jump or we could reduce the strength, J_I , of the interaction between the chains. Usually it is required that the topological operations which produce logic gates must be implemented slowly or the energy of the system may exceed the gap to excitations and extra quasiparticles could be created which will affect the state of the system, see e.g. ref. [80]. It would therefore be safer to explore methods which don't require us to perform calculations within a

time-frame, we will then concentrate on the second option where the interaction is weakened.

In reverse order the plots, figures 4.21 - 4.24, show the effect of lowering the interaction strength. It is clear, as predicted in the previous section, that lowering the value of J_I affects the likelihood of the system moving into an opposite parity state. This is an indication that the description produced by perturbation theory for low values of J_I , i.e. equation (4.66), is still useful in the interpretation of the dynamics of strongly interacting systems.

Decreasing J_I from 6 to 1 lowers the maximum P_{opp} from ~ 0.8 to ~ 0.1 , which means the probability of the system remaining in the initial state is always considerably higher than the probability of it changing. For $J_I \leq 1$ the probability of changing state in this system becomes effectively zero. Thus, by lowering values of J_I , the state of the system becomes more robust. To ensure that the integrity of the qubit remains intact, it is then essential to engineer the interaction between the two rings to be as low as possible.

Regime 2

We now look at regime 2 where the edge interactions and ring interactions scale differently with size, specifically J_E scales linearly whereas J_R decays exponentially. For larger system sizes then, the difference between the two values will grow. Keeping $J_E = 1$ we can look at the effects of moving to a different system size (without a corresponding increase in the anyon density) by plotting the spread of eigenvalues as J_I is increased for $J_E = 0.5$ and $J_E = 0.1$. In the case $J_E = J_R$ we simply obtain the results of regime 1, however, unlike the system in regime 1, these results will only hold at this specific system size. Comparison with figure 4.20 will then indicate the effect of the faster decay of J_E as the system size increases.

Figure 4.25 shows that for regime 2, at larger J_I we again see a bigger spread of the interacting eigenvalues in both systems, similar to what was shown for regime 1. However, a clear interpretation of how the difference in J_E for the two systems influences the effect of J_I is not easily obtained from a comparison of these two plots.

In the absence of anyon-anyon interactions in the bulk we obtain a system

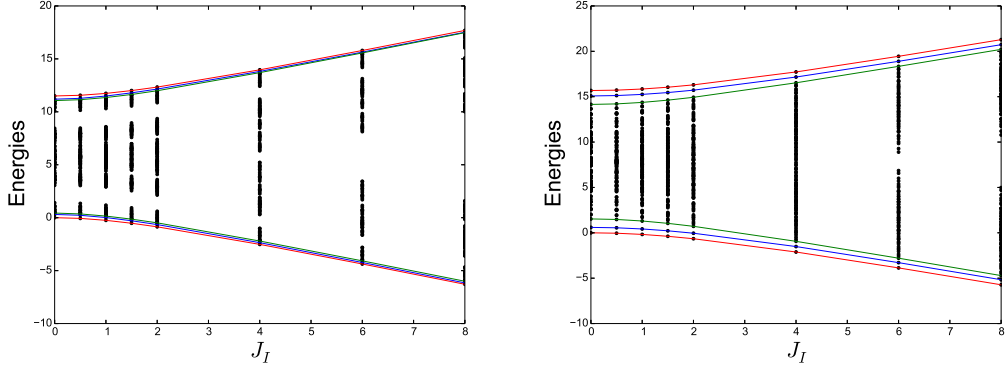


Figure 4.25: The spread of the eigenvalues of the systems with $J_E = 1$ and $J_R = 0.1$, $J_R = 0.5$ respectively, as J_I is increased.

of 2^N degenerate states, as discussed in section 4.3.3. It is the introduction of this bulk interaction which lifts the degeneracy of the system, producing the spectrum in figure 4.11. An increase in the bulk interaction, J_R , then will correspond to a decreases in the degeneracy of the states on the ring chain.

In figure 4.25 we see the system with lower J_R (on the left) has a smaller spread of the energies for the non-interacting case, i.e. there's a bigger degeneracy in the energies for the $J_R = 0.1$ system at $J_I = 0$. Because of this difference in the initial, $J_I = 0$ point, it is difficult to discern any useful information by comparing the plots at subsequent J_I . We then look to the time evolution plots to gain a clearer understanding of the how J_I affects the systems differently.

Similar to regime 1 then, for each system size, i.e. each value of J_E and J_R , we can see how a range of J_I values will affect the time evolution of the ground state of the non-interacting system.

We plot the time evolution for two systems; $J_R = 0.5$ and $J_R = 0.1$. The following figures should then be read left to right for increasing J_R values, at constant J_E and J_I , and top to bottom for increasing J_I , with constant J_E and J_R .

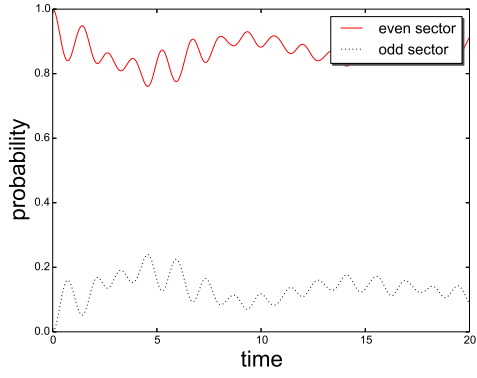


Figure 4.26: $J_E = 1, J_R = 0.1, J_I = 1$

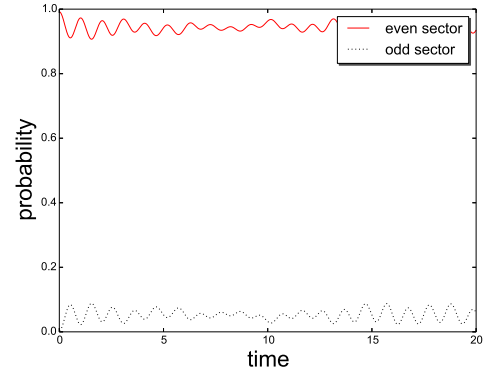


Figure 4.27: $J_E = 1, J_R = 0.5, J_I = 1$

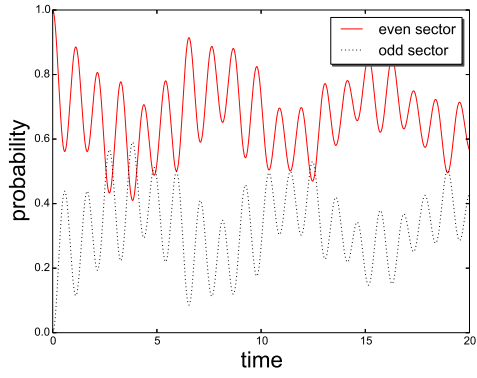


Figure 4.28: $J_E = 1, J_R = 0.1, J_I = 2$

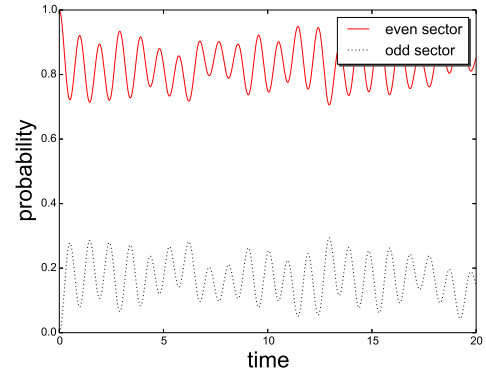


Figure 4.29: $J_E = 1, J_R = 0.5, J_I = 2$

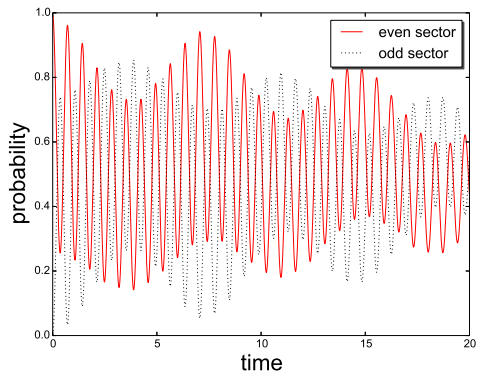


Figure 4.30: $J_E = 1, J_R = 0.1, J_I = 4$

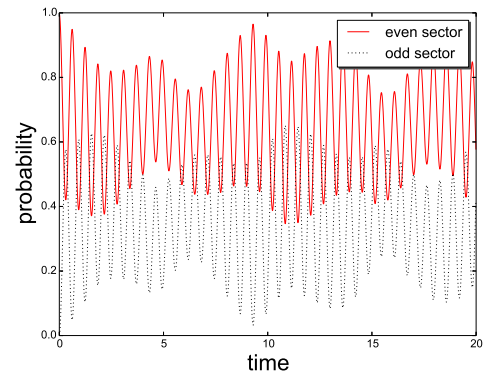


Figure 4.31: $J_E = 1, J_R = 0.5, J_I = 4$

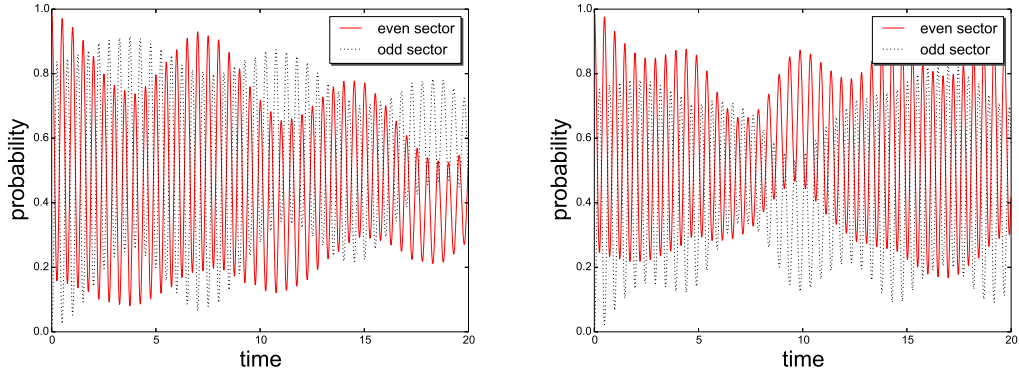


Figure 4.32: $J_E = 1$, $J_R = 0.1$, $J_I = 6$ Figure 4.33: $J_E = 1$, $J_R = 0.5$, $J_I = 6$

By reading left to right for each value of J_I it can be clearly seen that the interaction will have a more prominent effect on the system for weaker in-chain coupling on the ring. We see P_{opp} start to increase beyond P_{initial} for $J_I \approx 2$ when $J_E = 0.1$ but this does not happen in the $J_E = 0.5$ system until the interaction strength is $J_I \approx 4$.

For larger system sizes, figures 4.26 - 4.33 show that the state of the system becomes much more likely to change and operations must be performed in a much shorter time span to compensate for the faster oscillations between states. The integrity of the system, in regime 2, is then not only dependent on the separation between the ring and the edge but also the size of the system.

Edge Absorption

The strong coupling limit has been examined previously, refs. [100, 85] found that, when the interaction between a bulk anyon and the edge is very strong, the anyon effectively becomes absorbed into the edge of the system. This would suggest that figure 4.24 should present a similar plot to that obtained by considering a new system where a σ anyon from the chain has been absorbed into the edge of the system so $N_R \mapsto N_R - 1$ and $N_E \mapsto N_E + 1$.

However, these studies consider only single bulk anyons, or at least bulk anyons which don't interact with each other, and so the results cannot be so easily applied to our model. The interaction between the bulk anyons in our system means that, though the inter-chain interaction may be strong enough to absorb an anyon into the edge chain, the anyon has not decoupled from the ring chain and must still be considered a part of this chain also. It will likely

be difficult to apply this complex interaction to the anyon absorption interpretation, so our current method provides a more convenient representation of the strong coupling limit for our model.

If we were to return again to the system where anyons in the ring are permitted to be unevenly spaced, as described by the Hamiltonian in equation (4.17) and Lagrangian in equation (4.40), this absorption explanation would become relevant. With a non-constant, in-chain coupling, the ring structure becomes less strict, we can imagine moving one anyon in the ring closer and closer to the edge while keeping the others fixed. The interaction strength between this anyon and its neighbouring ring anyons diminishes, which is permitted thanks to the variable interaction strength in this model. Eventually, the anyon will be closer and more strongly coupled to the anyons on the edge, the anyon is now more a part of the edge chain and we can say it has been absorbed by it. The chain lengths are altered by the absorption, $N_E \mapsto N_E + 1$, $N_R \mapsto N_R - 1$, and the interaction between the two chains is now negligible at all points. Note that in the actual system, the edge will be chiral, there is then an anyon from a non-chiral chain being absorbed into a chiral chain, which represents a complex, non-trivial process (the effects of which are beyond the scope of this thesis).

It's interesting to note here, that the ring chain is now no longer a closed chain. There is no next-nearest neighbour interaction term in the Hamiltonian, the distance between next-neighbours is taken to be such that the interaction between them is negligible. So, with the removal of an anyon from the bulk, there is now a gap in the ring across which there is no interaction, the anyons in the bulk then form an open chain. We can model how this new system interacts with the edge relatively easily using the same methods as above, by replacing the Hamiltonian describing the bulk anyons with the open chain Hamiltonian from equation (4.13) or, alternatively, by introducing next-nearest neighbour interactions for the “end” anyons.

4.6.2 Chiral Edge System

We now reintroduce the chirality of the edge, allowing us to simulate our original model. Firstly, we look at the effect of reintroducing the chirality

of the edge on the non-interacting spectrum, figure 4.15. For the edge to be chiral, any operator which creates edge chain states with negative momentum must be eliminated (except for $\gamma_{-\pi/N}^\dagger$ which is needed to create states in the ψ sector, see section 4.4.1). We must, therefore, project onto the subspace of the Hilbert space containing states whose edge component only has operators with momentum $k \geq -\pi/N$ on the edge chain.

The number of remaining states in the edge spectrum is given by the number of even groupings of the momentum modes $(-1, \dots, N/2-1)$ and the number of odd groupings of the momentum modes $(0, \dots, N/2-1)$. For the ring chain however, we have the same number of states as before, thus we get a Hilbert (sub)space for the chiral model with dimension:

$$d_{\mathcal{H}} = n_{\text{odd}}^E \times n_{\text{odd}}^R + n_{\text{even}}^E \times n_{\text{even}}^R = (2^{N_E/2} \times 2^{N_R-1}) + (2^{N_E/2-1} \times 2^{N_R-1}) \quad (4.70)$$

For our simulated model, with $N_E = N_R = 4$, this gives a 48-dimensional Hilbert space.

We also must introduce a lowering of the energy of the states on the edge, halving the conformal dimensions of the sectors, as mentioned in section 4.4.1. Figure 4.15 shows the ψ and σ sector states appropriately lowered in relation to the 1 sector.

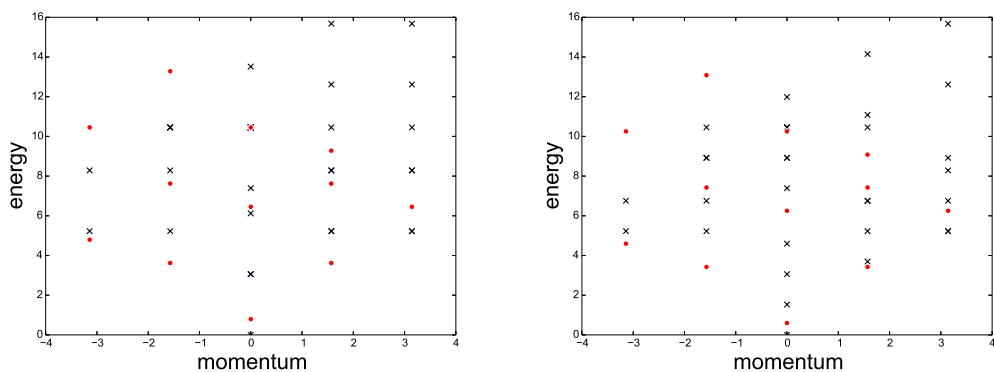


Figure 4.34: The non-interacting spectrum for a chiral edge without (left) and with (right) lowered ψ and σ state energies, for $J_E = J_R = 1$.

We expect this energy lowering to have an effect on the likelihood of the state moving to a different sector, as states from different sectors, e.g. the 1 and σ sectors, are now closer in energy. Looking to the perturbation theory interpretation of the interacting eigenstates (equation (4.56)), terms which

correspond to different parity states now have a lower energy denominator and so the probability of them overlapping is higher.

Regime 1

We can reintroduce the inter-chain coupling now, i.e. set $J_I \neq 0$, and, as expected from our non-chiral calculations, we see that the magnitude of this coupling strength determines how disturbed the states are from their non-interacting energies. In regime 1 the linear density of anyons in the ring scales with the system size, thus $J_E \sim J_R$. As in the non-chiral case, J_I is undetermined so, setting the in-chain interactions to some particular value, we can observe the effects of various strengths of J_I . Again, a good indication of how strongly the interaction is affecting the system can be gained by following the spread of the energies for a set J_E and J_R as J_I is varied, with $J_E = J_R = 1$ we get the following plot;

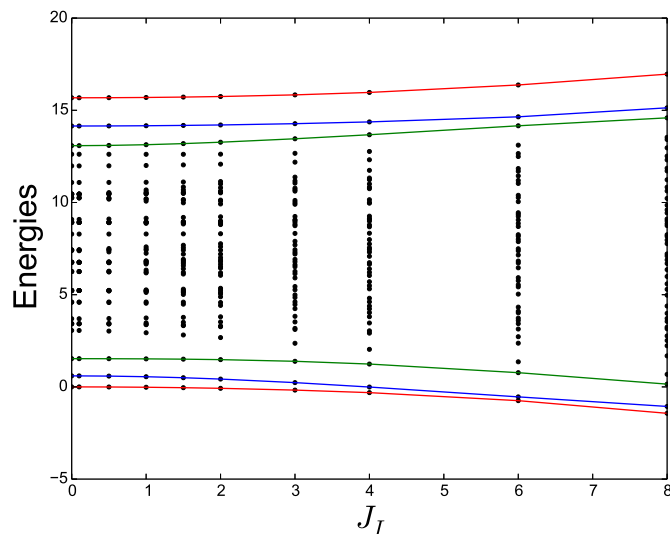


Figure 4.35: The spread of the eigenvalues of the system with $J_E = J_R = 1$ as J_I is increased. With guides to the eye shown to highlight the evolution of the 3 lowest and highest energy states.

Note that $J_I = 0$ in figure 4.35 gives the spread of the non-interacting, lowered spectrum from figure 4.34. We again see that, with increasing J_I , the spectrum becomes more distorted from the non-interacting case. It should be noted, however, that the degree to which the states have moved is less than in the non-chiral, regime 1 case, as seen by comparison with figure 4.20. This indicates that the energies of the states of the system are then less affected by

the interaction than in the non-chiral case.

This is surprising as we stated earlier that the lowering of the edge energies, and consequent ‘‘closeness’’ of the states in the chiral case, should increase the contribution from other states, as indicated in the perturbation theory results (section 4.5). We would then expect the eigenvalues to undergo a more drastic change due to the introduction of the coupling. However, while this is true and terms arising from overlaps with different sectors states will indeed contribute more to the interacting eigenstates in the chiral case, the number of such terms in the non-chiral case is larger by a factor of $2^{N_R-1} [2^{N_E} - (3)2^{N_E/2-1}]$. The contribution from this number of extra states will, in general, be much greater than the slight change we see in the energy difference denominators, thus the gain produced by the states moving closer is overcome by the loss from the discarded antiholomorphic states.

Again, keeping J_E and J_R constant, we can plot the time evolution of the ground state of the non-interacting system for varying values of J_I .

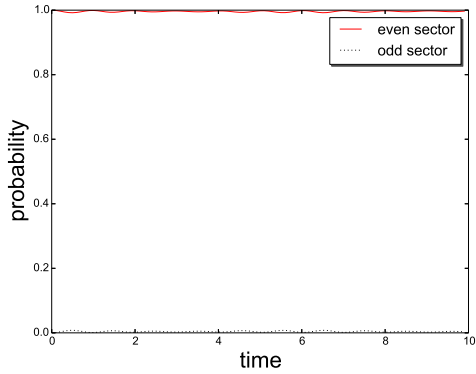


Figure 4.36: $J_E = J_R = 1, J_I = 1$

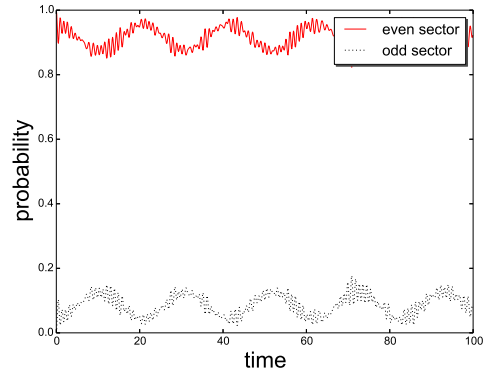


Figure 4.37: $J_E = J_R = 1, J_I = 4$

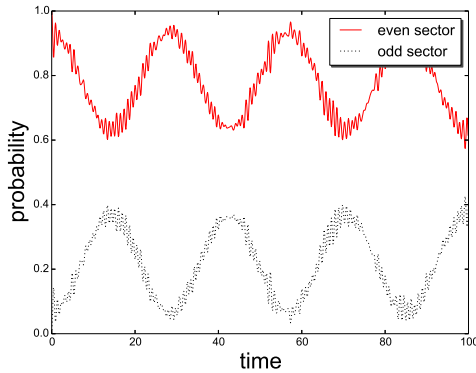


Figure 4.38: $J_E = J_R = 1, J_I = 5$

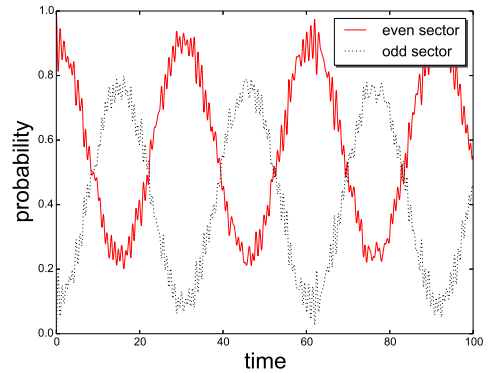


Figure 4.39: $J_E = J_R = 1, J_I = 6$

The time evolution plots clearly show that the increase in J_I leads to an increase in the likelihood of the system decaying into an opposite parity state, along with a speed up in the oscillations of the state. These plots display a somewhat similar behaviour to the non-chiral plots, figures 4.21 - 4.24, but, as with the spectra, the effect of the interaction is diminished by the reintroduction of the edge chirality (due to a lower number of states to sum over in the perturbation theory). As a result, for the system to be likely to change state, the interaction between the edge and the ring must be significantly stronger than in the non-chiral case. We see that the probability of the state flipping to an odd parity state only becomes larger than the probability of it remaining in the even sector only for $J_I > 5$.

Also the oscillations of the state of the system are much more rapid in the non-chiral case than the chiral case, note that figures 4.21 - 4.24 are for a range $t \in [0, 20]$ whereas figures 4.36 - 4.39 plot over a range of $t \in [0, 100]$. This is further indication that equation (4.66), derived from perturbation theory, still describes many of dynamics of the system for strong interactions. The interacting eigenvalues determining the rate of oscillation of the state have a contribution from a sum over all states of the system, as shown in equation (4.67). As there is more states in which to sum over in the non-chiral Hilbert space this term could lead to larger interacting eigenvalues, for large J_I , and thus faster oscillations in the time evolution of the state.

Regime 2

Moving to regime 2, similar to the non-chiral case, the scaling of the system will now have an effect on the spectrum. Remember for this regime, as the system grows J_E will scale linearly whereas J_R scales exponentially to zero, meaning the coupling for the ring will fall off much quicker than the edge couplings. For a set J_E and J_I then we can observe the effect of increasing the system size. We will again look at two separate systems with $J_R = 0.1$ and $J_R = 0.5$, for which we can produce the spectrum spread plots.

As with the non-chiral, regime 2 case (figure 4.25), we find that the difference in the degeneracies of the spectra at $J_I = 0$ makes it difficult to compare the plots for increasing interaction strength. The time evolution plots must

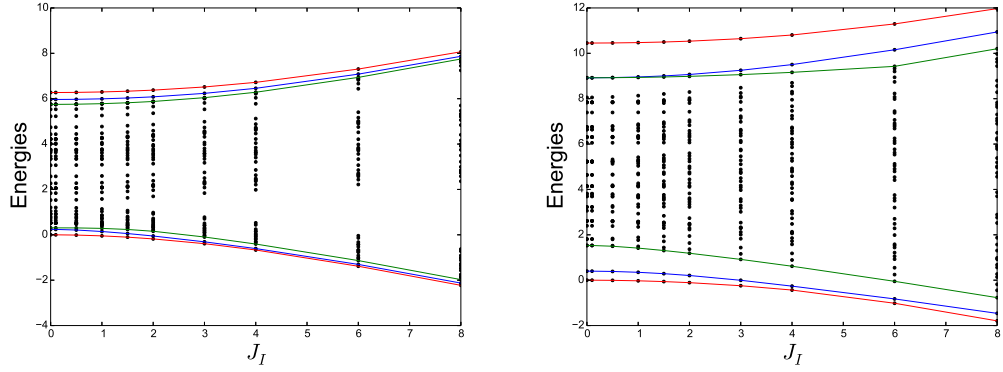


Figure 4.40: The spread of the eigenvalues of the systems with $J_E = 1$ and $J_R = 0.1$, $J_R = 0.5$ respectively, as J_I is increased.

again be relied upon to give a clearer understanding of how the effects of J_I change with decaying J_R values.

We provide an equivalent layout to that used in the non-chiral regime 2 section above. The plots then should again be read from left to right for constant J_I and J_E with decreasing J_R , and top to bottom for constant J_R and J_E , with increasing J_I .

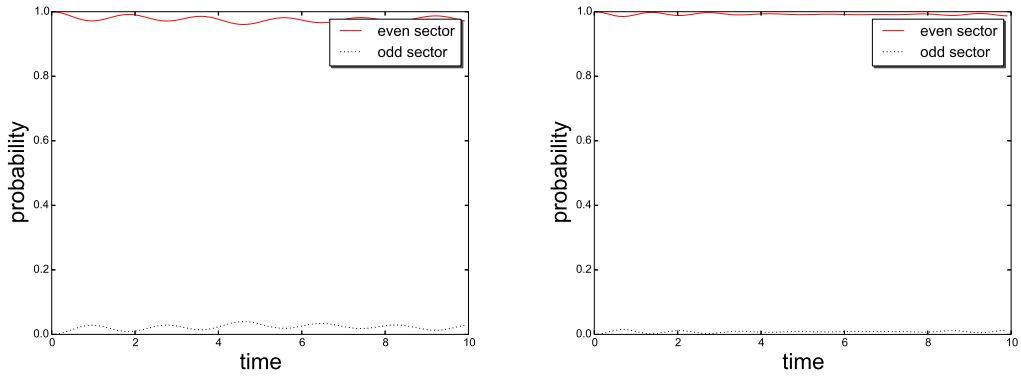


Figure 4.41: $J_E = 1$, $J_R = 0.1$, $J_I = 1$ Figure 4.42: $J_E = 1$, $J_R = 0.5$, $J_I = 1$

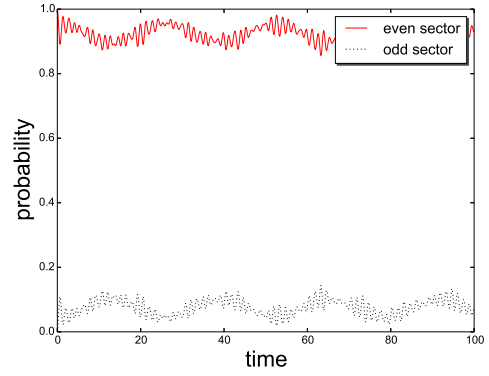
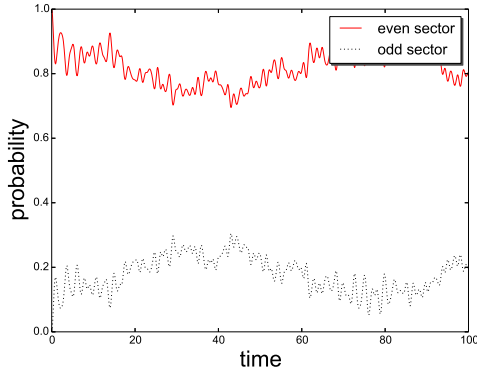


Figure 4.43: $J_E = 1, J_R = 0.1, J_I = 3$ Figure 4.44: $J_E = 1, J_R = 0.5, J_I = 3$

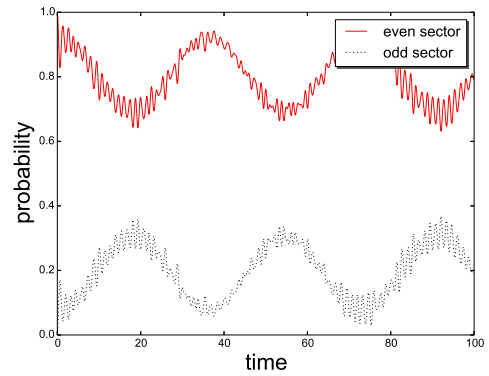
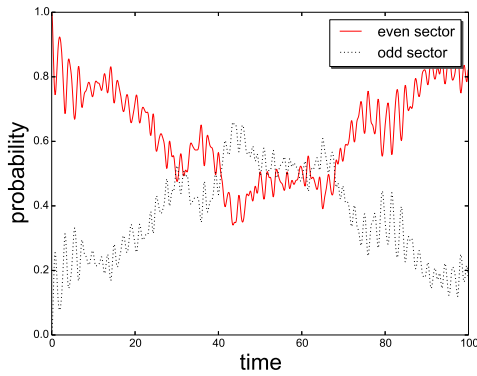


Figure 4.45: $J_E = 1, J_R = 0.1, J_I = 4$ Figure 4.46: $J_E = 1, J_R = 0.5, J_I = 4$

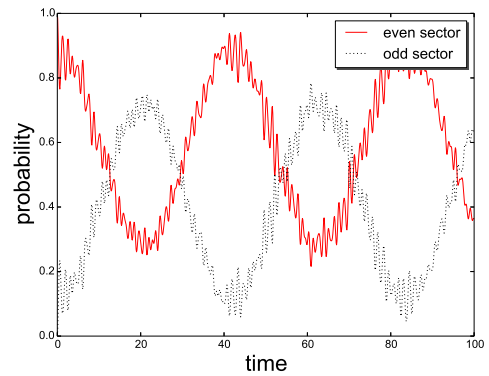
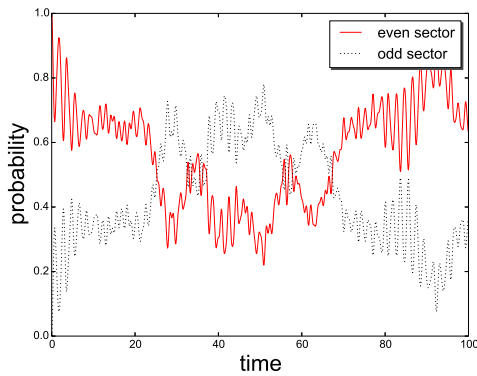


Figure 4.47: $J_E = 1, J_R = 0.1, J_I = 5$ Figure 4.48: $J_E = 1, J_R = 0.5, J_I = 5$

Clearly, in this regime, the system size will have a large impact on the robustness of the state of the system. We see, as the system is scaled and J_R decreases relative to J_E , that the probability of the system slipping into an opposite parity state increases steeply, along with the rate of oscillation of the states.

As we saw for the plots in regime 1, this behaviour is very similar to that seen in figures 4.26 - 4.33 for the non-chiral, regime 2 case. The same interpretation can then be applied, i.e. as the system grows it becomes much more susceptible to the interaction between the ring and the edge. The major difference produced by the reintroducing the chiral edge is again a slowing of the oscillation of the system between the states. As discussed previously, this can be attributed to the lower number of states contributing to the magnitude of the eigenvalues of the interacting states in the chiral system, for large J_I .

4.7 Optimal Design

From the numerics in the previous section, we can discuss some design considerations that should be taken into account when constructing a topological qubit using Ising anyons in a $\nu = 5/2$ fractional quantum Hall fluid. How optimally we can construct the system will depend on its exact behaviour, some elements of which have not yet been determined. However, we can safely say that, if the parity of the anyon ring is intended to be used as a qubit, then the inter-chain interaction must be kept to an absolute minimum. Regardless of the other properties of the system, the interaction between the ring and the edge is the main avenue by which the reliability of the qubit is compromised.

If the ring interacts strongly with the edge, it causes the interacting eigenstates of the system to deviate more from the initial, non-interacting states and, also, to have strong overlaps with a larger number of these initial states. This ultimately leads to a larger probability that the system will oscillate into an opposite parity state over time. We see this for weak inter-chain coupling in the perturbation theory, equations (4.55) and (4.56), and the numerics suggest that, in our simulated system, this relationship holds for stronger couplings strengths as well.

The optimal case would then be to engineer the system so that the separation between the ring and the edge is as large as possible. However, this distance is likely to be out of our control, as it is determined by the natural decrease in density of the fluid towards the edge of the system. This distance, along with the nature of how the anyon number is affected by scaling the system, are properties which have yet to be determined but using our assumed

regimes from the previous section we can make some general statements about what should be expected.

In regime 1, bulk quasiparticles are created in proportion to the linear size of the system so $J_E \sim J_R$ for all system sizes. We see from the plots, figures 4.36 - 4.39, that as J_I increases past 4 it starts to become more probable that the system will flip to an opposite parity state over time, rather than remain in its initial state. We can plot the difference between the highest value of P_{opp} and the lowest value of P_{initial} for a given range of t . With a set value of J_E and J_R , this will indicate the exact value of J_I for which it becomes more likely than not that the system will migrate into opposite parity states over time. The plot in figure 4.49 then identifies the values of J_I for which $P_{\text{opp}} < 0.5$, this gives some indication limiting values of J_I for which this particular qubit can be considered reliable.

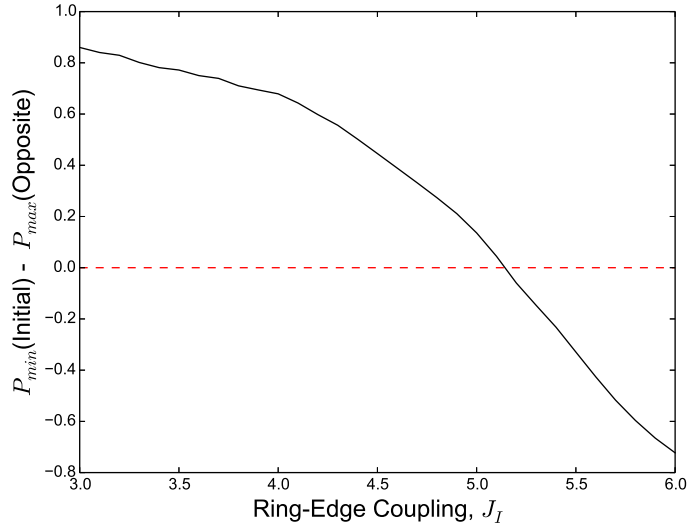


Figure 4.49: The gap between the likelihood of staying in the initial state and entering an opposite parity state for increasing J_I . Note below the red line indicates where the probability of changing to an opposite parity state is greater than that of remaining in the initial state.

Regime 2 describes a system in which the number of bulk quasiparticles is fixed and so J_R scales exponentially to zero with system size. The plots in section 4.2 show that, for a set value of J_E , a weaker in-chain coupling for the ring, J_R , will result in a less reliable qubit. This would seem to indicate that, in this regime, one should strive to keep the system as small as possible in order to maximize J_R and approach the more robust $J_R \sim J_E$ system described by regime 1.

However, in reality this will not be the case, as we are considering only the parity sector qubit and not all qubits of the system. For small J_R , we in fact approach a regime where there is N isolated qubits in the system, described in section 4.3.3 as the “ideal” regime. In this regime, the qubit which is closest to the edge will be unreliable, for strong enough J_I , but the other qubits are isolated from this interaction effect and will provide a more versatile implementation of TQC than the parity sector qubit. Thus, if regime two is really a possible realisation of the system it would be much more beneficial for us to sacrifice the reliability of the parity state qubit in favour of the $N - 1$ protected qubits which emerge for small J_R .

If, however, one still desires to use the parity qubit in this regime, an indication of its reliability for varying values of J_R and J_I may prove useful. The following plot (figure 4.50) then shows, for a range of J_R values, the minimum value of J_I for which $P_{\max}(\textit{opposite}) \geq 0.5$. Similar to figure 4.49 for regime 1, this gives a rough guide of the limiting values of J_I for which a system with given J_R can be considered reliable.

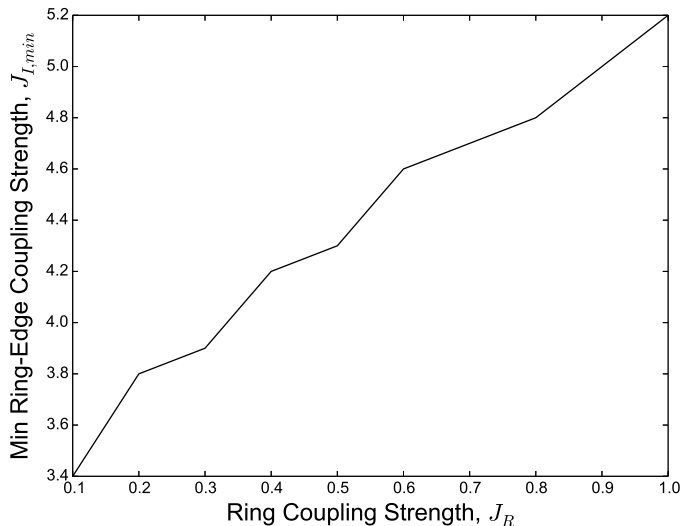


Figure 4.50: Lowest value of J_I for which the system is more likely to be in an opposite parity state to the initial state.

How to proceed with the design of the qubit then depends heavily on what we are able to manipulate in the system. It seems natural to assume J_I will be beyond our control if the anyons composing the ring are created in response to the density fall off towards the edge of the fluid. It would be more likely that we have some influence over the values of J_E and J_R , through appropriate

scaling of the system. However, we cannot say exactly how this scaling will affect the qubit, as other physical properties of the system, which we have not accounted for in this simple model, will likely be affected also.

In short, the results of the simulations in section 4.6 can not be assumed to accurately describe the dynamics in the thermodynamic limit. Larger systems will need to be simulated before we can provide a clear picture of the implications of the interactions on the various qubit designs. More concrete values for some of the physical properties of the system, such as the interaction strengths and their scaling behaviour, is also needed to understand which regimes should be focused on.

An alternative realisation of the model was mentioned in section 4.2, i.e. a model in which the anyon ring is created by physically manipulating the magnetic field, electron density or impurities of the system. Assuming this level of control is possible, it presents us with a vastly more manageable system, one which can be tuned much more precisely to our needs. We can then influence the properties of the system to ensure the anyon ring is located at the optimal distance from the edge, according to the plots above. There are some issues with this realisation however, namely, the level of control of the physical properties of the fractional quantum Hall fluid required here has not yet been achieved. Experiments can not yet influence the fractional quantum Hall in such a precise way as to create anyons in, or move them to, desired locations, as indicated in experimental review papers such as ref. [113].

We have also referred to a variation of our model in which the spacing of the anyons is not constant, i.e. J_R is site dependent. This model is worth considering, especially if a regime could be reached in which a number of the anyons have a large separation from their neighbours and so could be used to create near-ideal qubits. However, we discussed earlier how the interaction between a ring such as this and the edge will likely be difficult to model due to the lack of translational invariance even in the non-interacting system. This complicates the insertion of the chirality of the edge ring, as the problem cannot be easily expressed in the momentum basis. More sophisticated diagonalisation methods will then be necessary to obtain the eigenstates of the interacting system.

4.8 Conclusion

The goal of this chapter was to provide a simplified model of Ising anyons in a fractional quantum Hall fluid and to investigate the effects of the interactions on the system and their implications for TQC.

We argued that the bulk anyons could be approximated by a ring of interacting Ising anyons and this was shown to behave exactly like the 1-dimensional, transverse Ising model for a closed chain. It was seen that the interactions within the ring lift the degeneracy of the states and compromise the integrity of isolated qubits defined by the fusion channels of anyon pairs. As an alternative we considered a qubit defined by the parity of the number of fermions in the system, which remains well defined for large system sizes and interaction strengths.

We then examined the effect of the interaction between the ring and the edge on the state of this parity qubit. The edge was approximated by a similar 1-dimensional transverse Ising chain to facilitate the introduction of an interaction between the two. Under the assumption that the interaction between the two chains was only significant at their closest point, we derived a form for the interaction term and projected the model onto the subspace where the outer chain contains only positive momentum states, i.e. the edge is chiral, obtaining the interacting Hamiltonian of the original model.

For a general system, it is likely impossible to evaluate the eigenstates of the interacting Hamiltonian in general, thus numerical simulations were deemed to be necessary in order to observe the dynamics of the model. For one particular system with $N_E = N_R = 4$, we were able to diagonalise the Hamiltonian and obtain the eigenstates of the interacting system. However, as the states of the qubit are the eigenstates of the non-interacting system, it was clear that, with the interaction, such states would change over time and introduce the possibility for the system to decay out of a state we have placed it in making the qubit unreliable.

Through simulations we displayed that, while not completely unavoidable, the probability of such errors occurring could be reduced if the system could be engineered in such a way as to ensure the strength of the interaction between the ring and the edge is significantly lower than the strength of the interaction

between the anyons in the ring. Examining two possible regimes of the system, we showed how the coupling strengths affected the behaviour of the system and provided some plots (figures 4.49 and 4.50) which give an indication of the conditions under which the parity qubit should be considered unreliable.

However, it is not clear that these simulations at small system size represent the system's behaviour in the thermodynamic limit and we hope future simulations at larger system sizes may provide a more definite result.

Conclusions

In this thesis, we examined the design of topological qubits and assesses their efficiency and practicality as applied to topological quantum computation. Chapters 2 and 3 studied methods of optimally constructing a qubit using various different designs. Chapter 4 provides a simplified model for considering the behaviour of a qubit composed of interacting anyons within a fractional quantum Hall system. Here we outline the most important results of the thesis and propose some future work in the area.

Optimal Qudit Design in 2 Dimensions

Chapter 2 focused on qubits created using collections of anyonic excitations in a 2-dimensional system. With the braid group, B_n , dictating the possible operations that could be implemented on such a system, we used representations of this group to determine what design considerations should be made. We found that a qubit should be composed of either 3 or 4 anyons to ensure it can be efficient, universal and robust.

We generalised this result to d -dimensional qudits to show the maximum number, N , of anyons from which a qudit can be composed, without introducing leakage into single qubit operations, will always be related to its dimension by: $N = d + 2$.

Information leakage becomes an unavoidable issue when multi-qudit gates are implemented. We again used the representation theory of the braid group to look into the possibility of producing multi-qubit systems with no leaking operations. We found that such gates do in fact exist in some very special cases, but they do not provide universality for quantum computation.

Generalised Qudit Construction

The braid group is not the only method of implementing logic gates on anyons. In chapter 2, we tried to derive a formula for the maximum number of anyon-like excitations from which to compose a qudit if the logic operations on those anyons are not restricted to any particular exchange group.

While an exact relation proved elusive, we were able to show that the optimal number of constituent anyonic excitations will be related to the number and the multiplicity of the anyon species in the system. We also gave an extreme upper limit on the number of anyons which could comprise such a qubit, in equation (2.8).

Motion Group Anyons

In chapter 3, we studied a possible implementation of TQC in (3+1) dimensions. We specifically focused on a system of ring-shaped anyonic excitations in 3 dimensions which can be exchanged using the motion group, \mathfrak{Mot}_n , to produce quantum gates.

By constructing two-dimensional representations of \mathfrak{Mot}_n , we obtained results for the maximum number of rings a qudit can contain that closely resembled the results obtained for (2+1)-dimensional qubits in chapter 2. This similarity was attributed to the presence of the Yang-Baxter relation common to both exchange groups and thus the similarity of the representations is expected to continue to higher dimensional qudits.

Local Representations

In an effort to find non-Abelian, possibly universal representations of the motion group of rings we introduced the concept of local representations.

For a system where internal vector spaces are assigned to the excitations, the local representation of the operators of the motion group was defined as acting non-trivially only on those vector spaces related to the rings which are involved in the motion. We showed how such representations might be simpler to calculate due to requiring the computation of only three independent operators, \mathcal{R} , τ and f , regardless of the system size. We also argued how such representations may be more likely to be non-Abelian as the dimension of the

Hilbert space increases with the number of generators.

Using results from Dye [47], we gave a detailed characterisation of all non-Abelian, 2-dimensional local representations. We showed that non-Abelian representations of \mathfrak{Mot}_n of this form exist but the representation of the slide group, which we expect to make a large contribution to the universality of the representation, is always Abelian in these representations.

For local representations in higher dimensions we produced a general formula for calculating the local representation of the slide group operator, \mathcal{R} , and showed that it was related to the R -matrix of the quantum double of some gauge group acting on the local vector spaces.

Using this formula for \mathcal{R} we showed that non-Abelian, local representations of the motion group exist for which we can possibly be used for universal quantum computation. These representations alone will likely never be universal (we saw in section 3.5 that they are related to finite permutation groups), however, with the addition of some extra operations, such as measurement of topological charge, certain non-Abelian local representation may prove to be universal (as seen in ref. [52]).

Ising Anyon Ring

In chapter 4, we modelled a ring of Ising anyons in a fractional quantum Hall fluid at filling factor $\nu = 5/2$ under interaction with the edge of the fluid.

We showed how the model could be related to a transverse field Ising model on a closed chain interacting with a chiral Ising conformal theory describing the edge. We discussed various implementations of qubits arising from this model and mentioned some motivation for the study of a qubit composed from the fermion number parity sectors of the ring spectrum in detail.

Extending to a system of two transverse Ising chains which interact at a single point, we were able to obtain an approximate term for the interaction between the anyon ring and the edge. Projecting this system onto a subspace where the spectrum of the edge contains only chiral states we could then study how this ring-edge interaction affected the state of the parity sector qubit.

Numerical Simulations

We showed that analytical analysis of the system through perturbation theory was problematic and this prompted the use of numerical simulations. With many physical characteristics of the system yet undetermined, we outlined different possible regimes of the system which are dependant on how the various interaction energies scale with the system size.

Finally, we performed time evolution simulations under these various regimes for a single system size and produced a picture of how reliable the parity sector qubit remains after interactions are taken into consideration. For a single, small system ($N_E = N_R = 4$) we were able to indicate how relationships between the interaction strengths, J_E , J_R and J_I , affected the dynamics of the model. However, the connection to the thermodynamic limit is unclear at this point and will require substantial numerical work at larger system sizes.

Outlook

The work discussed in this thesis presents many opportunities for continued research.

For the generalised qudit, discussed in chapter 2, we would like to devise a way in which to obtain an exact relation between the dimension of a qudit and the optimal number of anyons. This would improve upon our upper limit result and give a more clear idea of how to optimally construct such systems.

In terms of leakage, we would like to prove (or disprove) our conjecture for the non-existence of universal, non-leaking, multi-qudit gates for general d . The existence of such gates would be a strong motivation for searching for anyon types with larger numbers of fusion channels. Alternatively, the existence of an anyon model for which only some subset of all multi-qudit gates is leakage free would be sufficient for universal, leakage-free quantum computation. It may prove more fruitful to search for such a system.

The next step for the ring-shaped anyonic excitations, discussed in chapter 3, should be to find a real system where such excitations could possibly exist. Ref. [114] shows that such quantised vortex rings do exist in ^3He , however it remains to be seen if any such excitations exist which also display anyonic exchange statistics. Our framework could then be used to predict the behaviour

of these systems and provide a method for analysing their usefulness for TQC, if the excitations are shown to exist.

Further research on the Ising anyon ring model, discussed in chapter 4, should include numerical simulations for larger systems sizes. Though our results give an indication of some of the dynamics to be expected from this model, larger system sizes are needed in order to accurately compare with experimental results and to predict the behaviour in the thermodynamic limit. A greater number of systems must also be evaluated for any general properties to be determined. More sophisticated computational procedures, such as DMRG techniques [115], along with more advanced resources, should allow the methods we have described in chapter 4 to be extended to much larger systems.

It will also be useful to look more in depth at the more generalised case of the model wherein the couplings between the σ anyons are allowed to vary. A more general result will allow us to model a greater number of regimes of the system, giving a greater probability of accurately modelling the real system. However, due to breaking of the translational invariance, analytic results will be more difficult to obtain even for the noninteracting Hamiltonian and a numerical approach will likely have to be introduced at an earlier stage than in our model.

Bibliography

- [1] A. Kitaev, “Fault-tolerant quantum computation by anyons,” *Ann. Phys.*, vol. 303, p. 2, 2003.
- [2] A. Kitaev, “Anyons in an exactly solved model and beyond,” *Ann. Phys.*, vol. 321, no. 1, pp. 2–111, 2006.
- [3] J. Alicea, Y. Oreg, G. Rafael, F. von Oppen, and M. P. A. Fisher, “Non-Abelian statistics and topological quantum information processing in 1d wire networks,” *Nature Physics*, vol. 7, pp. 412–417, 2010.
- [4] F. E. Camino, W. Zhou, and V. J. Goldman, “Realization of a Laughlin quasiparticle interferometer: Observation of fractional statistics,” *Phys. Rev. B*, vol. 72, p. 075342, Aug 2005.
- [5] R. L. Willett, L. N. Pfeiffer, and K. W. West, “Alternation and interchange of $e/4$ and $e/2$ period interference oscillations as evidence for filling factor $5/2$ non-Abelian quasiparticles,” *preprint*, 2009. [arXiv:0911.0345](https://arxiv.org/abs/0911.0345).
- [6] S. An, P. Jiang, H. Choi, W. Kang, S. H. Simon, L. N. Pfeiffer, K. W. West, and K. W. Baldwin, “Braiding of Abelian and non-Abelian anyons in the fractional quantum Hall effect,” *preprint*, 2011. [arXiv:1112.3400](https://arxiv.org/abs/1112.3400).
- [7] M. H. Freedman, A. Kitaev, M. J. Larsen, and Z. Wang, “Topological quantum computation,” *Bull. Amer. Math. Soc. (N.S.)*, vol. 40, no. 31, 2003.
- [8] J. Preskill, “Topological quantum computation,” *Lecture notes*, 2004. <http://theory.caltech.edu/people/preskill/ph229/>.

- [9] C. Nayak, S. H. Simon, A. Stern, M. Freedman, and S. Das Sarma, “Non-abelian anyons and topological quantum computation,” *Rev. Mod. Phys.*, vol. 80, pp. 1083–1159, 2008.
- [10] J. K. Pachos, *Introduction to Topological Quantum Computation*. Cambridge University Press, 2012.
- [11] M. A. Nielsen and I. L. Chuang, *Quantum Computation and Quantum Information*. Cambridge University Press, 2000.
- [12] S. Das Sarma, M. Freedman, and C. Nayak, “Topologically protected qubits from a possible non-Abelian fractional quantum Hall state,” *Phys. Rev. Lett.*, vol. 94, no. 166802, 2005.
- [13] J. M. Leinaas and J. Myrheim, “On the theory of identical particles,” *Nuovo Cimento B*, vol. 37B, no. 1, 1977.
- [14] M. A. Armstrong, *Basic Topology*. Springer, 1983.
- [15] F. Wilczek, “Magnetic flux, angular momentum, and statistics,” *Phys. Rev. Lett.*, vol. 48, no. 17, 1982.
- [16] F. Wilczek, “Quantum mechanics of fractional-spin particles,” *Phys. Rev. Lett.*, vol. 49, no. 14, 1982.
- [17] N. E. Bonesteel, L. Hormozi, G. Zikos, and S. H. Simon, “Braid topologies for quantum computation,” *Phys. Rev. Letters.*, vol. 95, no. 140503, 2005.
- [18] E. Artin, “Theory of braids,” *Ann. Math.*, p. 101, 1947.
- [19] G. Moore and N. Read, “Nonabelions in the fractional quantum Hall effect,” *Nucl. Phys. B*, vol. 360, pp. 362–396, 1991.
- [20] K. Drühl, R. Haag, and J. E. Roberts, “On parastatistics,” *Commun. Math. Phys.*, vol. 18, pp. 204 – 226, 1970.
- [21] H. Bombin, “Topological order with a twist: Ising anyons from an Abelian model,” *Phys. Rev. Lett.*, vol. 105, p. 030403, Jul 2010.

- [22] J. Liptrap, “Generalized Tambara-Yamagami categories,” *preprint*, 2010. [arXiv:1002.3166v2](https://arxiv.org/abs/1002.3166v2).
- [23] L. Hormozi, G. Zikos, N. E. Bonesteel, and S. H. Simon, “Topological quantum compiling,” *Phys. Rev. B*, vol. 75, no. 165310, 2007.
- [24] S. Trebst, M. Troyer, Z. Wang, and A. W. W. Ludwig, “A short introduction to Fibonacci anyon models,” *Prog. Theor. Phys. Supp.*, vol. 176, pp. 384–407, 2008.
- [25] Z. Wang, *Topological Quantum Computation*. American Mathematical Society, 2010.
- [26] G. Moore and N. Seiberg, “Polynomial equations for rational conformal field theories,” *Physics Letters B*, vol. 212, no. 4, 1988.
- [27] X. G. Wen, “Chiral Luttinger liquids and the edge excitations in the fractional quantum Hall effect,” *Phys. Rev. B*, vol. 41, no. 18, 1990.
- [28] A. A. Belavin, A. M. Polyakov, and A. B. Zamolodchikov, “Infinite conformal symmetry in two-dimensional quantum feild theory,” *Nucl. Phys. B*, vol. 241, pp. 333–380, 1984.
- [29] P. Di Francesco, *Conformal Field Theory*. Springer, 1997.
- [30] M. R. Gaberdiel, “An introduction to conformal field theory,” *Rep. Prog. Phys*, vol. 63, pp. 607–668, 2000.
- [31] P. Ginsparg, *Applied Conformal Field Theory in Fields Strings and Critical Phenomenon (Les Houches, Session XLIX, 1988)*, E. Brézin and J. Zinn-Justin (eds.). Elsevier, 1989.
- [32] A. M. Polyakov, “Conformal symmetry of critical fluctuations,” *JETP Lett.*, vol. 12, pp. 381–383, 1970.
- [33] V. G. Kac, “Contravariant form for infinite-dimensional lie algebras and superalgebras,” in *Group Theoretical Methods in Physics* (W. Beiglbcck, A. Bhm, and E. Takasugi, eds.), vol. 94 of *Lecture Notes in Physics*, pp. 441–445, Springer Berlin Heidelberg, 1979.

- [34] L. S. Georgiev, “Computational equivalence of the two inequivalent spinor representations of the braid group in the Ising topological quantum computer,” *J. Stat. Mech.*, no. P12013, 2009.
- [35] R. Ainsworth and J. K. Slingerland, “Topological qubit design and leakage,” *New Journal of Physics*, vol. 13, no. 065030, 2011.
- [36] S. Bravyi, “Universal quantum computation with the $\nu = 5/2$ fractional quantum Hall state,” *Phys. Rev. A*, vol. 73, no. 042313, 2006.
- [37] C. Vafa, “Toward classification of conformal theories,” *Physics Letters B*, vol. 206, no. 3, pp. 421 – 426, 1988.
- [38] M. H. Freedman, M. J. Larsen, and Z. Wang, “The two-eigenvalue problem and density of the Jones representation of braid groups,” *Comm. Math. Phys.*, vol. 228, pp. 177–199, 2002.
- [39] G. Kuperberg, “Denseness and Zariski denseness of Jones braid representations,” *Geom. Topol.*, vol. 15, no. 1, pp. 11–39, 2011.
- [40] D. Dahm, *A generalisation of braid theory*. Ph. D. Thesis, Princeton University, 1962.
- [41] D. L. Goldsmith, “The theory of motion groups,” *Michigan Math. J.*, vol. 28, no. 1, pp. 3–17, 1981.
- [42] E. Formanek, “Braid group representations of low degree,” *Proc. London Math. Soc.*, vol. 2, no. s3-73, pp. 279–322, 1996.
- [43] E. Formanek, W. Lee, I. Sysoeva, and M. Vazirani, “The irreducible representations of the braid group on n strings of degree $\leq n$,” *J. Algebra and its Applications*, vol. 2, no. 3, pp. 317–333, 2003.
- [44] I. Tuba and H. Wenzl, “Representations of the braid group B_3 and of $SL(2, \mathbf{Z})$,” *Pacific J. Math.*, vol. 197, no. 2, pp. 491–510, 2001.
- [45] E. Rowell, R. Stong, and Z. Wang, “On classification of modular tensor categories,” *Commun. Math. Phys.*, vol. 292, pp. 343–389, 2009.
- [46] E. C. Rowell and Z. Wang, “Localization of unitary braid group representations,” *Commun. Math. Phys.*, vol. 311, pp. 595–5615, 2012.

- [47] H. A. Dye, “Unitary solutions to the yang-baxter equation in dimension four,” *Quantum Information Processing*, vol. 2, pp. 117 – 151, 2003.
- [48] M. P. Drazin, J. W. Dungey, and K. W. Gruenberg, “Some generalizations of matrix commutativity,” *Proc. London Math Soc.*, vol. s3-1, pp. 22–231, 1952.
- [49] V. G. Drinfeld in *Proceedings of the international congress of mathematicians*, Berkeley, 1986, Amer. Math. Soc, Providence, 1987.
- [50] V. G. Drinfeld in *Problems of modern quantum field theory*, Proceedings of the Conference, Alushta, 1989, Springer, Berlin, 1989.
- [51] M. de Wild Propitius and F. A. Bais, *Discrete Gauge Theories in Particles and Fields*, edited by G.W. Semenoff, CRM Series in Maths. Phys. Springer, 1998.
- [52] C. Mochon, “Anyons from nonsolvable finite groups are sufficient for universal quantum computation,” *Phys. Rev. A*, vol. 67, p. 022315, Mar 2004.
- [53] K. v. Klitzing, G. Dorda, and M. Pepper, “New method for high-accuracy determination of the fine-structure constant based on quantised Hall resistance,” *Phys. Rev. Lett.*, vol. 45, no. 494, 1980.
- [54] D. C. Tsui, H. L. Stormer, and A. C. Gossard, “Two-dimensional magnetotransport in the extreme quantum limit,” *Phys. Rev. Lett.*, vol. 48, no. 22, 1982.
- [55] L. D. Landau and E. M. Lifshitz, *Quantum mechanics, non-relativistic theory, volume 3 of Course of theoretical physics*. Pergamon Press, London-Paris, 1958.
- [56] T. Ando, Y. Matsumoto, and Y. Uemura, “Theory of Hall effect in a two-dimensional electron system,” *J. Phys. Soc. Jpn.*, pp. 279–288, 1975.
- [57] R. E. Prange and S. M. Girvin, *The Quantum Hall Effect*. Springer-Verlag, New York, 1987.

- [58] S. M. Girvin, “The quantum hall effect: Novel excitations and broken symmetries,” in *Aspects topologiques de la physique en basse dimension. Topological aspects of low dimensional systems* (A. Comtet, T. Jolicur, S. Ouvry, and F. David, eds.), vol. 69 of *Les Houches - Ecole d’Ete de Physique Theorique*, pp. 53–175, Springer Berlin Heidelberg, 1999.
- [59] J. K. Jain, *Composite Fermions*. Cambridge University Press, 2007.
- [60] R. Willett, J. P. Eisenstein, H. L. Störmer, D. C. Tsui, A. C. Gosard, and J. H. English, “Observation of an even-denominator quantum number in the fractional quantum hall effect,” *Phys. Rev. Lett.*, vol. 59, pp. 1776–1779, Oct 1987.
- [61] J. S. Xia, W. Pan, C. L. Vicente, E. D. Adams, N. S. Sullivan, H. L. Stormer, D. C. Tsui, L. N. Pfeiffer, K. W. Baldwin, and K. W. West, “Electron correlation in the second Landau level: A competition between many nearly degenerate quantum phases,” *Phys. Rev. Lett.*, vol. 93, no. 17, 2004.
- [62] O. E. Dial, R. C. Anshoori, N. Pfeiffer, and K. W. West, “Anomalous structure in the single particle spectrum of the fractional quantum Hall effect,” *Nature*, vol. 464, pp. 566–570, 2010.
- [63] R. B. Laughlin, “Anomalous quantum Hall effect: An incompressible quantum fluid with fractionally charged excitations,” *Phys. Rev. Lett.*, vol. 50, no. 1395, 1983.
- [64] S. C. Zhang, T. H. Hansson, and S. Kivelson, “Effective-field-theory model for the fractional quantum hall effect,” *Phys. Rev. Lett.*, vol. 62, pp. 82–85, 1989.
- [65] F. D. M. Haldane, “Fractional quantisation of the Hall effect: A hierarchy of incompressible quantum fluid states,” *Phys. Rev. Lett.*, vol. 51, no. 7, 1983.
- [66] J. K. Jain, “Composite-fermion approach for the fractional quantum hall effect,” *Phys. Rev. Lett.*, vol. 63, pp. 199–202, 1989.

- [67] D. Arovas, J. R. Schrieffer, and F. Wilczek, “Fractional statistics and the quantum hall effect,” *Phys. Rev. Lett.*, vol. 53, pp. 722–723, 1984.
- [68] M. Levin, B. I. Halperin, and B. Rosenow, “Particle-hole symmetry and the Pfaffian state,” *Phys. Rev. Lett.*, vol. 99, no. 236806, 2007.
- [69] S.-S. Lee, S. Ryu, C. Nayak, and M. P. A. Fisher, “Particle-hole symmetry and the $\nu = 5/2$ quantum Hall state,” *Phys. Rev. Lett.*, vol. 99, no. 236807, 2007.
- [70] R. H. Morf, “Transition from quantum Hall to compressible states in the second Landau level: New light on the $\nu = 5/2$ enigma,” *Phys. Rev. Lett.*, vol. 80, no. 1505, 1998.
- [71] X. Wan, Z.-X. Hu, E. H. Rezayi, and K. Yang, “Fractional quantum Hall effect at $\nu = 5/2$: Ground states, non-Abelian quasiholes, and edge modes in a microscopic model,” *Phys. Rev. B*, vol. 77, no. 165316, 2008.
- [72] M. Storni, R. H. Morf, and S. Das Sarma, “Fractional quantum Hall state at $\nu = 5/2$ and the Moore-Read Pfaffian,” *Phys. Rev. Lett.*, vol. 104, no. 076803, 2010.
- [73] I. D. Rodriguez, A. Sterdyniak, M. Hermanns, J. K. Slingerland, and N. Regnault, “Quasiparticles and excitons for the Pfaffian quantum Hall state,” *Phys. Rev. B*, vol. 85, 2012.
- [74] A. Wójs, C. Tóke, and J. K. Jain, “Landau-level mixing and the emergence of Pfaffian excitations for the $5/2$ fractional quantum Hall effect,” *Phys. Rev. Lett.*, vol. 105, no. 096802, 2010.
- [75] E. H. Rezayi and S. H. Simon, “Breaking of particle-hole symmetry by Landau level mixing in the $\nu = 5/2$ quantized Hall state,” *Phys. Rev. Lett.*, vol. 106, no. 116801, 2011.
- [76] M. P. Zaletel, R. S. K. Mong, and F. Pollmann, “Topological characterization of fractional quantum Hall ground states from microscopic Hamiltonians,” *Phys. Rev. Lett.*, vol. 110, no. 236801, 2013.

- [77] V. Gurarie and C. Nayak, “A plasma analogy and Berry matrices for non-Abelian quantum Hall states,” *Nucl. Phys. B*, vol. 506, no. 3, pp. 685 – 694, 1997.
- [78] Y. Tserkovnyak and S. H. Simon, “Monte Carlo evaluation of non-Abelian statistics,” *Phys. Rev. Lett.*, vol. 90, p. 016802, 2003.
- [79] S. Bravyi and A. Kitaev, “Universal quantum computation with ideal Clifford gates and noisy ancillas,” *Phys. Rev. A*, vol. 71, no. 022316, 2005.
- [80] M. Freedman, C. Nayak, and K. Walker, “Towards universal topological quantum computation in the $\nu = 5/2$ fractional quantum Hall state,” *Phys. Rev. B*, vol. 73, no. 245307, 2006.
- [81] N. Read and E. Rezayi, “Beyond paired quantum Hall states: Parafermions and incompressible states in the first excited Landau level,” *Phys. Rev. B*, vol. 59, pp. 8084–8092, 1999.
- [82] E. H. Rezayi and N. Read, “Non-Abelian quantized Hall states of electrons at filling factors $12/5$ and $13/5$ in the first excited Landau level,” *Phys. Rev. B*, vol. 79, no. 075306, 2009.
- [83] P. Bonderson and J. Slingerland, “Fractional quantum Hall hierarchy and the second Landau level,” *Phys. Rev. B*, vol. 78, no. 125323, 2008.
- [84] P. Bonderson, A. E. Feiguin, G. Möller, and J. K. Slingerland, “Competing topological orders in the $\nu = 5/2$ quantum Hall state,” *Phys. Rev. Lett.*, vol. 108, no. 036806, 2012.
- [85] B. Rosenow, I. H. Bertrand, S. H. Simon, and A. Stern, “Exact solution for bulk-edge coupling in the non-Abelian $\nu = 5/2$ quantum Hall interferometer,” *Phys. Rev. B*, vol. 80, no. 155305, 2009.
- [86] C. R. Laumann, D. A. Huse, A. W. W. Ludwig, G. Rafael, S. Trebst, and M. Troyer, “Strong-disorder renormalization for interacting non-Abelian anyon systems in two dimensions,” *Phys. Rev. Lett.*, vol. 85, no. 224201, 2012.

- [87] A. H. MacDonald, “Introduction to the physics of the quantum Hall regime,” *preprint*, 1994. [arXiv:cond-mat/9410047](https://arxiv.org/abs/cond-mat/9410047).
- [88] M. Büttiker, “Absence of backscattering in the quantum Hall effect in multiprobe conductors,” *Phys. Rev. B*, vol. 38, no. 14, 1988.
- [89] X. G. Wen, “Theory of the edge states in fractional quantum Hall effects,” *Int J. Mod. Phys. B*, vol. 6, no. 1711, 1992.
- [90] X. G. Wen, “Edge excitations in the fractional quantum Hall states at general filling fractions,” *Mod. Phys. Lett. B*, vol. 5, 1991.
- [91] D.-H. Lee and X.-G. Wen, “Edge excitations in the fractional quantum Hall liquids,” *Phys. Rev. Lett.*, vol. 66, no. 1765, 1991.
- [92] N. Kawakami and S.-K. Yang, “Conformal field theory approach to one-dimensional quantum liquids,” *Prog. of Theo. Phys. Supp.*, vol. 107, no. 59, 1992.
- [93] J. Voit, “One-dimensional Fermi liquids,” *Rep. Prog. Phys.*, vol. 58, no. 977, 1995.
- [94] A. Feiguin, S. Trebst, A. W. W. Ludwig, M. Troyer, A. Kitaev, Z. Wang, and M. H. Freedman, “Interacting anyons in topological quantum liquids: The golden chain,” *Phys. Rev. Lett.*, vol. 98, no. 160409, 2007.
- [95] S. Trebst, E. Ardonne, A. Feiguin, D. A. Huse, A. W. W. Ludwig, and M. Troyer, “Collective states of interacting Fibonacci anyons,” *Phys. Rev. Lett.*, vol. 101, no. 050401, 2008.
- [96] P. Bonderson, “Splitting of topological degeneracy of non-Abelian anyons,” *Phys. Rev. Lett.*, vol. 103, no. 110403, 2009.
- [97] P. Kakashvili and E. Ardonne, “Intergrability in anyonic quantum spin chains via a composite height model,” *Phys. Rev. B*, vol. 85, no. 115116, 2012.
- [98] M. Baraban, G. Zikos, N. Bonesteel, and S. H. Simon, “Numerical analysis of quasiholes of the Moore-Read wave function,” *Phys. Rev. Lett.*, vol. 103, no. 076801, 2009.

- [99] P. Pfeuty, “The one-dimensional Ising model with transverse field,” *Ann. of Phys.*, vol. 57, pp. 79–90, 1970.
- [100] B. Rosenow, B. I. Halperin, S. H. Simon, and A. Stern, “Bulk-edge coupling in the non-Abelian $\nu = 5/2$ quantum Hall interferometer,” *Phys. Rev. Lett.*, vol. 100, no. 226803, 2008.
- [101] S. Sachdev, *Quantum Phase Transitions*. Cambridge University Press, 2000.
- [102] B. Douçot, M. V. Feigel’man, L. B. Ioffe, and A. S. Ioselevich, “Protected qubits and Chern-Simmons theories in Josephson junction arrays,” *Phys. Rev. B*, vol. 71, no. 024505, 2005.
- [103] G. Misguich, V. Pasquier, F. Mila, and C. Lhuillier, “Quantum dimer model with \mathbb{Z}_2 liquid ground-state: interpolation between cylinder and disk topologies and toy model for a topological quantum-bit,” *Phys. Rev. B*, vol. 71, no. 184424, 2005.
- [104] P. Jordan and E. Wigner, “Über das Paulische äquivalenzverbot,” *Zeitschrift für Physik*, vol. 47, pp. 631–651, 1928.
- [105] N. Bogoliubov, “On the theory of superfluidity,” *J. Phys. (USSR)*, vol. 11, p. 23, 1947.
- [106] A. Kitaev, “Unpaired Majorana fermions in quantum wires,” *Phys.-Usp.*, vol. 44, no. 131, 2001.
- [107] J. Bardeen, L. N. Cooper, and J. R. Schrieffer, “Microscopic theory of superconductivity,” *Phys. Rev.*, vol. 106, no. 162, 1957.
- [108] J. Bardeen, L. N. Cooper, and J. R. Schrieffer, “Theory of superconductivity,” *Phys. Rev.*, vol. 108, no. 1175, 1957.
- [109] G. Kells, D. Sen, J. K. Slingerland, and S. Vishveshwara, “Topological blocking in quantum quench dynamics,” *Phys. Rev. B*, vol. 89, no. 235130, 2014.
- [110] E. Dagotto and T. M. Rice, “Suprises on the way from one to two-dimensional quantum magnets: The ladder materials,” *Science*, vol. 271, no. 5249, pp. 618–623, 1996.

- [111] D. Poilblanc, A. W. W. Ludwig, S. Trebst, and M. Troyer, “Quantum spin ladders of non-abelian anyons,” *Phys. Rev. B*, vol. 83, p. 134439, 2011.
- [112] C. Cohen-Tannoudji, B. Diu, and F. Laloë, *Quantum Mechanics*. Wiley, 1977.
- [113] R. L. Willett, “The quantum Hall effect at $\nu = 5/2$ filling factor,” *Rep. Prog. Phys.*, vol. 76, no. 076501, 2013.
- [114] G. W. Rayfield and F. Reif, “Quantized vortex rings in superfluid helium,” *Phys. Rev.*, vol. 136, pp. A1194–A1208, Nov 1964.
- [115] S. White, “Density matrix formulation for quantum renormalization groups,” *Phys. Rev. Lett.*, vol. 69, no. 2863, 1992.